EXACT BER ANALYSIS AND DESIGN OF PRERAKE COMBINING SCHEMES FOR DIRECT SEQUENCE ULTRA-WIDEBAND MULTIPLE ACCESS SYSTEMS

CAO WEI

NATIONAL UNIVERSITY OF SINGAPORE

2007

EXACT BER ANALYSIS AND DESIGN OF PRERAKE COMBINING SCHEMES FOR DIRECT SEQUENCE ULTRA-WIDEBAND MULTIPLE ACCESS SYSTEMS

CAO WEI

(*B. Eng, M. Eng*)

A THESIS SUBMITTED

FOR THE DEGREE OF DOCTOR OF PHILOSOPHY

DEPARTMENT OF ELECTRICAL AND COMPUTER ENGINEERING

NATIONAL UNIVERSITY OF SINGAPORE

2007

Acknowledgment

The work in this thesis could not have been accomplished without the contribution of friendship, support and guidance of many people.

First of all, I would like to express my sincere gratitude to my supervisors, Dr. Arumugam Nallanathan, Dr. Chin Choy Chai and Dr. Balakrishnan Kannan, for their valuable guidance and helpful technical support throughout my PhD study. Had it not been for their advices, direction, patience and encouragement, this thesis would certainly not be possible. Not only their serious attitude towards research but also their courage to face difficulties make a great impact on me.

I specially thank Dr. Yong Huat Chew, Dr. Yan Xin and Dr. Meixia Tao, who are always willing to share their research experiences. I also thank Mr. Siow Hong Lin, who gives full technical support for a good working environment.

My sincere thanks go to my colleagues in the laboratory for their genuine friendship and many stimulating discussions in research. Special thanks to Sheusheu Tan, Feng Wang, Ronghong Mo, Kainan Zhou, Cheng Shan, Tek Ming Ng, Feifei Gao, Pham The Hanh, Hon Fah Chong, Yan Li, Le Cao, Jianwen Zhang, Yonglan Zhu, Jinhua Jiang, Lan Zhang, Rong Li, Jun He and Yang Lu.

I am also grateful to all my friends for their deep concern and enthusiastic support. Sharing with them the joy and frustration has made my life fruitful and complete.

I dedicate this thesis to my husband, my parents and my brother for their

great care and endless love to me throughout the years. I will be forever indebted to them for all that they have done.

Last but not least, I acknowledge National University of Singapore for supporting my PhD study.

Contents

Acknowledgment **i**

Contents **iii**

Summary **viii**

List of Tables **x**

List of Figures **xi**

List of Acronyms **xvi**

List of Notations **xviii**

Chapter 1. Introduction **1**

1.1 Background of UWB Communications 1

1.2 Current Research and Challenges 4

1.3 Objective and Contribution 6

1.4 Organization of the Thesis 9

Chapter 2. Overview of UWB Communication Systems **11**

2.1 Signal Generating Schemes 11

2.2 UWB Pulse Shapes 13

2.3 Modulation Schemes 15
2.4 Multiple Access Schemes 16
2.5 Channel Model 17
2.6 Energy Combining Schemes 19

Chapter 3. Exact BER Evaluation for DS UWB systems in AWGN Channels 22

3.1 Introduction 23
3.2 System Model 25
3.2.1 Signal Format 25
3.2.2 Template Waveform 26
3.3 Characteristic Function Analysis of DS PAM UWB System 27
3.3.1 Decision Statistics 27
3.3.2 Characteristic Function Analysis 28
3.4 Characteristic Function Analysis of DS PPM UWB System 30
3.4.1 Decision Statistics 30
3.4.2 Characteristic Function Analysis 31
3.5 BER Formula 34
3.6 BER Derivation Using the GA Method 34
3.7 Numerical Results 35
3.8 Conclusions 41

Chapter 4. Exact BER Analysis and Comparison of DS PAM UWB and DS PPM UWB systems in Lognormal Multipath Fading Channels 43

4.1 Introduction 44
4.2 System and Channel Models 46
4.2.1 Signal Format 46

4.2.2 Channel Model 47
4.2.3 Received Signal 48
4.3 Characteristic Function Analysis of DS PAM UWB System 49
4.3.1 Decision Statistics 49
4.3.2 Characteristic Function Analysis 53
4.4 Characteristic Function Analysis of DS PPM UWB System 55
4.4.1 Decision Statistics 55
4.4.2 Characteristic Function Analysis 59
4.5 BER Formula 61
4.6 BER Derivation Using the GA Method 62
4.7 Numerical Results and Comparison 63
4.7.1 System Parameters Setting 63
4.7.2 BER Results and Comparison 66
4.7.3 Explanation Based on Characteristic Functions 69
4.8 Conclusions 73

Chapter 5. Design and Analysis of Prerake DS UWB Multiple Access Systems Under Imperfect Channel Estimation 75

5.1 Introduction 76
5.2 System Model 78
5.2.1 Channel Model 78
5.2.2 Transmitted Signal 79
5.2.3 Received Signal 80
5.2.4 Channel Estimation 81
5.3 Signal Modeling and Decision Statistics 82
5.3.1 Signal Modeling 82
5.3.2 Decision Statistics 83

5.4 BER Performance Analysis 85
5.5 Multiple Access Performance Analysis 87
5.5.1 Definition of Degradation Factor 87
5.5.2 Degradation Factor and Number of Users 88
5.6 Numerical Results and Discussion 88
5.7 Conclusions 94

Chapter 6. Design and Analysis of High Data Rate Prerake DS UWB Multiple Access Systems 96

6.1 Introduction 96
6.2 System Model 98
6.2.1 Channel Model 98
6.2.2 Transmitted Signal 99
6.2.3 Received Signal 99
6.2.4 Channel Estimation 100
6.3 Signal Modeling and Decision Statistics 101
6.3.1 Signal Structure 101
6.3.2 Signal Modeling 101
6.3.3 Decision Statistics 104
6.4 Distribution of Interference 105
6.4.1 Inter-Chip Interference 107
6.4.2 Multiple Access Interference 107
6.5 BER Performance Analysis 109
6.6 Numerical Results and Discussion 111
6.6.1 Distribution of Interference 111
6.6.2 BER Performance 113
6.6.3 Effect of Imperfect Channel Estimation 115

6.7 Conclusions 120

Chapter 7. Conclusions and Future Work **122**

Bibliography **125**

Appendix A. Expectation Related to $\tilde{g}_{j,k}$ **134**

A.1 The 2nd Moment 134

A.1.1 $j \neq L_p - 1$ 134

A.1.2 $j = L_p - 1$ 135

A.2 The 4th Moment 135

A.2.1 $j \neq L_p - 1$ 135

A.2.2 $j = L_p - 1$ 136

A.3 Expectation of Square Product 136

List of Publications **137**

Summary

Recently, direct sequence ultra-wideband (DS UWB) communication systems have attracted much attention of both academia and industry because of its potential for high data rate applications within a short range. In this thesis, we study two important aspects of DS UWB communication systems: The first one is to exactly evaluate the bit error rate (BER) performance of DS UWB multiple access systems. The second one is to effectively capture energy using Prerake combining schemes.

Although the Gaussian approximation (GA) on the distribution of multiple access interference (MAI) prevails in previous performance studies of UWB systems, validity of the GA method is found to be questionable. Hence we propose to use a novel method based on characteristic function (CF) to compute BER values. We make use of the Fourier transform pair of probability density function (PDF) and characteristic function to find the distribution of total noise at the receiver. Then BER formula is derived based on the distribution of total noise. Our results show that the CF method outperforms the GA method in both additive white Gaussian noise (AWGN) channels and lognormal multipath fading channels. Furthermore, the BER formula enables us to accurately compare the performance of different modulation schemes and provides useful criteria for choosing appropriate modulation schemes in practical UWB applications.

Rich multipath diversity is an attractive feature of UWB communications.

However, how to utilize this advantage is not straightforward. We propose to use the Prerake combining in DS UWB communication systems, which enables effective energy capture with a simple correlation receiver instead of complex Rake receivers. Most of previous studies on the Prerake combining address single user scenario and/or perfect channel estimation, which are impractical for most UWB applications. Here we consider imperfect channel estimation and highlight the tradeoff between data rate and system performance in a multiple access environment. On the other hand, the Prerake combining allows higher data rate transmission. Hence, we design a high data rate (HDR) Prerake DS UWB system and employ the CF method to accurately analyze its performance.

List of Tables

3.1 The system parameters used in numerical study 36

5.1 The system parameters used in numerical study 89

6.1 The system parameters used in numerical study 111

List of Figures

1.1 FCC regulated spectral mask for indoor and outdoor UWB communication systems 2

2.1 The Gaussian pulse and its second derivative, the duration of the pulse is 1ns, the energy is normalized as 1. 14
2.2 Commonly used modulation methods in UWB communication systems: (a) binary PAM, (b) binary PPM, (c) OOK. 15
2.3 Comparison of Rake MRC and Prerake combining 20

3.1 The autocorrelation functions of $z(t)$: (1) is $R_{PAM}(\Delta T_k)$, (2) is $\hat{R}_{PAM}(\Delta T_k)$. 37
3.2 The cross correlation functions of $z(t)$ and $q(t)$: (1) is $R_{PPM}(\Delta T_k)$, (2) is $R_{PPM}(\Delta T_k + T_p)$. 38
3.3 The BER performance of the DS PAM UWB system under perfect power control ($P_0 = P_1$), number of users is $K = 2$. 39
3.4 The BER performance of the DS PPM UWB system under perfect power control ($P_0 = P_1$), number of users is $K = 2$. 40
3.5 The BER performance of the DS PAM UWB system under imperfect power control ($P_2 = 5P_0 = 5P_1$), number of users is $K = 3$. 41

3.6 The BER performance of the DS PPM UWB system under imperfect power control ($P_2 = 5P_0 = 5P_1$), number of users is $K = 3$. 42

4.1 The autocorrelation functions of $z(t)$: (1) is $R_{PAM}(\Delta T_k)$, (2) is $\hat{R}_{PAM}(\Delta T_k)$. 64

4.2 The cross correlation functions of $z(t)$ and $q(t)$: (1) is $R_{PPM}(\Delta T_k, 0)$, (2) is $R_{PPM}(\Delta T_k, 1)$, (3) is $\hat{R}_{PPM}(\Delta T_k, 0)$, (4) is $\hat{R}_{PPM}(\Delta T_k, 1)$. 65

4.3 Comparison of the GA and CF methods for the DS UWB systems: 2 users, 3 paths, Nr=64 66

4.4 Comparison of the GA and CF methods for the DS UWB systems: 2 users, 3 paths, Nr=128 67

4.5 Comparison of the GA and CF methods for the DS UWB systems: 2 users, 3 paths, Nr=256 68

4.6 Comparison of the GA and CF methods for the DS UWB systems: 2 users, 3 paths, Nr=512 69

4.7 The characteristic functions of the DS PAM UWB system: 2 users, 3 paths, Nr=64 70

4.8 The characteristic functions of the DS PAM UWB system: 2 users, 3 paths, Nr=512 71

4.9 The characteristic functions of the DS PPM UWB system: 2 users, 3 paths, Nr=64 72

4.10 The characteristic functions of the DS PPM UWB system: 2 users, 3 paths, Nr=512 73

5.1 BER performance of the Prerake DS UWB system in UWB channel model CM1 under imperfect channel estimation, the data rate increasing factor $N_c = 1, 4, 8, 20$, the number of users $K = 1$, the number of training monocycles $N_t = 100$. 90

5.2 BER performance of the Prerake DS UWB system in UWB channel model CM1 under imperfect channel estimation, the data rate increasing factor $N_c = 1, 8$, the number of users $K = 10, 50$, the number of training monocycles $N_t = 100$. 91

5.3 BER performance of the Prerake DS UWB system in UWB channel model CM1 under imperfect and perfect channel estimation, the data rate increasing factor $N_c = 1, 8$, the number of users $K = 50$, the number of training monocycles $N_t = 100, 200, \infty$. 92

5.4 BER performance of the Prerake DS UWB system in UWB channel model CM1 and CM3 with different number of users, the data rate increasing factor $N_c = 1$, the number of training monocycles $N_t = 100, 200, \infty$. 93

5.5 The number of users K as a function of degradation factor in CM1 and CM3 under perfect channel estimation. The desired BER is set as 10^{-3}. The data rate increasing factor $N_c = 1, 4, 8$. 94

6.1 Comparison of HDR Prerake and Partial-Prerake schemes, (a) is the channel impulse response $h^{(k)}(t)$ with $L = 10$, (b) is the reversal of $h^{(k)}(t)$, (c) is the structure of two chips (one in dashed lines, the other in solid lines) in the HDR Prerake scheme, with $L_c = 4$, $L_p = 6$, (d) is the structure of two chips (one in dashed lines, the other in solid lines) in the Partial-Prerake scheme, with $L_c = L_p = 4$. 102

6.2 The variance of $\tilde{g}_{j,k}$, (a) is in CM1, $L_p = 200$ with perfect channel estimation ($N_t = \infty$), (b) is in CM1, $L_p = 45$ with imperfect channel estimation ($N_t = 200$), (c) is in CM3, $L_p = 400$ with perfect channel estimation ($N_t = \infty$), (d) is in CM3, $L_p = 125$ with imperfect channel estimation ($N_t = 200$). 106

6.3 Comparison of the simulation PDF of I_M and its generalized Gaussian fitting and Gaussian fitting in CM1, $R_b = 50$Mbps, $L_p = 200$, $L_c = 5$, perfect channel estimation ($N_t = \infty$), 4 users. . 113

6.4 Comparison of the simulation PDF I_M and its generalized Gaussian fitting and Gaussian fitting in CM3, $R_b = 25$Mbps, $L_p = 125$, $L_c = 10$, imperfect channel estimation ($N_t = 200$), 4 users. 114

6.5 Comparison of the simulation PDF of I_C and its Gaussian fitting in CM3, $R_b = 25$Mbps, $L_p = 125$, $L_c = 10$, imperfect channel estimation ($N_t = 200$), 4 users. 115

6.6 BER performance comparison of the HDR Prerake DS UWB system and the Partial-Prerake DS UWB system in CM1, $R_b = 25$Mbps, under both perfect ($N_t = \infty$) and imperfect channel estimation ($N_t = 200$). 116

6.7 Comparison of the accuracy of the GA and the CF methods in BER calculation under perfect channel estimation ($N_t = \infty$) in CM1, $R_b = 50$Mbps, $L_p = 45$, the number of users $K = 4$ and 8 respectively. 117

6.8 Comparison of the accuracy of the GA and the CF methods in BER calculation under imperfect channel estimation ($N_t = 200$) in CM3, $R_b = 25$Mbps, $L_p = 125$, the number of users $K = 4$ and 8 respectively. 118

6.9 The effect of imperfect channel estimation ($N_t = 200$) with different number of taps L_p in Prerake filter in CM1, $R_b = 50$Mbps, $L_c = 5$, 4 users. 119

6.10 Multiple access performance of the HDR Prerake DS UWB system and the Partial-Prerake DS UWB system under perfect ($N_t = \infty$) and imperfect channel estimation ($N_t = 200$), $R_b = 25$Mbps, $L_c = 10$, $E_b/N_0 = 16dB$. 120

6.11 The output SNIR as a function of number of taps L_p in the Prerake filter under perfect ($N_t = \infty$) and imperfect channel estimation ($N_t = 200, 500, 1000$) with $E_b/N_0 = 16$dB in CM1, $R_b = 50$Mbps, 4 users. 121

List of Acronyms

AWGN	additive white Gaussian noise
BER	bit error rate
CDMA	code division multiple access
CF	characteristic function
CLT	central limit theorem
DF	degradation factor
DS	direct sequence
FCC	Federal Communications Commission
FDMA	frequency division multiple access
GA	Gaussian approximation
HDR	high data rate
ICI	inter-chip interference
IPI	inter-pulse interference
IR	impulse radio
ISI	inter-symbol interference
LOS	line-of-sight
MAI	multiple access interference
MMSE	minimum mean-square error
MRC	maximal ratio combining

NBI	narrow band interference
NLOS	nonline-of-sight
OFDM	orthogonal frequency division multiplexing
OOK	on-off keying
PAM	pulse amplitude modulation
PDF	probability density function
PPM	pulse position modulation
PSD	power spectral density
SI	self interference
SINR	signal-to-interference-plus-noise ratio
SNR	signal-to-noise ratio
TDD	time division duplex
TDL	tapped delay line
TDMA	time division multiple access
TH	time hopping
TR	transmitted reference
UWB	ultra-wideband
WPAN	wireless personal area network

List of Notations

a	lowercase letters are used to denote scalars
$\mathbf{a}$	boldface lowercase letters are used to denote column vectors
$\mathbf{A}$	boldface uppercase letters are used to denote matrices
$(\cdot)^T$	the transpose of a vector or a matrix
$\mathrm{E}[\cdot]$	the statistical expectation operator
$\otimes$	the Kronecker product
$\mathbf{0}_x$	the zero vector with x elements
$\mathbf{I}_x$	the $x \times x$ identity matrix
$\lfloor \cdot \rfloor$	the integer floor operation
$*$	convolution operation

Chapter 1

Introduction

In this chapter, the background of UWB communications and an overview of our work are given. Section 1.1 briefly describes the basic principle of UWB communications. Current research on UWB communication systems is summarized in Section 1.2. The objective and contribution of our work are presented in Section 1.3. The organization of this thesis is given in Section 1.4.

1.1 Background of UWB Communications

With rapid growth of number of wireless devices and ever-increasing demand on high data rate applications, radio spectrum becomes very precious resource. Though elaborate effort on well allocating spectrum resources has been continuously taken, it is necessary to find alternative approaches to exploit spectrum resources efficiently. In recent years, UWB technique has received significant interest from both research community and industry. The novel and unconventional approach employed by UWB communications is based on optimally sharing already occupied spectrum by means of the overlay principle, rather than looking for still available but possibly unsuitable new frequency bands.

In 2002, the US Federal Communications Commission (FCC) approved the use of UWB technique for both indoor and outdoor communications in the frequency band of 3.1GHz to 10.6GHz [1]. According to the FCC regulations, UWB communication systems are defined as those where the bandwidth is greater than 500MHz, or where the signal fractional bandwidth is greater than 0.2. The fractional bandwidth is defined by $2(f_H - f_L)/(f_H + f_L)$, where f_H is the upper frequency and f_L is the lower frequency at the -10dB emission points.

The main limiting factor of UWB communication systems is power spectral density (PSD) rather than bandwidth. In order to coexist harmoniously with those existing radio systems in the same frequency band, UWB communication systems must fulfill certain restriction with respect to both bandwidth and PSD. In Fig. 1.1, the emission limits and spectral mask assigned by FCC for indoor and outdoor UWB communication systems are illustrated.

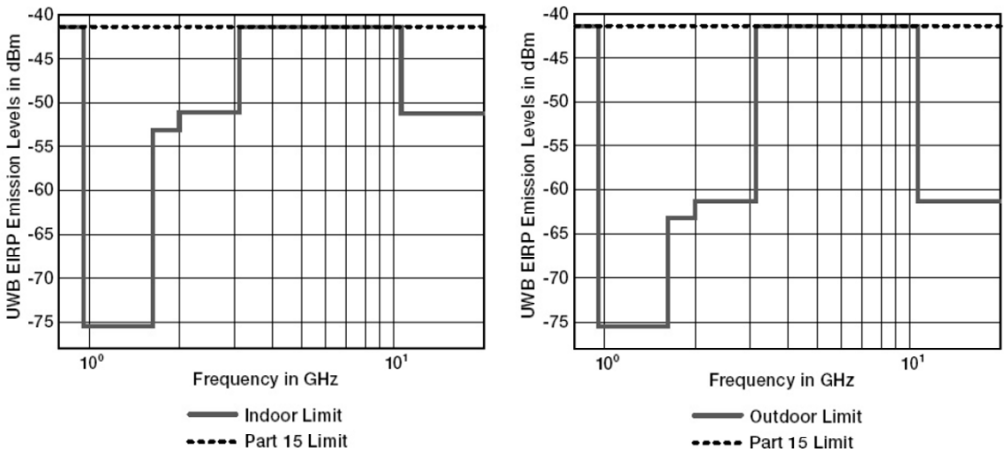

Figure 1.1: FCC regulated spectral mask for indoor and outdoor UWB communication systems

Due to the super large bandwidth, UWB communications come with unique advantages including enhanced capability to penetrate through obstacles, ultra

high precision ranging at the centimeter level, potential for high data rate transmission along with a commensurate increase in user capacity, and potentially small size/processing power. All these advantages enable us to use the UWB technique in various wireless applications, which include:

1. Wireless personal area networks (WPANs): WPANs allow short range ad hoc connectivity among portable consumer electronic and communication devices. They are envisioned to provide high-quality real-time multimedia distribution, file exchange among storage systems, and cable replacement for home entertainment systems. UWB technique emerges as a promising physical layer candidate for WPANs, because it offers high data rate transmission over short range, with low cost and high power efficiency.

2. Sensor networks: Sensor networks consist of a large number of static/mobile nodes spread across a geographical area. Key requirements for sensor networks operating in challenging environments include low cost, low power, and multifunctionality. High data rate UWB communication systems are well motivated for real-time gathering/disseminating/exchanging a vast quantity of sensory data. Typically, energy is more limited in sensor networks than in WPANs because of the nature of sensing devices and the difficulty in recharging their batteries. Studies have shown that current commercial Bluetooth devices are less suitable for sensor network applications because of their energy requirements and system cost [2]. In addition, exploiting the precise localization capability of UWB promises wireless sensor networks with improved positioning accuracy.

3. Radar imaging systems: Different from conventional radar systems where targets are typically considered as point scatterers, UWB radar pulses (also called UWB monocycle) are generally shorter than the target dimensions.

The reflected UWB pulses exhibit changes in both amplitude/time shift and pulse shape. As a result, UWB waveforms exhibit pronounced sensitivity to scattering relative to conventional radar signals. This property has been readily adopted by radar systems and can be extended to additional applications, such as underground and ocean imaging, as well as medical diagnostics and border surveillance devices.

1.2 Current Research and Challenges

Interest in UWB technique prior to 2001 was primarily limited to military applications, where supporting large number of users is not necessarily a main objective. However, multiple access scheme becomes much more important in commercial applications. Hence choosing an effective multiple access scheme is the first step in commercialization of UWB. Most of early research focuses on time hopping (TH) UWB systems [3]. In a typical UWB system, each data symbol is represented by a number of pulses, and each pulse is put in a frame. For a TH UWB system, multiple access is achieved by altering the pulse *position* from frame to frame, according to the TH code of a specific user. Later, DS UWB systems [4] attract much attention from both industry and academia, which enable multiple access by modifying the pulse *phase* from frame to frame. Intuitively, TH UWB system is suitable for low data rate applications because of its relatively low duty cycle, while DS UWB system has the potential to support high data rate applications. In addition, some research [5][6][7] has shown that DS UWB systems outperform TH UWB systems in terms of BER performance, multiple access capability and achievable data rate. Therefore, we concentrate on DS UWB systems in this thesis.

Unlike those narrow-band wireless communication systems, UWB systems

suffer much less from channel fading effects. The reason is that extremely narrow UWB pulses propagate over different paths and cause a large number of independently fading multipath components. These multipath components can be distinguished due to fine time resolution, which results in significant multipath diversity. Although UWB systems feature a certain inherent robustness to multipath effects, they are not entirely immune to them. For example, when a symbol sequence goes through multipath channels with large delay spread, inter-symbol interference (ISI) could occur due to overlapped multipath components. In a multiple user scenario, MAI and ISI could severely limit the system performance. In performance study of DS code division multiple access (CDMA) systems, MAI and ISI are generally assumed to be Gaussian distributed. However, recent studies [8][9] have shown that the Gaussian approximation of MAI is not suitable in UWB systems. To accurately analyze the performance and effectively mitigate the interference in UWB systems, it is necessary to study the statistical properties of the interference.

Another particularly challenging task is the receiver design. The first proposed UWB receiver is the correlation (matched filter) receiver [3][10][11], where received signal is correlated with the transmitted pulse. Later, efforts have been made to exploit rich multipath diversity, which has motivated research towards designing correlation-based Rake receivers to collect signal energy on multipaths [12][13]. However, Rake reception generally requires a large number of fingers with corresponding channel amplitudes and delays which are cumbersome to obtain [14][15]. In addition, hardware complexity, power consumption and system cost scale up significantly with increasing number of Rake fingers. To utilize the multipath diversity, an alternative approach is to use an autocorrelation receiver which correlates the received signal with a previously received signal [16][17]. The autocorrelation receiver can capture the entire received signal energy

for slowly varying channels without channel estimation. The primary drawback of autocorrelation receivers, nevertheless, is performance degradation associated with employing noisy received signals as reference signal in demodulation. Furthermore, an analog delay line required at the autocorrelation receiver is not easy to implement [18]. In a nutshell, although rich multipath diversity is enabled with UWB communications, effective energy capture with a low cost receiver still faces technical difficulties.

1.3 Objective and Contribution

The objective of this thesis is twofold: First, a CF method is proposed for precisely calculating BER values of DS UWB multiple access systems using pulse amplitude modulation (PAM) and pulse position modulation (PPM) in both AWGN channels and lognormal multipath fading channels. Using the CF method, analytical expressions of the average BER are derived, which enables accurate performance comparison of different modulation schemes. Second, two Prerake DS UWB systems are designed for medium and high data rate transmission respectively. The main advantages of these Prerake DS UWB systems include low complexity/cost receiver, alleviating ISI and allowing higher data rates in transmission.

Performance analysis is an important topic in any communication system from both practical and theoretical viewpoints. Performance evaluation of DS UWB multiple access systems can be found in some literature in both AWGN channels [5][6][7] and multipath fading channels [19][20][21]. In most of these works [5][6][7][20][21], the GA method is used, i.e., the total noise (could include ISI, MAI and AWGN) at the receiver is approximated as a Gaussian random variable. Though the GA method is simple to apply in AWGN channels, some

study [8][22] has shown that the GA method is inaccurate in the presence of MAI, especially under imperfect power control. Similarly, validity of the GA method should be considered carefully in multipath fading channels with near-far scenarios [49]. Furthermore, it is noted that only the conditional BER can be obtained by the GA method in multipath fading channels. And numerical averaging on the channel fading parameters (so-called semi-analytical/simulation approach) is needed to assist the GA method to obtain the average BER. So, in multipath fading channels, the GA method losses its main advantages: simplicity and closed form formula. In [19], though the Gaussian assumption on MAI is not required, only a Chernoff bound is derived on BER performance. In order to accurately evaluate the BER performance of DS UWB multiple access systems under imperfect power control, we propose to use a method based on characteristic function (called the CF method) in this thesis. The relation between PDF and characteristic function is utilized to find the distribution of the total noise at the receiver. Thereafter average BER values are computed based on exact PDF of the total noise. Our study shows that more accurate BER evaluation can be obtained by the CF method. Then performance comparison based on the exact BER formula indicates actual performance difference among commonly used modulation schemes and provides valuable criteria for choosing appropriate modulation schemes in practical UWB applications. The characteristic function and distribution analysis of interference in DS UWB systems also provides the theoretical basis for further study on interference suppression.

In UWB systems with a centralized topology (including a few fixed access points and a lot of portable receivers), low complexity receivers are very desirable to reduce the whole system cost. This is the key motivation for us to find a way to effectively capture signal energy in multipath fading channels using a simple receiver. We take the advantage of slow varying channels in most WPAN

applications [23][24] and design two Prerake DS UWB multiple access systems for medium and high data rate transmission respectively. In the proposed Prerake DS UWB systems, the temporal reverse channel impulse response is used as a prefilter at the transmitter. When the "preraked" transmitted signal passes through the channel, a strong peak is produced at the output of the channel. A simple receiver with only one finger is used to capture the peak, which carries energy equivalent to Rake maximal ratio combining (MRC). Recent works [25][26][27][28][29] on Prerake UWB systems have considered single user scenario under perfect channel estimation only. Since MAI is one of the major difference between Prerake and Rake systems [30], it is of interest to study the Prerake UWB multiple access systems. Also a study [31] has shown that channel estimation error largely degrades the performance of Prerake time division duplex (TDD) CDMA systems, especially in a multiple access environment. Hence the effect of imperfect channel estimation should be considered with carefulness in study of Prerake UWB systems. We propose a Prerake DS UWB multiple access system and examine its performance under imperfect channel estimation. It is found that the BER performance does not decrease monotonically with the increasing data rate under imperfect channel estimation. The expression of maximum number of users is derived. And the multiple access performance is evaluated in terms of maximum number of users supported for a desired BER. In order to support higher data rate, we propose another HDR Prerake DS UWB system, in which high data rate is achieved by superposition of chip waveforms. In the HDR Prerake DS UWB system, the constraint between data rate and captured signal energy existing in our first proposed Prerake DS UWB system is removed. We analyze the statistical property of MAI and adopt a generalized Gaussian distribution to well model the distribution of MAI. An accurate BER formula based on the CF method is derived and verified. Similar to our first proposed Prerake DS UWB system, we highlight

the tradeoff between signal energy captured and channel estimation noise in the HDR Prerake DS UWB system.

1.4 Organization of the Thesis

This thesis is organized as follows.

In Chapter 2, we outline several relevant technical aspects in UWB communication systems which is helpful to peruse this thesis.

In Chapter 3, an exact BER evaluation method based on the characteristic function is proposed for DS UWB multiple access systems using PAM and PPM in the AWGN channels. The accurate BER formula is derived and verified by numerical results. The accuracy of the CF method and the GA method is compared.

In Chapter 4, we extend the exact BER analysis for DS PAM/PPM UWB multiple access systems to a more practical channel model for UWB indoor communications: the lognormal multipath fading channels. DS PAM UWB and DS PPM UWB systems are accurately compared based on the exact BER formula derived.

Chapter 5 is devoted to describe the design and analysis of a Prerake DS UWB multiple access system under imperfect channel estimation. For the first time, the analytical signal model of Prerake DS UWB multiple access systems is presented. Then we analyze the BER performance and the multiple access performance of the proposed system.

In Chapter 6, we propose a HDR Prerake DS UWB multiple access system and analyze its performance. The distribution of different interference in the system is discussed and a generalized Gaussian distribution is adopted to model the distribution of MAI. Then we use the CF method to derive the BER formula

and verify it using simulations.

Finally, we summarize and conclude our work in Chapter 7. In this chapter, we also discuss a few interesting questions for further study.

Chapter 2

Overview of UWB Communication Systems

In this chapter, we present the physical layer issues of UWB communication systems, including channel model, modulation and multiple access schemes, energy combining schemes and receiver design.

2.1 Signal Generating Schemes

Existing UWB communication systems are generally based on two main signal generating schemes: impulse radio (IR) scheme [32][33][34] and multiband orthogonal frequency division multiplexing (OFDM) scheme [35][36][37]. The IR UWB scheme has been used in military radar measurements and communications since 1960's [38][39]. The basic principle of IR UWB scheme is to develop, transmit and receive pulses with extremely short duration, often on the order of nanoseconds or even less. As a result, energy of the UWB signal spreads very thinly from near direct current to a few GHz even in the absence of modulation. On the other side, in OFDM UWB scheme, the spectrum of 3.1GHz to 10.6GHz is divided into multiple subbands of 528MHz each. Within every subband, data

modulation/demodulation is realized using OFDM.

IR UWB scheme has following advantages: **1)** IR UWB signal can be generated by a low complexity/cost transmitter [40] with relatively low power consumption [41]. **2)** The inherent fine time resolution of IR UWB signal significantly reduces fading effects even in dense multipath environments [15][42]. This can considerably reduce the fading margins in link budgets and allow low transmission power. **3)** Low transmission power leads to low probability of detection and interception, which is very desirable in secure and covert communications. Besides, low transmission power alleviates interference to existing radio systems. **4)** Rich resolvable multipaths components enable multipath diversity reception. And robust performance can be achieved in the presence of narrow band interference because of large multipath diversity gain. **5)** Fine time resolution promises improved positioning accuracy in UWB radar applications.

The major advantages of OFDM UWB scheme are listed as follows: **1)** OFDM UWB scheme permits adaptive selection of subbands to provide good interference robustness and coexistence properties. **2)** Smaller bandwidth in each subbands helps reduce linearity requirements on antenna. **3)** Transmitted pulse is longer so that distortion by integrated circuit package and antenna is less. **4)** It is capable of utilizing frequency division multiple access (FDMA) in severe near-far scenarios.

Compared to IR UWB scheme, the system structure in OFDM UWB scheme is more complex because it needs communications digital signal processor to perform the fast Fourier transform and inverse fast Fourier transform operations. And the peak-to-average ratio of OFDM UWB scheme is higher than that of IR UWB scheme. The most important drawback of OFDM UWB scheme is that it loses the attractive features of accurate timing and locating, since the large

bandwidth is divided into many small subbands. Therefore, IR UWB scheme can support more types of applications than OFDM UWB scheme. In this thesis, we will focus on IR UWB scheme only. Hereinafter, the word "UWB" means IR UWB, unless otherwise mentioned.

2.2 UWB Pulse Shapes

Pulse shape plays an important role in UWB systems since it largely determines the spectrum of the system. Generally, the duration T_p of a UWB pulse $z(t)$ is on the order of nanosecond. Thus the bandwidth of $z(t)$ can be approximately calculated as $B \approx 1/T_p$. As mentioned before, such a super short pulse $z(t)$ enables rich multipath diversity by giving rise to a large number of resolvable replicas.

The Gaussian pulse and its n^{th} derivative are the most widely used pulse shapes in UWB systems. The reason behind the popularity of these pulses is twofold: First, Gaussian pulses come with the smallest possible time-bandwidth product of 0.5, which maximizes the range-rate resolution. Second, the Gaussian pulses are readily available from the antenna pattern [43]. For example, the Gaussian pulse can be generated by applying a step function current to the antenna. Later, an orthogonal pulse set based on modified Hermite polynomials is introduced in [44], which can be used to differentiate symbol in pulse shape modulation or to differentiate users in multiple access systems. More recently, a novel pulse design algorithm utilizing the concepts of prolate spheroidal functions is proposed in [45]. The performance of these pulse shapes are examined and compared in [46]. The Gaussian pulses are shown to achieve the same performance as the prolate spheroidal function based pulses with the same effective bandwidths. Further, the Gaussian pulses outperform the modified

Hermite polynomial based pulses. Therefore, in the numerical study section of each chapter, we use the Gaussian pulse and its second derivative for the purpose of illustration. Nevertheless, the analysis throughout this thesis is applicable for any UWB pulse shape. In Fig. 2.1, the Gaussian pulse and its second derivative are plotted. The duration of these pulses is set as 1ns. Both pulses are energy-normalized.

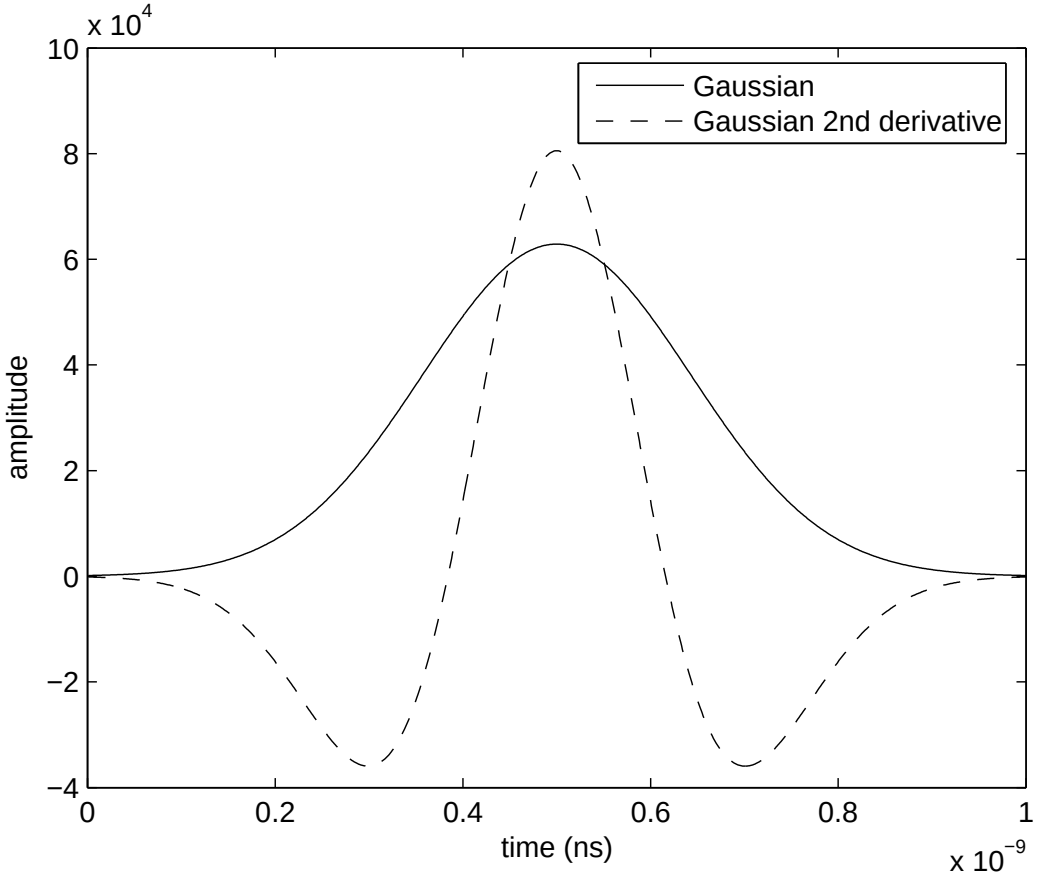

Figure 2.1: The Gaussian pulse and its second derivative, the duration of the pulse is 1ns, the energy is normalized as 1.

2.3 Modulation Schemes

A number of modulation schemes may be used with UWB systems. The potential modulation schemes include both orthogonal and antipodal schemes, such as PPM [11], on-off keying (OOK) [47] and PAM [48]. The binary PAM, binary PPM and OOK modulation are illustrated in Fig. 2.2.

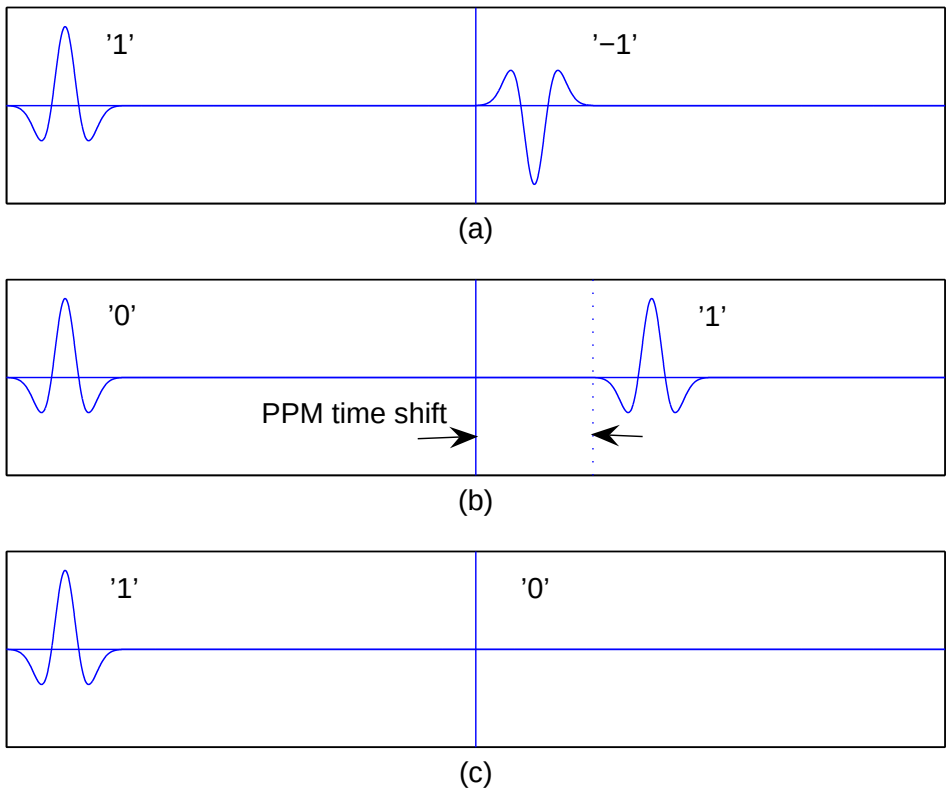

Figure 2.2: Commonly used modulation methods in UWB communication systems: (a) binary PAM, (b) binary PPM, (c) OOK.

In the early research on UWB communications, PPM was almost exclusively adopted since the negative UWB pulses were difficult to implement. In the M-ary PPM scheme, M delayed pulses $\{z(t-\Delta_m)\}_{m=0}^{M-1}$ are used to represent

different symbols. Generally, the modulation indices Δ_m are chosen as $\Delta_m = m\Delta$ with $\Delta \geq T_p$, which corresponds to an orthogonal PPM. In binary PPM, the delay Δ can also be chosen to minimize the correlation of $\int z(t)z(t-\Delta)dt$ [20]. Another binary modulation scheme that does not require negative pulse is OOK, where symbol "1" is represented by transmitting a pulse, and symbol "0" by transmitting nothing. Lately, generating negative pulses becomes easier and PAM attracts more attention. In particular, the classic binary PAM using antipodal pulses is widely adopted.

It should be noted that PPM and OOK signals have discrete spectral lines [11][49][50][51], which could cause severe interference to narrow band wireless communication systems operating in the same frequency band. On the other side, the PAM scheme inherently offers smooth PSD because of the random polarities of data symbols. In this sense, PAM signaling is more attractive.

More complex modulation schemes, such as hybrid amplitude and position modulation [52], and pulse shape modulation [44] have also been reported.

2.4 Multiple Access Schemes

Time hopping is the first suggested multiple access scheme [3] for the UWB systems. In a TH UWB system, each data symbol is represented by a number (N_r) of frames. In each frame (with duration of T_f), there is one and only one pulse. The positions of N_r pulses are determined by a user-specific TH sequence c_n^k. Each frame is divided into N_c chips with duration of T_c ($T_c > T_p$), i.e., $T_f = N_c T_c$. And the k^{th} user's TH code $\{c_n^k\}_{n=0}^{N_r-1} \in [0, 1, \cdots, N_c - 1]$ corresponds to a time delay of $c_n^k T_c$ during the n^{th} frame [11]. Consequently, the k^{th} user's

transmitted waveform using PAM is given by the following expression.

$$s_{TH}^{(k)}(t) = \sum_{i=-\infty}^{\infty} b_i^k \sum_{n=0}^{N_r-1} z(t - iN_rT_f - nT_f - c_n^kT_c) \tag{2.1}$$

DS is another traditional spread spectrum technique that can be combined with UWB to accommodate multiple users. In a DS UWB system, the users are distinguished by a user-specific DS code. Each symbol still consists of N_r pulses of duration T_p, each pulse occupying a frame with duration of T_f. The transmitted signal is analytically expressed as follows.

$$s_{DS}^{(k)}(t) = \sum_{i=-\infty}^{\infty} b_i^k \sum_{n=0}^{N_r-1} a_n^k z(t - iN_rT_f - nT_f) \tag{2.2}$$

where b_i^k is the i^{th} symbol and $\{a_n^k\}_{n=0}^{N_r-1} \in [-1, 1]$ is the direct sequence assigned to the k^{th} user.

In both TH UWB and DS UWB systems, the symbol duration is N_rT_f, which corresponds to a data rate of $R_b = 1/(N_rT_f)$ in binary PAM scheme. It is noted that in the TH UWB system, the frame duration must be large enough to allow the time hopping delay, i.e., $T_f = N_cT_c > N_cT_p$. In contrast, the frame duration in the DS UWB system can be much smaller as long as it can accommodate the pulse itself, i.e., $T_f \geq T_p$. Therefore, DS UWB inherently can support higher data rate than TH UWB.

2.5 Channel Model

The channel model adopted by the IEEE 802.15.3a task group is basically a modified version of the well-known S-V indoor channel model [53]. To reach an analytically tractable channel model, the total number of paths is defined as the number of multipath arrivals with expected power within 10dB from that of the strongest arrival.

Analytically, the channel model is defined by the following channel impulse response.

$$h(t) = X \sum_{l=0}^{L-1} \alpha_l \delta(t - \tau_l) \tag{2.3}$$

where X represents the lognormal shadowing, L denotes the number of multipaths. The path gain α_l consists of two parts, i.e., $\alpha_l = \theta_l \beta_l$, where $\theta_l \in \{\pm 1\}$ represents the random phase due to reflection and β_l is the lognormal fading amplitude. For different l, α_l are independent random variables. Since the multipath components arrive in clusters [54], the l^{th} path can be expressed as the j^{th} ray in the i^{th} cluster. Therefore the delay of the l^{th} path, τ_l can be split as $\tau_l = \mu_i + \nu_{j,i}$, where μ_i is delay of the i^{th} cluster and $\nu_{j,i}$ is delay of the j^{th} ray in the i^{th} cluster relative to μ_i. Similar to the S-V channel model, cluster arrivals are Poisson distributed with rate Λ. Within each cluster, ray arrivals are also Poisson distributed with rate $\lambda > \Lambda$.

The power delay profile of the channel is double exponential decaying by rays and clusters.

$$\mathrm{E}\left[\beta_l^2\right] = \Omega_0 \exp(-\mu_i/\Gamma) \exp(-\nu_{j,i}/\gamma) \tag{2.4}$$

where Ω_0 is the mean energy of the 0^{th} path in the 0^{th} cluster. Γ and γ represent the cluster decay factor and ray decay factor, respectively. The channel is normalized to have unit energy, i.e., $\sum_{l=0}^{L-1} \mathrm{E}\left[\beta_l^2\right] = 1$.

Model parameters corresponding to several ranges are provided in [54], for both line-of-sight (LOS) and nonline-of-sight (NLOS) scenarios. Since the shadowing factor X renders this model less tractable for theoretical performance analysis, X is generally ignored in most of UWB study for simplicity.

2.6 Energy Combining Schemes

The UWB systems enjoy a large multipath diversity gain owing to the fine time resolution. On one hand, a large number of multipaths significantly combat channel fading since the probability of all paths suffering from deep fading simultaneously is low [55][56]. On the other hand, the dense multipath environment makes effective energy capture a challenging task.

The correlation receiver [32][57] is originally used in the UWB systems. However, it can not handle well the energy capture in multipath fading channels. Then the Rake receiver [58][59][60][61] has been widely adopted in UWB systems. The main drawback of the Rake receiver is its complexity when applied in dense multipath channels. A Rake receiver with tens or even hundreds of fingers, performing accurate acquisition and channel estimation, seems to be unaffordable. To achieve low complexity without sacrificing performance, the autocorrelation receiver proposed 40 years ago [62], has regained interest from UWB researchers [17][63][64]. The autocorrelation receivers are generally used together with the transmitted reference (TR) UWB systems. The primary disadvantage of autocorrelation receivers, however, is the performance degradation associated with employing noisy received signals as reference signals in demodulation. Further, the transmission of reference pulses decreases the power efficiency. To avoid this problem, the differential TR UWB is proposed [65][66], where each pulse is differentially modulated with respect to the previous one and acts as reference for the next one. In both the TR UWB and the differential TR UWB systems, channel estimation is avoided with a autocorrelation receiver. However, an analogy delay line is required at the receiver, which is not easy to implement [18] especially in channels with large delay spread. Furthermore, the delay between pulses is generally set to be larger than the channel delay spread

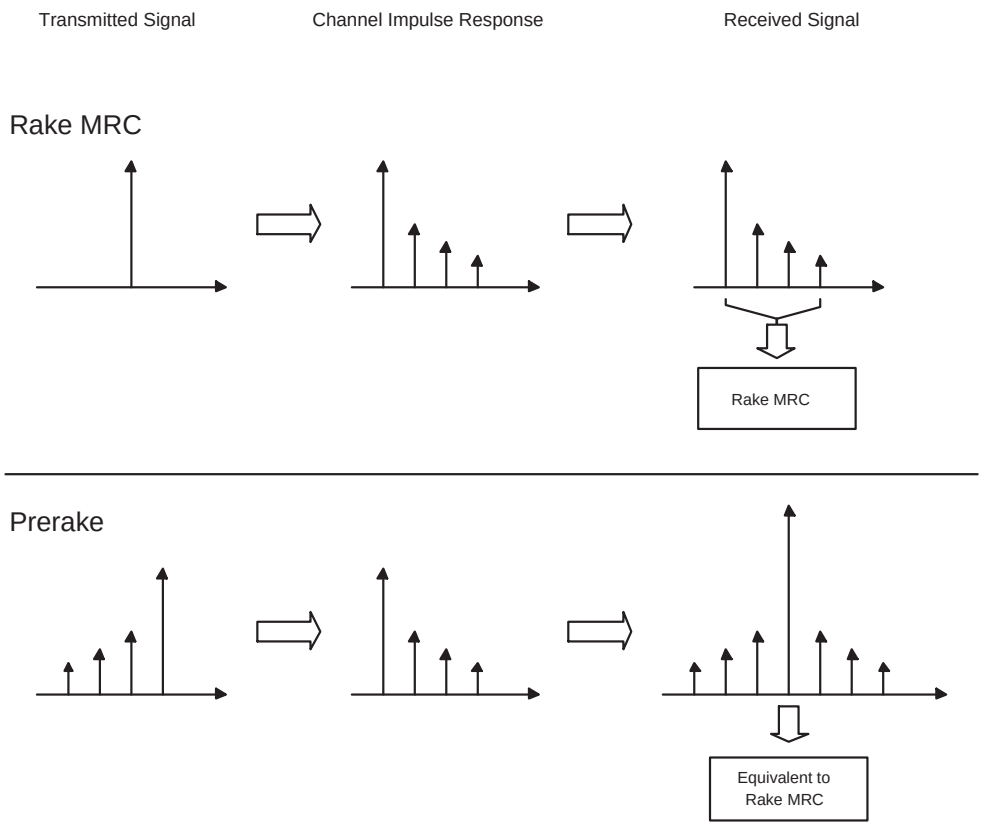

Figure 2.3: Comparison of Rake MRC and Prerake combining

to avoid inter-pulse interference, which inevitably sacrifices data rate.

An alternative approach to exploiting the multipath diversity with a simple receiver structure is to use the Prerake combing. The Prerake technique (also called time reversal) is originally used in wideband transmission in underwater acoustic [67] and TDD CDMA systems [30]. The temporal reverse channel impulse response is used as a prefilter at the transmitter. When the "preraked" transmitted signal convolves with the channel impulse response, a strong peak is produced at output of the channel due to coherent summation of the multipath components. Using Prerake combining, we can use a very simple correlation receiver to capture the peak. As shown in Fig. 2.3, comparison of Rake combing and Prerake combining is illustrated. Some study [25] has shown that in a

single user scenario, Prerake and Rake combining achieve almost the same BER performance when the same number of multipaths are combined. However, the multiple access performance of Prerake combining, the tradeoff between performance and data rate, and the effect of imperfect channel estimation have not been examined yet.

Chapter 3

Exact BER Evaluation for DS UWB systems in AWGN Channels

In this chapter, a method is proposed to evaluate the exact BER of DS PAM/PPM UWB multiple access systems. Section 3.1 introduces the prior works on performance study for various UWB systems in AWGN channels. The system model of DS PAM/PPM UWB systems are described in Section 3.2. The characteristic function analysis for DS PAM UWB and DS PPM UWB systems is presented in Section 3.3 and Section 3.4 respectively. In Section 3.5, the BER formula is derived based on characteristic functions. For comparison, the BER formula obtained by the GA method is briefly explained in Section 3.6. Numerical results are presented in Section 3.7 to show the accuracy of the CF method and the GA method. Finally, conclusions are drawn in Section 3.8.

3.1 Introduction

Performance evaluation of UWB communication systems in AWGN channels has been studied in the literature before the UWB channel model was formally released by the IEEE 802.15.3a task group. On one hand, performance analysis in AWGN channels presents important intermediate results for further study on general cases in more complex channel models. On the other hand, performance in AWGN channels can serve as a benchmark for UWB communication systems as shown in [68]. The fading margin of a PPM UWB system with single user is examined in [68] by comparing the system performance in AWGN channel and dense multipath channel. To achieve a desired BER of 10^{-5}, the transmission signal-to-noise ratio (SNR) required in AWGN channel and multipath channel is 13.5dB and 15dB, respectively, when the channel information is perfectly known. The small fading margin (1.5dB only) implies that performance of UWB systems in real UWB channels approaches the benchmark performance in the AWGN channel if multipath diversity is fully exploited.

Most of the earlier work on performance study focuses on TH UWB systems, which is the first multiple access scheme suggested for UWB communications [32][57]. The multiple access performance of TH UWB systems using binary PPM is discussed in [32] and [11], and the results show that a large number of users can be supported in a low data rate of 19.2Kbps under perfect power control. Then TH UWB systems with more complex modulation schemes have been studied in [33][69]. The union bound of BER is derived for the TH UWB system with M-ary PPM [69]. It is found that larger values of M bring better BER performance under perfect power control. The analytical BER expression of a UWB system using the pseudochaotic time hopping modulation (which combines pseudochaotic coding and multilevel PPM) is presented in [33]. The analysis emphasizes that

the cross correlation amongst the pseudochaotic code plays a dominant role in BER performance.

Later, DS UWB has attracted much attention as an alternative multiple access scheme for UWB communication systems. Comparison between TH UWB and DS UWB systems is carried out in [5][6][7]. The same conclusion is reached in all these works: Performance of DS UWB system, in terms of BER performance, multiple access capability and achievable data rate, is better than that of TH UWB system.

In all the works listed above, the GA method is used (i.e., the total noise in the system, including MAI and AWGN, is approximated as a Gaussian random variable) and the BER is expressed in terms of the output signal-to-interference-plus-noise ratio (SINR) using a Gaussian tail integral (the well-known erfc function). However, validity of the Gaussian approximation is questionable as shown in [8][22]. The BER performance of a TH PPM UWB system is studied and the results clearly show that the GA method significantly underestimates the BER values.

In order to accurately evaluate BER performance of TH UWB multiple access systems, a method based on the characteristic function is proposed in [70][71][72]. The characteristic function of MAI is derived to obtain the distribution of the total noise. It is shown that the CF method offers more accurate BER evaluation than the GA method at the expense of higher computational complexity.

In this chapter, we use the CF method to derive the BER formula of DS UWB multiple access systems, which can be used to precisely assess the system performance in AWGN channels. The analytical expressions are validated by simulation results. BER computation using the GA method is also briefly explained for comparison. The numerical results show that the CF method yields exact BER evaluation, while the GA method is inaccurate in medium

and large SNR range. The analysis in this chapter provides valuable performance benchmark for DS UWB multiple access systems.

3.2 System Model

3.2.1 Signal Format

The DS PAM UWB and the DS PPM UWB systems use the same multiple access scheme but different modulation schemes.

A typical DS binary PAM UWB signal is modeled as

$$s_{PAM}^{(k)}(t) = \sqrt{P_k} \sum_{i=-\infty}^{\infty} b_i^k \sum_{n=0}^{N_r-1} a_n^k z(t - iT_r - nT_c) \tag{3.1}$$

And a DS binary PPM UWB signal is modeled as

$$s_{PPM}^{(k)}(t) = \sqrt{P_k} \sum_{i=-\infty}^{\infty} \sum_{n=0}^{N_r-1} a_n^k z(t - iT_r - nT_c - b_i^k T_p) \tag{3.2}$$

where k is the index of user, i is the index of data symbol and $z(t)$ represents the UWB monocycle with normalized energy and duration of T_p. Other parameters are explained as below.

1. $\{a_n^k\}_{n=0}^{N_r-1}$ is the DS signature of the k^{th} user, which provides the multiple access capability for the UWB system. Random DS sequence is assumed, i.e., for every n and k, $a_n^k \in \{\pm 1\}$ with equal probability.

2. $\{b_i^k\}_{i=-\infty}^{\infty}$ represents the data symbol sequence of the k^{th} user. In the DS binary PAM UWB system, b_i^k takes value from $\{\pm 1\}$ with equal probability. In the DS binary PPM UWB system, b_i^k is chosen from $\{0, 1\}$ with equal probability.

3. N_r stands for the number of chips in one data symbol. In each chip, there is one and only one UWB monocycle $z(t)$.

4. P_k is the transmitted signal power of the k^{th} user. Under imperfect power control, P_k is different for different users. The energy of each transmitted symbol is $E_b^k = P_k N_r$.

5. T_c is the chip duration and T_r is the symbol duration, i.e., $T_r = N_r T_c$. To accommodate one UWB monocycle in each chip, we set $T_p = T_c$ in the DS PAM UWB system. In the DS PPM UWB system, we set $T_p = T_c/4$ to allow the pulse position shift.

6. The time shift associated with PPM is set as T_p in the orthogonal binary PPM signal set.

In a multiple access environment with K asynchronous users, the received signal in an AWGN channel is expressed as

$$r_{PAM/PPM}(t) = \sum_{k=0}^{K-1} s^{(k)}_{PAM/PPM}(t - \tau_k) + n(t) \tag{3.3}$$

where τ_k is the asynchronous transmission delay of the k^{th} user uniformly distributed over $[0, T_r)$, $n(t)$ is the AWGN with double sided PSD of $N_0/2$.

3.2.2 Template Waveform

The template waveforms used in the correlation receiver of the k^{th} user for the DS PAM UWB and the DS PPM UWB systems are listed as below.

$$v^{(k)}_{PAM}(t) = \sum_{n=0}^{N_r-1} a^k_n z(t - nT_c) \tag{3.4}$$

$$v^{(k)}_{PPM}(t) = \sum_{n=0}^{N_r-1} a^k_n q(t - nT_c) \tag{3.5}$$

where $q(t) = z(t) - z(t - T_p)$ is the template waveform in one chip for the orthogonal binary PPM signal set.

3.3 Characteristic Function Analysis of DS PAM UWB System

3.3.1 Decision Statistics

Without loss of generality, we consider the 0^{th} user as the desired user. Under the assumption of perfect synchronization with the 0^{th} user, we set $\tau_0 = 0$ in Eq. (3.3). To detect the 0^{th} symbol (i.e., $i = 0$) of the 0^{th} user, the decision statistic Z_{PAM} at the output of the 0^{th} receiver is given by

$$\begin{aligned} Z_{PAM} &= \int_0^{T_r} r_{PAM}(t) v_{PAM}^{(0)}(t) dt \\ &= \underbrace{\int_0^{T_r} s_{PAM}^{(0)}(t) v_{PAM}^{(0)}(t) dt}_{Z_{PAM}^{(0)}} + \underbrace{\sum_{k=1}^{K-1} \int_0^{T_r} s_{PAM}^{(k)}(t-\tau_k) v_{PAM}^{(0)}(t) dt}_{I_{PAM}} \\ &\quad + \underbrace{\int_0^{T_r} n(t) v_{PAM}^{(0)}(t) dt}_{N_{PAM}} \end{aligned} \tag{3.6}$$

As shown in Eq. (3.6), Z_{PAM} consists of three terms:

1. $Z_{PAM}^{(0)}$ is the desired term contributed by the 0^{th} user.

$$Z_{PAM}^{(0)} = \int_0^{T_r} s_{PAM}^{(0)}(t) \sum_{n=0}^{N_r-1} a_n^0 z(t - nT_c) dt = b_0^0 \sqrt{P_0} N_r \tag{3.7}$$

2. I_{PAM} is the MAI from the $K-1$ interfering users.

$$I_{PAM} = \sum_{k=1}^{K-1} \underbrace{\int_0^{T_r} s_{PAM}^{(k)}(t-\tau_k) \sum_{n=0}^{N_r-1} a_n^0 z(t - nT_c) dt}_{I_{PAM}^{(k)}} \tag{3.8}$$

where $I_{PAM}^{(k)}$ is the interference from the k^{th} interfering user.

$$\begin{aligned} I_{PAM}^{(k)} &= b_{-1}^k \sqrt{P_k} \int_0^{\tau_k} \sum_{m=0}^{N_r-1} a_m^k z(t + T_r - mT_c - \tau_k) \sum_{n=0}^{N_r-1} a_n^0 z(t - nT_c) dt \\ &\quad + b_0^k \sqrt{P_k} \int_{\tau_k}^{T_r} \sum_{m=0}^{N_r-1} a_m^k z(t - mT_c - \tau_k) \sum_{n=0}^{N_r-1} a_n^0 z(t - nT_c) dt \end{aligned} \tag{3.9}$$

3. N_{PAM} is the AWGN term, which follows Gaussian distribution with zero mean and variance of $\sigma^2_{N_{PAM}} = N_0 N_r/2$.

3.3.2 Characteristic Function Analysis

The MAI from the k^{th} user, $I^{(k)}_{PAM}$, is rewritten as below

$$I^{(k)}_{PAM} = \sqrt{P_k} R_{PAM}(\Delta T_k) X_k + \sqrt{P_k} \hat{R}_{PAM}(\Delta T_k) Y_k \tag{3.10}$$

where we introduce following ancillary definitions.

1. The asynchronous delay τ_k can be split into two parts: the integer multiple of T_c and the remaining part ΔT_k.

$$\tau_k = \gamma_k T_c + \Delta T_k \tag{3.11}$$

where $\gamma_k \in \{0, 1, \cdots, N_r - 1\}$ and $\Delta T_k \in [0, T_c)$, both with uniform distribution in their respective domains.

2. $R_{PAM}(\Delta T_k)$ and $\hat{R}_{PAM}(\Delta T_k)$ are defined as the autocorrelation functions of $z(t)$. Generally the UWB monocycle $z(t)$ is a symmetrical waveform, and $R_{PAM}(\Delta T_k) = \hat{R}_{PAM}(T_c - \Delta T_k)$.

$$\begin{aligned} R_{PAM}(\Delta T_k) &= \int_0^{\Delta T_k} z(t) z(t + T_c - \Delta T_k) dt \\ \hat{R}_{PAM}(\Delta T_k) &= \int_{\Delta T_k}^{T_c} z(t) z(t - \Delta T_k) dt \end{aligned} \tag{3.12}$$

3. X_k and Y_k are defined as follows. It is easy to prove that X_k and Y_k are two independent and identical Binomial random variables due to the random property of b^k_i and a^k_n.

$$\begin{aligned} X_k &= b^k_{-1} \sum_{n=0}^{\gamma_k} a^0_n a^k_{n+N_r-\gamma_k-1} + b^k_0 \sum_{n=\gamma_k+1}^{N_r-1} a^0_n a^k_{n-\gamma_k-1} \\ Y_k &= b^k_{-1} \sum_{n=0}^{\gamma_k-1} a^0_n a^k_{n+N_r-\gamma_k} + b^k_0 \sum_{n=\gamma_k}^{N_r-1} a^0_n a^k_{n-\gamma_k} \end{aligned} \tag{3.13}$$

The distribution of X_k and Y_k is given as

$$P(x) = \begin{pmatrix} N_r \\ \frac{x+N_r}{2} \end{pmatrix} \frac{1}{2^{N_r}} \tag{3.14}$$

where the range of x (or X_k, Y_k) is $\{-N_r, -N_r+2, \cdots, N_r-2, N_r\}$.

The characteristic function of $I_{PAM}^{(k)}$ is derived using Eq. (3.10). When ΔT_k is given, the values of $R_{PAM}(\Delta T_k)$ and $\hat{R}_{PAM}(\Delta T_k)$ are fixed accordingly. Therefore the two terms in Eq. (3.10), $\sqrt{P_k}R_{PAM}(\Delta T_k)X_k$ and $\sqrt{P_k}\hat{R}_{PAM}(\Delta T_k)Y_k$, become two statistically independent random variables. The characteristic function of $\sqrt{P_k}R_{PAM}(\Delta T_k)X_k$ conditioned on ΔT_k is $\left[\cos\left(\omega\sqrt{P_k}R_{PAM}(\Delta T_k)\right)\right]^{N_r}$. Similarly, the characteristic function of $\sqrt{P_k}\hat{R}_{PAM}(\Delta T_k)Y_k$ conditioned on ΔT_k is given by $\left[\cos\left(\omega\sqrt{P_k}\hat{R}_{PAM}(\Delta T_k)\right)\right]^{N_r}$.

Because of the conditional independence between $\sqrt{P_k}R_{PAM}(\Delta T_k)X_k$ and $\sqrt{P_k}\hat{R}_{PAM}(\Delta T_k)Y_k$, the conditional characteristic function of $I_{PAM}^{(k)}$ is in the form of a product as below.

$$\Phi_{I_{PAM}^{(k)}|\Delta T_k}(\omega) = \left[\cos\left(\omega\sqrt{P_k}R_{PAM}(\Delta T_k)\right)\cos\left(\omega\sqrt{P_k}\hat{R}_{PAM}(\Delta T_k)\right)\right]^{N_r} \tag{3.15}$$

Then the conditional PDF of $I_{PAM}^{(k)}$ is obtained by taking an inverse Fourier transform of $\Phi_{I_{PAM}^{(k)}|\Delta T_k}(\omega)$.

$$p_{I_{PAM}^{(k)}|\Delta T_k}(x) = \frac{1}{2\pi}\int_{-\infty}^{\infty}\Phi_{I_{PAM}^{(k)}|\Delta T_k}(\omega)\exp(-j\omega x)d\omega \tag{3.16}$$

The unconditional PDF of $I_{PAM}^{(k)}$ is derived by averaging $p_{I_{PAM}^{(k)}|\Delta T_k}(x)$ on the distribution of ΔT_k.

$$p_{I_{PAM}^{(k)}}(x) = \frac{1}{T_c}\int_0^{T_c} p_{I_{PAM}^{(k)}|\Delta T_k}(x)d\Delta T_k \tag{3.17}$$

Again, we use a Fourier transform to get the unconditional characteristic function of $I_{PAM}^{(k)}$.

$$\Phi_{I_{PAM}^{(k)}}(\omega) = \int_{-\infty}^{\infty} p_{I_{PAM}^{(k)}}(x)\exp(j\omega x)dx$$

$$= \int_{-\infty}^{\infty} \left(\frac{1}{T_c} \int_0^{T_c} p_{I_{PAM}^{(k)}|\Delta T_k}(x) d\Delta T_k \right) \exp(j\omega x) dx \tag{3.18}$$
$$= \frac{1}{T_c} \int_0^{T_c} \left[\cos\left(\omega \sqrt{P_k} R_{PAM}(\Delta T_k) \right) \cos\left(\omega \sqrt{P_k} \hat{R}_{PAM}(\Delta T_k) \right) \right]^{N_r} d\Delta T_k$$

Since the $K-1$ interfering users are mutually independent, the characteristic function of I_{PAM} is expressed as below according to Eq. (3.8).

$$\Phi_{I_{PAM}}(\omega) = \prod_{k=1}^{K-1} \Phi_{I_{PAM}^{(k)}}(\omega) \tag{3.19}$$

As in Eq. (3.6), set the total noise as $\varsigma_{PAM} = I_{PAM} + N_{PAM}$. And the characteristic function of ς_{PAM} is expressed as

$$\Phi_{\varsigma_{PAM}}(\omega) = \Phi_{I_{PAM}}(\omega) \Phi_{N_{PAM}}(\omega) \tag{3.20}$$

where $\Phi_{I_{PAM}}(\omega)$ is given by Eq. (3.19) and $\Phi_{N_{PAM}} = \exp\left(-\frac{N_0 N_r \omega^2}{4} \right)$.

3.4 Characteristic Function Analysis of DS PPM UWB System

3.4.1 Decision Statistics

We still assume the 0^{th} user is the desired user and consider the detection of the 0^{th} symbol. Under the assumption of perfect synchronization for the desired user, i.e., $\tau_0 = 0$ in Eq. (3.3), the correlation receiver computes the decision statistic as below

$$\begin{aligned} Z_{PPM} &= \int_0^{T_r} r_{PPM}(t) v_{PPM}^{(0)}(t) dt \\ &= \underbrace{\int_0^{T_r} s_{PPM}^{(0)}(t) v_{PPM}^{(0)}(t) dt}_{Z_{PPM}^{(0)}} + \underbrace{\sum_{k=1}^{K-1} \int_0^{T_r} s_{PPM}^{(k)}(t-\tau_k) v_{PPM}^{(0)}(t) dt}_{I_{PPM}} \\ &\quad + \underbrace{\int_0^{T_r} n(t) v_{PPM}^{(0)}(t) dt}_{N_{PPM}} \end{aligned} \tag{3.21}$$

As shown in Eq. (3.21), the decision statistic Z_{PPM} includes three terms:

1. $Z_{PPM}^{(0)}$ is the desired term from the 0^{th} user.

$$Z_{PPM}^{(0)} = \int_0^{T_r} s_{PPM}^{(0)}(t) \sum_{n=0}^{N_r-1} a_n^0 q(t - nT_c)dt = (1 - 2b_0^0)\sqrt{P_0}N_r \quad (3.22)$$

2. I_{PPM} is the MAI contributed by the $K-1$ interfering users.

$$I_{PPM} = \sum_{k=1}^{K-1} \underbrace{\int_0^{T_r} s_{PPM}^{(k)}(t - \tau_k) \sum_{n=0}^{N_r-1} a_n^0 q(t - nT_c)dt}_{I_{PPM}^{(k)}} \quad (3.23)$$

where $I_{PPM}^{(k)}$ is the contribution from the k^{th} interfering user.

$$\begin{aligned} I_{PPM}^{(k)} = \sqrt{P_k} \int_0^{\tau_k} \sum_{m=0}^{N_r-1} a_m^k z(t+T_r-\tau_k-mT_c-b_{-1}^k T_p) \sum_{n=0}^{N_r-1} a_n^0 q(t - nT_c)dt \\ +\sqrt{P_k} \int_{\tau_k}^{T_r} \sum_{m=0}^{N_r-1} a_m^k z(t-\tau_k-mT_c-b_0^k \tau) \sum_{n=0}^{N_r-1} a_n^0 q(t - nT_c)dt \end{aligned} \quad (3.24)$$

3. N_{PPM} is the AWGN term, which follows Gaussian distribution with zero mean and variance of $\sigma_{N_{PPM}}^2 = N_0 N_r$.

3.4.2 Characteristic Function Analysis

The MAI from the k^{th} user, $I_{PPM}^{(k)}$, is rewritten as

$$I_{PPM}^{(k)} = \sqrt{P_k}\,(A_k B_k + C_k D_k) \quad (3.25)$$

where we introduce following ancillary definitions.

1. A_k and C_k are defined as

$$\begin{aligned} A_k &= \sum_{n=0}^{\gamma_k-1} a_n^0 a_{n+N_r-\gamma_k}^k \\ C_k &= \sum_{n=\gamma_k}^{N_r-1} a_n^0 a_{n-\gamma_k}^k \end{aligned} \quad (3.26)$$

If γ_k is given, A_k and C_k are statistically independent due to the random property of a_n^k. It is easy to show that both A_k and C_k are Binomial random variables. The conditional distribution of A_k and C_k are given by

$$p_{A_k|\gamma_k}(x) = \begin{pmatrix} \gamma_k \\ \frac{x+\gamma_k}{2} \end{pmatrix} \frac{1}{2^{\gamma_k}} \tag{3.27}$$

where $x \in \{-\gamma_k, -\gamma_k + 2, \cdots, \gamma_k - 2, \gamma_k\}$. And

$$p_{C_k|\gamma_k}(x) = \begin{pmatrix} N_r - \gamma_k \\ \frac{x+N_r-\gamma_k}{2} \end{pmatrix} \frac{1}{2^{N_r-\gamma_k}} \tag{3.28}$$

where $x \in \{-(N_r - \gamma_k), -(N_r - \gamma_k) + 2, \cdots, N_r - \gamma_k - 2, N_r - \gamma_k\}$.

2. The asynchronous delay τ_k is split into two parts: the integer multiple of T_c and the remaining part ΔT_k.

$$\tau_k = \gamma_k T_c + \Delta T_k \tag{3.29}$$

where $\gamma_k \in \{0, 1, \cdots, N_r - 1\}$ and $\Delta T_k \in [0, T_c)$, both with uniform distribution in their respective domains.

3. We define the cross correlation functions of $z(t)$ and $q(t)$ as $R_{PPM}(x)$, where $x = \Delta T_k + b_i^k T_p$.

$$R_{PPM}(x) = \begin{cases} \int_0^{T_c} q(t)z(t-x)dt & x \in [0, 2T_p) \\ \int_0^{T_c} q(t)z(t-x+T_c)dt & x \in [3T_p, 5T_p) \\ 0 & \text{elsewhere} \end{cases} \tag{3.30}$$

4. B_k and D_k are defined as

$$\begin{aligned} B_k &= R_{PPM}(\Delta T_k + b_{-1}^k T_p) \\ D_k &= R_{PPM}(\Delta T_k + b_0^k T_p) \end{aligned} \tag{3.31}$$

If ΔT_k is given, B_k and D_k are identical and independent distributed random variables because of the random property of b_i^k.

When τ_k is given, ΔT_k and γ_k are fixed and A_k, B_k, C_k and D_k are four independent random variables. Hence the PDF of $I_{PPM}^{(k)}$ conditioned on τ_k can be obtained using existing formulae of product and sum of independent random variables as below.

$$p_{I_{PPM}^{(k)}|\tau_k}(x)=\frac{1}{2^{N_r+2}}\sum_{n=0}^{\gamma_k}\begin{pmatrix}\gamma_k\\ n\end{pmatrix}\begin{pmatrix}\delta\left(x-(2n-\gamma_k)\sqrt{P_k}R_{PPM}(\Delta T_k+T_p)\right)\\ +\delta\left(x-(2n-\gamma_k)\sqrt{P_k}R_{PPM}(\Delta T_k)\right)\end{pmatrix}$$
$$*\sum_{n=0}^{N_r-\gamma_k}\begin{pmatrix}N_r-\gamma_k\\ n\end{pmatrix}\begin{pmatrix}\delta\left(x-(2n-N_r+\gamma_k)\sqrt{P_k}R_{PPM}(\Delta T_k+T_p)\right)\\ +\delta\left(x-(2n-N_r+\gamma_k)\sqrt{P_k}R_{PPM}(\Delta T_k)\right)\end{pmatrix}$$

where $\delta(\cdot)$ is the Dirac Delta function and the operator $*$ denotes convolution.

The unconditional PDF of $I_{PPM}^{(k)}$ is obtained by averaging $p_{I_{PPM}^{(k)}|\tau_k}(x)$ over the distribution of τ_k as below.

$$p_{I_{PPM}^{(k)}}(x)=\int_0^{T_c}\frac{1}{N_rT_c}\sum_{\gamma_k=0}^{N_r-1}p_{I_{PPM}^{(k)}|\tau_k}(x)d\Delta T_k \tag{3.32}$$

The characteristic function of $I_{PPM}^{(k)}$ is given by

$$\Phi_{I_{PPM}^{(k)}}(\omega)=\int_{-\infty}^{\infty}p_{I_{PPM}^{(k)}}(x)\exp(j\omega x)dx \tag{3.33}$$

Since all users are independently transmitting data symbols, the characteristic function of I_{PPM} is expressed as

$$\Phi_{I_{PPM}}(\omega)=\prod_{k=1}^{K-1}\Phi_{I_{PPM}^{(k)}}(\omega) \tag{3.34}$$

We set the total noise in Eq. (3.21) as $\varsigma_{PPM}=I_{PPM}+N_{PPM}$. The characteristic function of ς_{PPM} is given by the following product

$$\Phi_{\varsigma_{PPM}}(\omega)=\Phi_{I_{PPM}}(\omega)\Phi_{N_{PPM}}(\omega) \tag{3.35}$$

where $\Phi_{N_{PPM}}(\omega)=\exp\left(-\frac{N_0N_r\omega^2}{2}\right)$.

3.5 BER Formula

In previous sections, the characteristic function of the total noise $\varsigma_{PAM/PPM}$ is derived. The PDF of $\varsigma_{PAM/PPM}$ is obtained by taking an inverse Fourier transform on Eq. (3.20) and Eq. (3.35).

$$p_{\varsigma_{PAM/PPM}}(x) = \frac{1}{2\pi}\int_{-\infty}^{\infty} \Phi_{\varsigma_{PAM/PPM}}(\omega)\exp(-j\omega x)d\omega \tag{3.36}$$

The decision rule for the DS UWB system using binary PAM/PPM is expressed as

$$\begin{cases} Z_{PAM/PPM} > 0 \Rightarrow b_0^0 = 1/0 \\ Z_{PAM/PPM} \leq 0 \Rightarrow b_0^0 = -1/1 \end{cases} \tag{3.37}$$

According to the decision rule, the BER P_e is given by the following PDF tail integral.

$$\begin{aligned} P_e &= \frac{1}{2}\text{Prob}(Z_{PAM/PPM} \leq 0 | b_0^0 = 1/0) + \frac{1}{2}\text{Prob}(Z_{PAM/PPM} > 0 | b_0^0 = -1/1) \\ &= \text{Prob}\left(\varsigma_{PAM/PPM} \geq N_r\sqrt{P_0}\right) \\ &= \frac{1}{2}\left(1 - \int_{-N_r\sqrt{P_0}}^{N_r\sqrt{P_0}} \underbrace{\frac{1}{2\pi}\int_{-\infty}^{\infty} \Phi_{\varsigma_{PAM/PPM}}(\omega)\exp(-j\omega x)d\omega}_{\text{PDF of } \varsigma_{PAM/PPM}} dx\right) \\ &= \frac{1}{2} - \frac{1}{\pi}\int_0^{\infty} \Phi_{\varsigma_{PAM/PPM}}(\omega)\frac{\sin\left(\sqrt{P_0}N_r\omega\right)}{\omega}d\omega \end{aligned} \tag{3.38}$$

3.6 BER Derivation Using the GA Method

For the sake of completeness and comparison, we briefly explain the BER derivation using the GA method in this section. The GA method is based on the assumption that the total noise $\varsigma_{PAM/PPM}$ follows Gaussian distribution. Since both the MAI and AWGN are with zero mean and mutually independent, the

variance of $\varsigma_{PAM/PPM}$ is given by

$$\begin{aligned}\sigma^2_{\varsigma_{PAM/PPM}} &= \sigma^2_{I_{PAM/PPM}} + \sigma^2_{N_{PAM/PPM}} \\ &= \sum_{k=1}^{K-1} \sigma^2_{I^{(k)}_{PAM/PPM}} + \sigma^2_{N_{PAM/PPM}} \end{aligned} \tag{3.39}$$

The variance of $I^{(k)}_{PAM}$ and $I^{(k)}_{PPM}$ is derived as

$$\begin{aligned}\sigma^2_{I^{(k)}_{PAM}} &= \mathrm{E}\left[\left(I^{(k)}_{PAM}\right)^2\right] \\ &= \frac{P_k N_r}{T_c}\int_0^{T_c}\left(R^2_{PAM}(\Delta T_k) + \hat{R}^2_{PAM}(\Delta T_k)\right) d\Delta T_k \\ &= \frac{2P_k N_r}{T_c}\int_0^{T_c} R^2_{PAM}(\Delta T_k)\, d\Delta T_k \end{aligned} \tag{3.40}$$

$$\begin{aligned}\sigma^2_{I^{(k)}_{PPM}} &= \mathrm{E}\left[\left(I^{(k)}_{PPM}\right)^2\right] \\ &= \frac{P_k N_r}{2T_c}\int_0^{T_c}\left(R^2_{PPM}(\Delta T_k) + R^2_{PPM}(\Delta T_k + T_p)\right) d\Delta T_k \\ &= \frac{P_k N_r}{T_c}\int_0^{T_c} R^2_{PPM}(\Delta T_k)\, d\Delta T_k \end{aligned} \tag{3.41}$$

The BER is evaluated using the following formula.

$$P_e = \frac{1}{2}\mathrm{erfc}\left(\frac{\sqrt{P_0}N_r}{\sqrt{2\sigma^2_{\varsigma_{PAM/PPM}}}}\right) \tag{3.42}$$

3.7 Numerical Results

In this section, the BER performance of the DS UWB systems with PAM and PPM is evaluated using both the CF method and the GA method. The simulation results are also provided for comparison.

The analysis in this chapter is applicable for any UWB monocycle waveform. In the numerical study, we choose a commonly used Gaussian monocycle $z(t)$ with following expression.

$$z(t) = A\exp\left(-0.5\left(\frac{t}{\sigma} - 3.5\right)^2\right) \tag{3.43}$$

The parameter settings in the DS PAM UWB and the DS PPM UWB systems are listed in Table 3.1.

Table 3.1: The system parameters used in numerical study

System Parameters	PAM	PPM
Monocycle amplitude A	6.2875×10^4	1.25687×10^5
Monocycle duration T_p (ns)	1	0.25
Time scale parameter σ (ns)	0.14286	0.035714
Length of DS signature N_r	10	10
Chip duration T_c (ns)	1	1
Symbol duration T_r (ns)	10	10

The autocorrelation function of $z(t)$ defined in Eq. (3.12), $\hat{R}_{PAM}(x)$, has a closed form as in Eq. (3.44).

$$\hat{R}_{PAM}(x) = \frac{T_c\sqrt{\pi}A^2}{56} \exp\left(-\left(\frac{x}{2\sigma}\right)^2\right) \operatorname{erfc}\left(\sqrt{2}\left(\frac{x}{\sigma} - 3.5\right) - \frac{x}{\sqrt{2}\sigma}\right) \quad (3.44)$$

In Fig. 3.1, the autocorrelation functions $R_{PAM}(x)$ and $\hat{R}_{PAM}(x)$ are plotted. The cross correlation function of $z(t)$ and $q(t)$ defined in Eq. (3.30), $R_{PPM}(x)$, is plotted in Fig. 3.2.

We consider two cases in the numerical analysis of the DS PAM UWB and the DS PPM UWB systems.

1. The first case is for those systems with small number of users under perfect power control. We set the number of users $K = 2$ and $P_0 = P_1$. The theoretical BER curves obtained using the CF method are plotted in solid line in Fig. 3.3 and Fig. 3.4 for the DS PAM UWB and the DS PPM UWB systems respectively. And the simulation results are marked by circles in both figures. It is observed that the theoretical curves generated by the

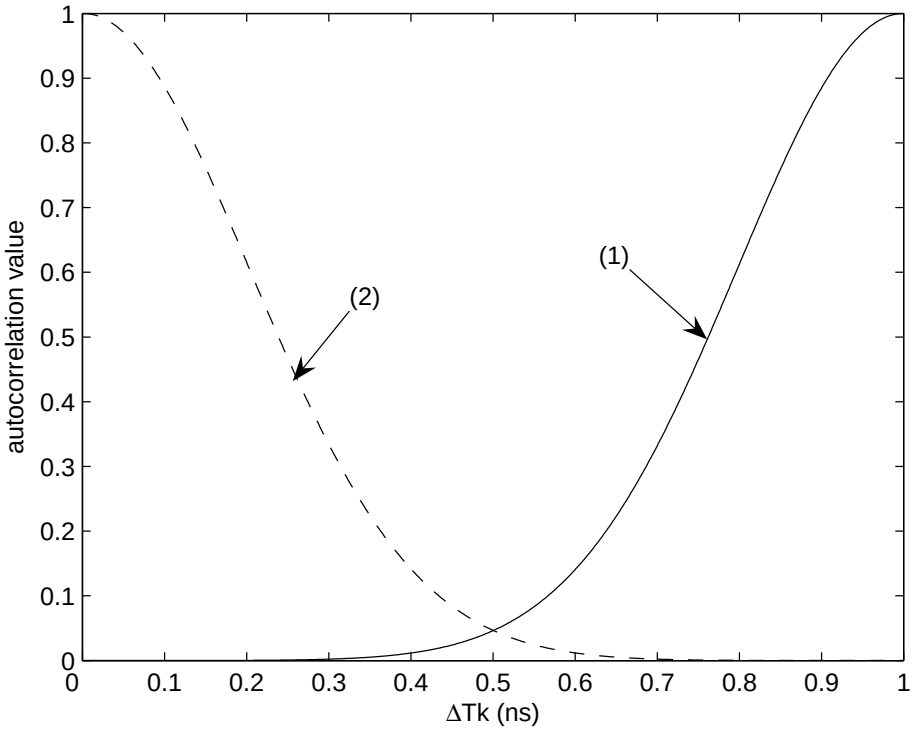

Figure 3.1: The autocorrelation functions of $z(t)$: (1) is $R_{PAM}(\Delta T_k)$, (2) is $\hat{R}_{PAM}(\Delta T_k)$.

CF method and the simulation results are in excellent agreement. The GA theoretical curves (dashed line) are also provided for comparison in these two figures. For the DS PAM UWB system, the theoretical curve obtained by the GA method matches the simulation result well in low SNR range (E_b^0/N_0 from 0 to 4dB). However, the GA method is not accurate for BER evaluation in medium and high SNR range (E_b^0/N_0 from 6dB and above). Similarly, for the DS PPM UWB system, the theoretical curve generated by the GA method matches the simulation result well only in low SNR range (E_b^0/N_0 from 0 to 8dB) and two curves deviate from each other in medium and high SNR range (E_b^0/N_0 from 10dB and above). In the high SNR range

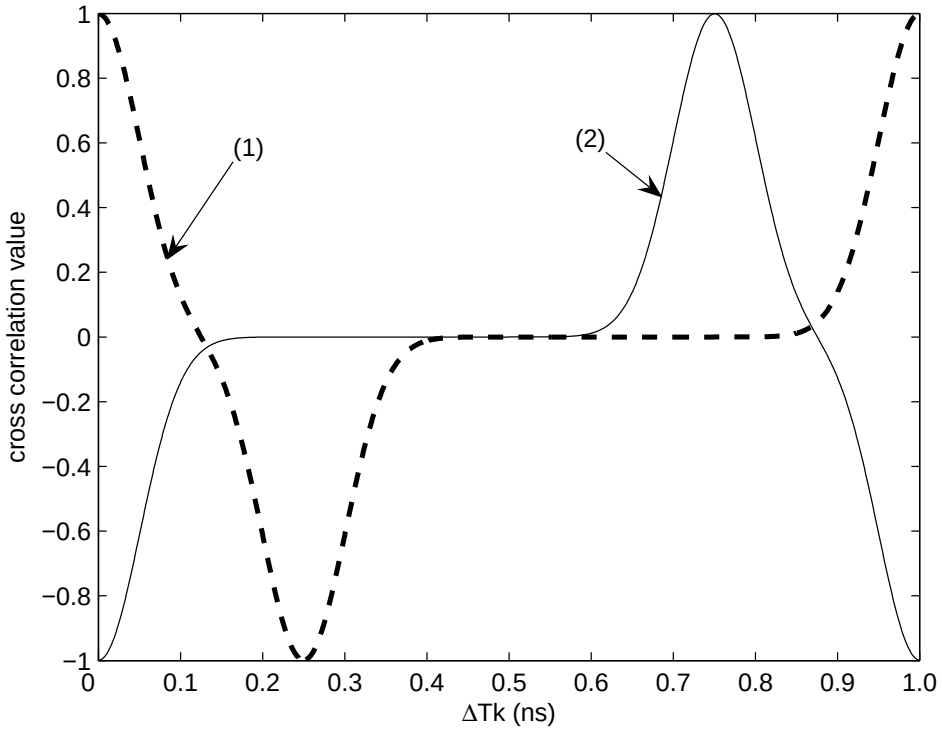

Figure 3.2: The cross correlation functions of $z(t)$ and $q(t)$: (1) is $R_{PPM}(\Delta T_k)$, (2) is $R_{PPM}(\Delta T_k + T_p)$.

(E_b^0/N_0 from 16 to 20dB), the BER results calculated by the GA method are too optimistic to show the error floor caused by the MAI.

2. The second case is for those systems under imperfect power control. There are more than one interfering users in the system, where some user dominates the total MAI value. We consider a system of three users, i.e., $K = 3$. The 0^{th} user is the desired user and the 1^{th} and 2^{th} users are the interfering users. We further assume that the 0^{th} user and the 1^{th} user have the same power, i.e., $P_0 = P_1$, while the 2^{th} user has a much higher power of $P_2 = 5P_0 = 5P_1$. Therefore the 2^{th} user gives major contribution to the MAI. In Fig. 3.5 and Fig. 3.6, the theoretical BER curves evaluated by

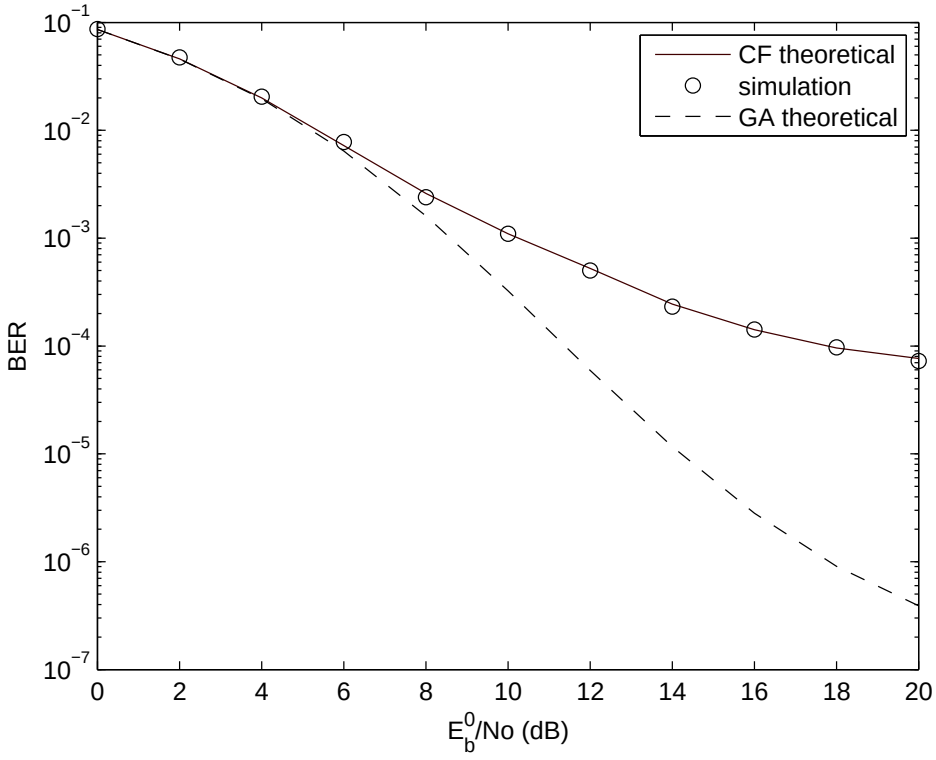

Figure 3.3: The BER performance of the DS PAM UWB system under perfect power control ($P_0 = P_1$), number of users is $K = 2$.

the CF method are plotted in solid line for the DS PAM UWB and the DS PPM UWB systems respectively. It is observed that the simulation results (circle marked) agree well with the theoretical curves generated by the CF method. On the other hand, the theoretical curves obtained by the GA method (dashed line) are not so accurate for high SNR values (E_b^0/N_0 from 8dB and above). Since the MAI is more severe than that in the first case, the overall BER performance gets worse.

In both cases studied in this section, the CF method outperforms the GA method in BER evaluation because the exact PDF of the total noise is used in the BER evaluation. In contrast, the MAI is approximated as a Gaussian random

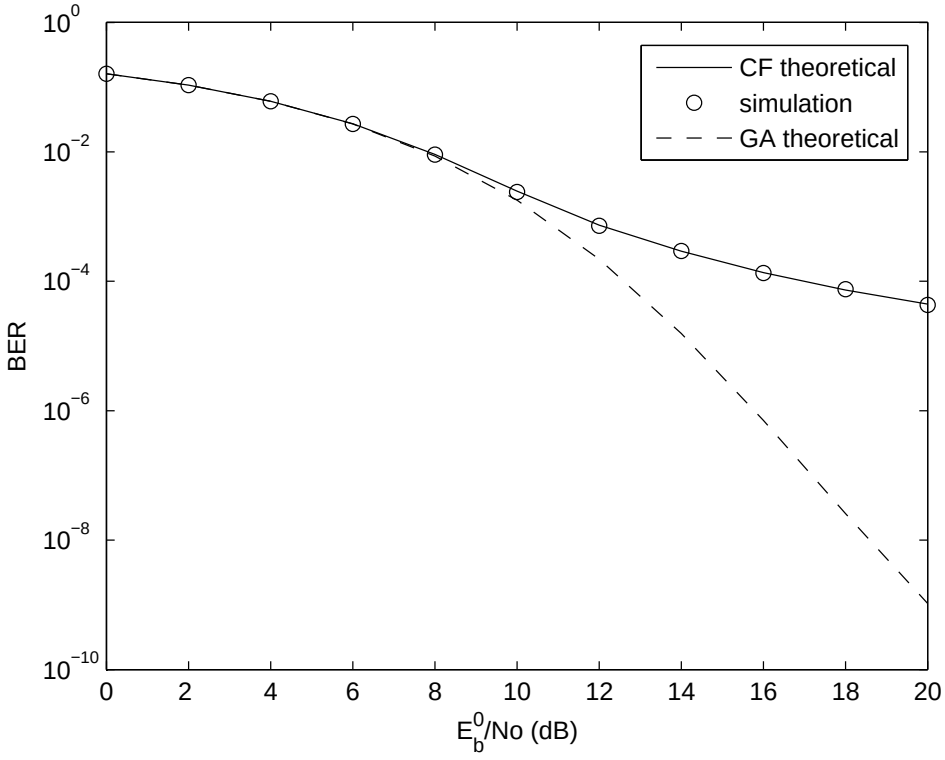

Figure 3.4: The BER performance of the DS PPM UWB system under perfect power control ($P_0 = P_1$), number of users is $K = 2$.

variable in the GA method. When the SNR value is small, the AWGN term $N_{PAM/PPM}$ dominates the total noise $\varsigma_{PAM/PPM}$. As a result, $\varsigma_{PAM/PPM}$ can be approximated as Gaussian distributed. However, in the medium or high SNR range, the dominant component in the total noise $\varsigma_{PAM/PPM}$ becomes the MAI $I_{PAM/PPM}$. Since the MAI in the UWB systems generally does not follow the Gaussian distribution [8][9], the GA method does not work well in the medium and high SNR range accordingly.

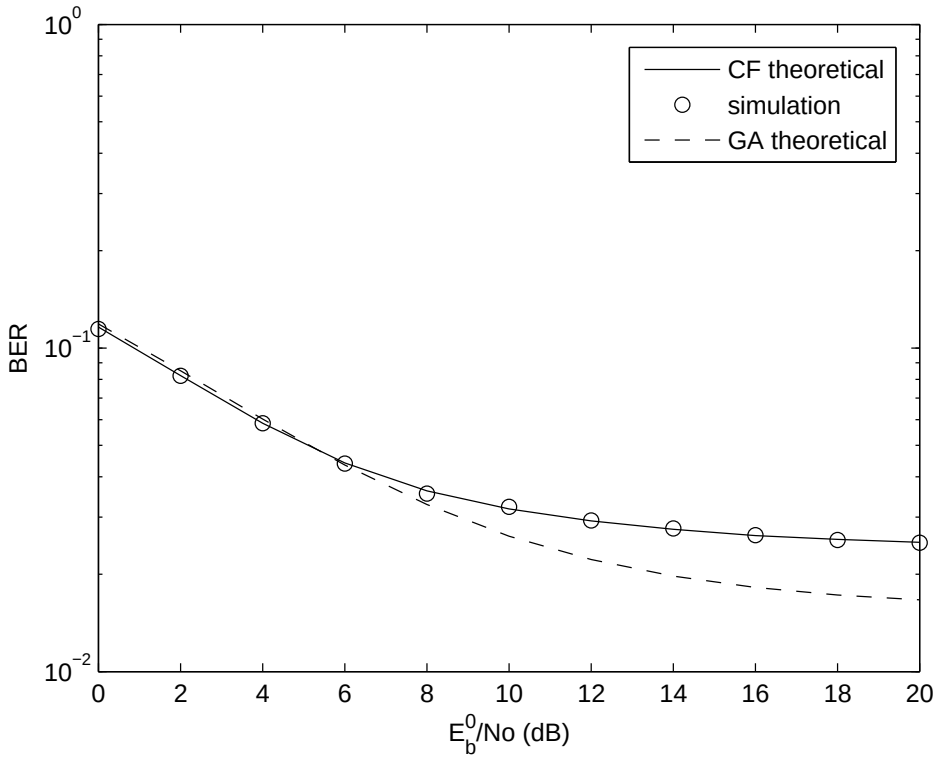

Figure 3.5: The BER performance of the DS PAM UWB system under imperfect power control ($P_2 = 5P_0 = 5P_1$), number of users is $K = 3$.

3.8 Conclusions

In this chapter, we propose a novel BER evaluation method based on the characteristic function for the DS PAM/PPM UWB multiple access systems under both perfect and imperfect power control. Instead of approximating the total noise (including MAI and AWGN) as a Gaussian random variable, we consider the exact PDF of the total noise. Then the accurate BER formula is derived based on the characteristic function of the total noise. The numerical analysis is carried out on two cases to compare the accuracy of the CF method and the GA method. It should be noted that the indoor UWB applications are limited to a short range of about 4 to 10 meters so that the number of users could

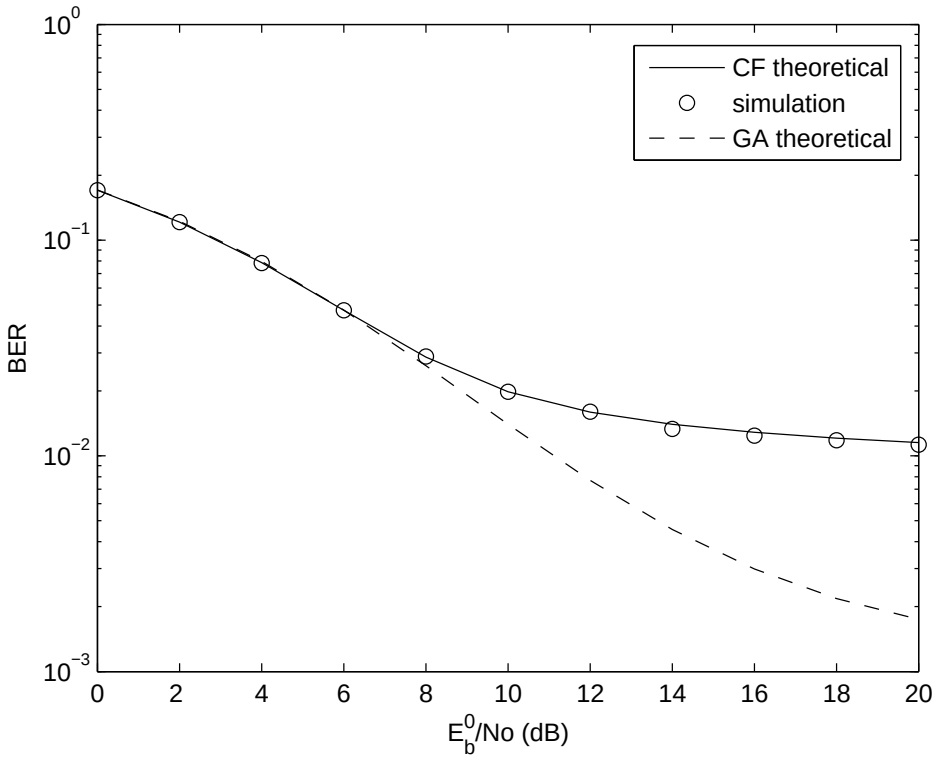

Figure 3.6: The BER performance of the DS PPM UWB system under imperfect power control ($P_2 = 5P_0 = 5P_1$), number of users is $K = 3$.

be small. In addition, non-centralized topology can be used in UWB networks, where it is relatively difficult to achieve perfect power control. Therefore we choose one case with small number of users and the other case with imperfect power control in our numerical study. The analytical and simulation results show that the CF method computes the BER value exactly in both cases. In contrast, the theoretical results obtained by the GA method do not match well with the simulation results in medium and large SNR range. The inaccuracy of the GA method is interpreted using the dominant component of the total noise.

Chapter 4

Exact BER Analysis and Comparison of DS PAM UWB and DS PPM UWB systems in Lognormal Multipath Fading Channels

In this chapter, we present the exact BER analysis using the CF method for DS PAM/PPM UWB multiple access systems in lognormal multipath fading channels. In the Section 4.1, we introduce previous works on performance analysis of various UWB systems in multipath fading channels. The system and channel models adopted in this chapter are described in Section 4.2. The characteristic function analysis for DS PAM UWB and DS PPM UWB systems is presented in Section 4.3 and Section 4.4 respectively. In Section 4.5, the BER formula is derived based on the characteristic functions. For the sake of completeness and comparison, BER evaluation using the GA method is briefly presented in Section 4.6. In Section 4.7, numerical results are provided to validate our derivations.

The DS PAM UWB and DS PPM UWB systems are accurately compared. Then explanations based on the characteristic functions give further interpretation on our findings. Finally, conclusions are drawn in Section 4.8.

4.1 Introduction

In Chapter 3, we have presented the exact BER evaluation of DS UWB PAM/PPM systems in AWGN channels. Here we will extend our study to a more practical channel model for UWB indoor communications: the lognormal multipath fading channels [54][23].

Theoretical computation of BER for various UWB systems in multipath fading channels has been discussed in some literature. Most of the earlier works focus on single user scenario. Performance of various modulation schemes is studied in [73][74][52]. The M-ary PAM UWB signal is investigated in [73]. Based on the same data rate, it is found that a larger M leads to a lower error floor due to the reduced ISI. This finding is consistent with the results in the TH M-ary PPM UWB systems [69]. The UWB systems using TH PAM, TH PPM and DS PAM are compared in [74], and the results show that the DS PAM UWB system yields the best overall performance. A more complex modulation scheme, the hybrid pulse amplitude and position modulation [52], is proven to be able to provide higher data rate than PAM and PPM. Different UWB receiver structures and their performance is another extensively studied topic. It is shown that employing more Rake fingers can improve the BER performance by capture more energy [13][34]. However, the tradeoff between performance and complexity is a crucial problem in practical receiver design.

Later the performance of multiple access UWB systems was reported in some other literature. In order to combat the effect of MAI in the UWB systems,

various signaling formats have been studied, including episodic transmission [19], PPM with optimized time shift [20] and advanced source coding [75]. In [19], an episodic transmission scheme (where off-time separation is inserted between UWB monocycles) is proposed for the DS UWB systems, whose performance approaches the performance of ideal time division multiple access (TDMA) system in very low data rate settings. The DS UWB systems using the optimally spaced PPM and the orthogonal PPM signal schemes are compared in [20], and the optimally spaced PPM outperforms the orthogonal PPM with a much lower error floor. A near optimal low rate convolution code is applied in the TH UWB systems [75]. The coded system is proven to have higher order of diversity, which is a function of the Hamming distance of the codes. Besides the effect of MAI, the impact of narrow band interference (NBI) [21][76] also arouses some academic interest. Though research in [21] and [76] is on the DS UWB and TH UWB systems respectively, similar conclusions are drawn: Both the DS and TH spreading can not effectively suppress the NBI. Therefore NBI suppression should be taken into consideration in receiver design.

In the works mentioned above, the BER performance analysis can be grouped into two categories. One is based on various bounds on BER, which provides an approximation of the exact BER performance [68][19][75]. The other is to assume the interference as Gaussian distributed and use the well-known GA method [34][73][74][20][21].

As shown in Chapter 3, the GA method is simple to apply in AWGN channels but the resultant BER expression (a closed form of erfc function) is not accurate. Similarly, validity of the GA method should be considered carefully in multipath fading channels, especially in near-far scenarios [19]. Furthermore, only the conditional BER can be obtained by the GA method in multipath fading channels. And numerical averaging on the channel fading parameters (so-called

semi-analytical/simulation approach) is needed to assist the GA method to obtain the average BER. Thus the GA method losses its main advantages: simplicity and closed form formula.

So far, the CF method has been used for exact BER analysis of UWB systems in AWGN channels only [71][77][78], which shows the power of the CF method and verifies that the GA method is not so suitable for BER evaluation of UWB systems. In this chapter, we apply the CF method to derive exact BER formula of DS PAM/PPM UWB multiple access systems in lognormal multipath fading channels. The accurate BER expressions can be used to provide useful performance evaluation of various UWB applications. Simulation results show that BER obtained by the CF method is more accurate than the GA method in large SNR range. Performance of the DS PAM UWB and DS PPM UWB systems is accurately compared for different length of spreading sequence. Furthermore, we plot the characteristic functions to provide explanation for the BER results.

4.2 System and Channel Models

4.2.1 Signal Format

The DS PAM UWB and the DS PPM UWB signals are given by the following expressions

$$\begin{aligned} s_{PAM}^{(k)}(t) &= \sqrt{P}\sum_{i=-\infty}^{\infty} b_i^k \sum_{n=0}^{N_r-1} a_n^k z(t - iT_r - nT_c) \\ s_{PPM}^{(k)}(t) &= \sqrt{P}\sum_{i=-\infty}^{\infty} \sum_{n=0}^{N_r-1} a_n^k z(t - 2iT_r - nT_c - b_i^k T_p) \end{aligned} \tag{4.1}$$

where k is the index of user, i is the index of symbol and $z(t)$ represents the energy normalized UWB monocycle with duration of T_p. Other parameters used here are explained as follows.

1. $\{a_n^k\}_{n=0}^{N_r-1}$ is the DS signature assigned to the k^{th} user. Random DS sequence is assumed, i.e., for every n and k, $a_n^k \in \{\pm 1\}$ with equal probability.

2. $\{b_i^k\}_{i=-\infty}^{\infty}$ represents the data symbol sequence of the k^{th} user. $b_i^k \in \{\pm 1\}$ in the DS binary PAM UWB system, while $b_i^k \in \{0, 1\}$ in the DS binary PPM UWB system. In both systems, b_i^k takes two possible values with equal probability.

3. N_r is the number of chips in one symbol. In each chip, there is one and only one UWB monocycle.

4. P is the transmitted signal power of each user. The energy of one transmitted symbol is $E_b = PN_r$. It should be noted that the received signal power from different users will be different (imperfect power control at receiver side) because of the fading channels.

5. T_c is the chip duration and T_r is the symbol duration, i.e., $T_r = N_r T_c$.

6. The time shift associated with PPM is T_p in the orthogonal binary PPM signal set, which equals to the duration of the UWB monocycle $z(t)$. Furthermore, we set $T_p = T_c/4$ so that the time shift associated with PPM is smaller than the chip duration.

7. In the DS PPM UWB system, a guarding interval T_r is inserted to avoid ISI, and T_r is assumed to be greater than the maximal delay spread of the channel.

4.2.2 Channel Model

The channel impulse response of the k^{th} user is modeled as

$$h^{(k)}(t) = \sum_{l=0}^{L-1} \alpha_{k,l} \delta(t - lT_c) \tag{4.2}$$

where L denotes the number of multipaths, $\alpha_{k,l} = \theta_{k,l}\beta_{k,l}$ is the path gain, $\theta_{k,l} \in \{\pm 1\}$ represents the random phase due to reflection, $\beta_{k,l}$ is the lognormal fading amplitude. For different k and l, $\alpha_{k,l}$ are independent random variables. In the practical UWB channels, the multipath delay (continuous random variable) may cause inter-pulse interference (IPI) and influence the system performance. However, one study [79] has shown that the optimum minimum mean-square error (MMSE) receiver with IPI considered performs exactly the same as the Rake MRC receiver with IPI ignored, which implies the effect of IPI is negligible. Therefore we can safely model the multipath channel using a tapped delay line (TDL) with tapped delay of T_c. The power delay profile of the channel is exponential decaying. Since the transmitter and receiver are slowly time-varying in most WPAN applications [54], we assume the channel remains invariant over a block of symbols.

4.2.3 Received Signal

The received signal $r_{PAM/PPM}(t)$ in a multiple access environment with K asynchronous users is given by

$$r_{PAM/PPM}(t) = \sum_{k=0}^{K-1} \sum_{l=0}^{L-1} \alpha_{k,l} s^{(k)}_{PAM/PPM}(t - \tau_k - lT_c) + n(t) \tag{4.3}$$

where τ_k is the transmission delay of the k^{th} user uniformly distributed over $[0, T_r)$, $n(t)$ is the AWGN with double sided PSD of $N_0/2$.

The template waveform used in the correlation receiver (or the Selection Rake receiver with one finger) of the k^{th} user are given as follows. The energy on the 0^{th} path is captured and $\alpha_{k,0}$ is assumed to be known at the k^{th} receiver.

$$\begin{aligned} v^{(k)}_{PAM}(t) &= \alpha_{k,0} \sum_{n=0}^{N_r-1} a^k_n z(t - nT_c) \\ v^{(k)}_{PPM}(t) &= \alpha_{k,0} \sum_{n=0}^{N_r-1} a^k_n q(t - nT_c) \end{aligned} \tag{4.4}$$

where $q(t) = z(t) - z(t - T_p)$ is the template waveform for the orthogonal binary PPM signal set in one chip.

4.3 Characteristic Function Analysis of DS PAM UWB System

4.3.1 Decision Statistics

We choose the 0^{th} user as the desired user and assume perfect synchronization, i.e. $\tau_0 = 0$ in Eq. (4.3). The output decision statistic Z_{PAM} is given by

$$\begin{aligned} Z_{PAM} &= \int_0^{T_r} r_{PAM}(t) v_{PAM}^{(0)}(t) dt \\ &= \underbrace{\int_0^{T_r} \alpha_{0,0} s_{PAM}^{(0)}(t) v_{PAM}^{(0)}(t) dt}_{Z_{PAM}^{(0)}} \\ &\quad + \underbrace{\int_0^{T_r} \sum_{l=1}^{L-1} \alpha_{0,l} s_{PAM}^{(0)}(t - lT_c) v_{PAM}^{(0)}(t) dt}_{I_{PAM}} \\ &\quad + \underbrace{\int_0^{T_r} \sum_{k=1}^{K-1} \sum_{l=0}^{L-1} \alpha_{k,l} s_{PAM}^{(k)}(t - \tau_k - lT_c) v_{PAM}^{(0)}(t) dt}_{M_{PAM}} \\ &\quad + \underbrace{\int_0^{T_r} n(t) v_{PAM}^{(0)}(t) dt}_{N_{PAM}} \end{aligned} \tag{4.5}$$

where $Z_{PAM}^{(0)}$ is the desired signal, I_{PAM} is the self interference (SI) caused by the multipath, M_{PAM} is the MAI and N_{PAM} is the AWGN term.

A. Desired Signal

The desired signal $Z_{PAM}^{(0)}$ is the contribution from the 0^{th} path of the 0^{th} user.

$$Z_{PAM}^{(0)} = \int_0^{T_r} \alpha_{0,0} s_{PAM}^{(0)}(t) \alpha_{0,0} \sum_{n=0}^{N_r-1} a_n^0 z(t - nT_c) dt = \alpha_{0,0}^2 b_0^0 \sqrt{P} N_r \tag{4.6}$$

B. Multiple Access Interference

The MAI term M_{PAM} is the summation of signals from other $K-1$ interfering users. If we regard every path of an interfering user as an interfering source, then MAI is the summation of $(K-1) \times L$ terms.

$$M_{PAM} = \sum_{k=1}^{K-1} \sum_{l=0}^{L-1} \underbrace{\int_0^{T_r} \alpha_{k,l} s_{PAM}^{(k)}(t - \tau_k - lT_c) \alpha_{0,0} \sum_{n=0}^{N_r-1} a_n^0 z(t - nT_c) dt}_{M_{PAM}^{(k,l)}} \tag{4.7}$$

The contribution of the l^{th} path of the k^{th} user, $M_{PAM}^{(k,l)}$, is modeled as

$$\begin{aligned} M_{PAM}^{(k,l)} &= \int_0^{T_r} \alpha_{k,l} s_{PAM}^{(k)}(t - \tau_k - lT_c) \alpha_{0,0} \sum_{n=0}^{N_r-1} a_n^0 z(t - nT_c) dt \\ &= \alpha_{0,0} \alpha_{k,l} \sqrt{P} \left[R_{PAM}(\Delta T_k) X_{PAM}^{(k,l)} + \hat{R}_{PAM}(\Delta T_k) Y_{PAM}^{(k,l)} \right] \end{aligned} \tag{4.8}$$

where we introduce following ancillary definitions.

1. τ_k, the asynchronous transmission delay, can be split into two parts: the integer multiple of T_c and the remaining part ΔT_k.

$$\tau_k = \gamma_k T_c + \Delta T_k \tag{4.9}$$

   where $\gamma_k \in \{0, 1, \cdots, N_r - 1\}$ and $\Delta T_k \in [0, T_c)$, both with uniform distribution in their respective domains.

2. $R_{PAM}(\Delta T_k)$ and $\hat{R}_{PAM}(\Delta T_k)$ are defined as the autocorrelation functions of $z(t)$. Generally $z(t)$ is symmetrical and $R_{PAM}(\Delta T_k) = \hat{R}_{PAM}(T_c - \Delta T_k)$.

$$\begin{aligned} R_{PAM}(\Delta T_k) &= \int_0^{\Delta T_k} z(t) z(t + T_c - \Delta T_k) dt \\ \hat{R}_{PAM}(\Delta T_k) &= \int_{\Delta T_k}^{T_c} z(t) z(t - \Delta T_k) dt \end{aligned} \tag{4.10}$$

3. $X_{PAM}^{(k,l)}$ and $Y_{PAM}^{(k,l)}$ are defined as follows.

$$\begin{aligned} X_{PAM}^{(k,l)} &= b_{-1}^k \sum_{n=0}^{\gamma_k+l} a_n^0 a_{n+N_r-\gamma_k-l-1}^k + b_0^k \sum_{n=\gamma_k+l+1}^{N_r-1} a_n^0 a_{n-\gamma_k-l-1}^k \\ Y_{PAM}^{(k,l)} &= b_{-1}^k \sum_{n=0}^{\gamma_k+l-1} a_n^0 a_{n+N_r-\gamma_k-l}^k + b_0^k \sum_{n=\gamma_k+l}^{N_r-1} a_n^0 a_{n-\gamma_k-l}^k \end{aligned} \tag{4.11}$$

It is easy to prove that for different k and l, all $X_{PAM}^{(k,l)}$, $Y_{PAM}^{(k,l)}$ are independent and identical Binomial random variables due to the random property of b_i^k and a_n^k. The distribution of $X_{PAM}^{(k,l)}$ and $Y_{PAM}^{(k,l)}$ is given by

$$P(x) = \begin{pmatrix} N_r \\ \frac{x+N_r}{2} \end{pmatrix} \frac{1}{2^{N_r}} \tag{4.12}$$

where the range of x (or $X_{PAM}^{(k,l)}$, $Y_{PAM}^{(k,l)}$) is $\{-N_r, -N_r+2, \cdots, N_r-2, N_r\}$.

Using Eq. (4.8), the interference from the k^{th} user, $M_{PAM}^{(k)}$, is given by

$$\begin{aligned} M_{PAM}^{(k)} &= \sum_{l=0}^{L-1} M_{PAM}^{(k,l)} \\ &= \alpha_{0,0}\sqrt{P}\left[R_{PAM}(\Delta T_k)\sum_{l=0}^{L-1}\alpha_{k,l}X_{PAM}^{(k,l)} + \hat{R}_{PAM}(\Delta T_k)\sum_{l=0}^{L-1}\alpha_{k,l}Y_{PAM}^{(k,l)}\right] \end{aligned} \tag{4.13}$$

At least one of $R_{PAM}(\Delta T_k)$ and $\hat{R}_{PAM}(\Delta T_k)$ is zero for any $\Delta T_k \in [0, T_c)$ under the assumption of $T_p = T_c/4$. Therefore Eq. (4.13) is rewritten as piecewise functions, which helps to simplify the numerical calculation.

$$M_{PAM}^{(k)} = \begin{cases} \alpha_{0,0}\sqrt{P}R_{PAM}(\Delta T_k)\sum\limits_{l=0}^{L-1}\alpha_{k,l}X_{PAM}^{(k,l)} & \Delta T_k \in [3T_p, T_c) \\ \alpha_{0,0}\sqrt{P}\hat{R}_{PAM}(\Delta T_k)\sum\limits_{l=0}^{L-1}\alpha_{k,l}Y_{PAM}^{(k,l)} & \Delta T_k \in [0, T_p) \\ 0 & \text{elsewhere} \end{cases} \tag{4.14}$$

C. Self Interference

The self interference from the l^{th} path is modeled as

$$I_{PAM}^{(l)} = \int_0^{T_r} \alpha_{0,l} s_{PAM}^{(0)}(t - lT_c)\alpha_{0,0} \sum_{n=0}^{N_r-1} a_n^0 z(t - nT_c)dt$$

$$
\begin{aligned}
&= \alpha_{0,0}\alpha_{0,l}\sqrt{P}[R_{PAM}(0)X_{PAM}^{(0,l)} + \hat{R}_{PAM}(0)Y_{PAM}^{(0,l)}] \\
&= \alpha_{0,0}\alpha_{0,l}\sqrt{P}Y_{PAM}^{(0,l)} \qquad (4.15)
\end{aligned}
$$

The self interference I_{PAM} is given by

$$
I_{PAM} = \sum_{l=1}^{L-1} I_{PAM}^{(l)} = \alpha_{0,0}\sqrt{P}\sum_{l=1}^{L-1}\alpha_{0,l}Y_{PAM}^{(0,l)} \qquad (4.16)
$$

D. AWGN

The AWGN term N_{PAM} in Eq. (4.5) is expressed as

$$
N_{PAM} = \int_0^{T_r} n(t)\alpha_{0,0}\sum_{n=0}^{N_r-1} a_n^0 z(t-nT_c)dt \qquad (4.17)
$$

E. Decision Variables

The channel gain $\alpha_{0,0}$ is a common factor of $Z_{PAM}^{(0)}$, M_{PAM}, I_{PAM} and N_{PAM}. Here a series of auxiliary variables is defined by removing $\alpha_{0,0}$.

$$
\begin{aligned}
\hat{Z}_{PAM}^{(0)} &= \alpha_{0,0}b_0^0\sqrt{P}N_r \\
\hat{M}_{PAM}^{(k)} &= \sum_{l=0}^{L-1}\hat{M}_{PAM}^{(k,l)} = \sum_{l=0}^{L-1}\alpha_{k,l}\sqrt{P}\left[R_{PAM}(\Delta T_k)X_{PAM}^{(k,l)} + \hat{R}_{PAM}(\Delta T_k)Y_{PAM}^{(k,l)}\right] \\
\hat{M}_{PAM} &= \sum_{k=1}^{K-1}\hat{M}_{PAM}^{(k)} \\
\hat{I}_{PAM} &= \sum_{l=1}^{L-1}\hat{I}_{PAM}^{(l)} = \sqrt{P}\sum_{l=1}^{L-1}\alpha_{0,l}Y_{PAM}^{(0,l)} \\
\hat{N}_{PAM} &= \int_0^{T_r} n(t)\sum_{n=0}^{N_r-1} a_n^0 z(t-nT_c)dt \qquad (4.18)
\end{aligned}
$$

Recall that the channel fading gain $\alpha_{k,l} = \theta_{k,l}\beta_{k,l}$. It is easy to show that the distribution of $\alpha_{k,l}X_{PAM}^{(k,l)}$ and $\beta_{k,l}X_{PAM}^{(k,l)}$ are the same. Therefore the equivalent formulae Eq. (4.19a) and Eq. (4.19b) stand from the view point of statistical property. In the following analysis, we will use the equivalent formulae Eq.

(4.19a) and Eq. (4.19b).

$$\hat{M}_{PAM}^{(k)}=\sum_{l=0}^{L-1}\hat{M}_{PAM}^{(k,l)}=\sum_{l=0}^{L-1}\beta_{k,l}\sqrt{P}\left[R_{PAM}(\Delta T_k)X_{PAM}^{(k,l)}+\hat{R}_{PAM}(\Delta T_k)Y_{PAM}^{(k,l)}\right] \quad (4.19a)$$

$$\hat{I}_{PAM}=\sum_{l=1}^{L-1}\hat{I}_{PAM}^{(l)}=\sqrt{P}\sum_{l=1}^{L-1}\beta_{0,l}Y_{PAM}^{(0,l)} \quad (4.19b)$$

The decision statistic Z_{PAM} is rewritten as

$$Z_{PAM}=\alpha_{0,0}(\hat{Z}_{PAM}^{(0)}+\hat{M}_{PAM}+\hat{I}_{PAM}+\hat{N}_{PAM}) \quad (4.20)$$

4.3.2 Characteristic Function Analysis

A. CF of MAI

It is observed from Eq. (4.19a) that $\hat{M}_{PAM}^{(k)}$ is the summation of signals from L paths of the k^{th} user, where ΔT_k is a common factor. For a given ΔT_k, the values of $R_{PAM}(\Delta T_k)$ and $\hat{R}_{PAM}(\Delta T_k)$ are fixed, and the L terms in the summation become statistically independent. Let the characteristic function of $\hat{M}_{PAM}^{(k,l)}$ conditioned on ΔT_k and $\beta_{k,l}$ be $\Phi_{\hat{M}_{PAM}^{(k,l)}|\Delta T_k,\beta_{k,l}}(\omega)$.

$$\Phi_{\hat{M}_{PAM}^{(k,l)}|\Delta T_k,\beta_{k,l}}(\omega)=\left[\cos\left(\sqrt{P}R_{PAM}(\Delta T_k)\beta_{k,l}\omega\right)\cos\left(\sqrt{P}\hat{R}_{PAM}(\Delta T_k)\beta_{k,l}\omega\right)\right]^{N_r} \quad (4.21)$$

The characteristic function of $\hat{M}_{PAM}^{(k)}$ is given by

$$\Phi_{\hat{M}_{PAM}^{(k)}}(\omega)=\int_0^{Tc}\frac{1}{T_c}\left[\prod_{l=0}^{L-1}\int_0^{\infty}\Phi_{\hat{M}_{PAM}^{(k,l)}|\Delta T_k,\beta_{k,l}}(\omega)p_{\beta_{k,l}}(\beta_{k,l})d\beta_{k,l}\right]d\Delta T_k \quad (4.22)$$

where $p_{\beta_{k,l}}(\beta_{k,l})$ is the PDF of the channel fading amplitude $\beta_{k,l}$.

Since all the interfering users are mutually independent, the characteristic function of the MAI is a product of $\Phi_{\hat{M}_{PAM}^{(k)}}(\omega)$.

$$\Phi_{\hat{M}_{PAM}}(\omega)=\prod_{k=1}^{K-1}\Phi_{\hat{M}_{PAM}^{(k)}}(\omega) \quad (4.23)$$

B. CF of Self Interference

The self interference $\hat{I}_{PAM}$ is the summation of $L-1$ independent terms as shown in Eq. (4.19b). The characteristic function of $\hat{I}_{PAM}^{(l)}$ is given by

$$\Phi_{\hat{I}_{PAM}^{(l)}}(\omega) = \int_0^\infty \left[\cos(\sqrt{P}\beta_{0,l}\omega)\right]^{N_r} p_{\beta_{0,l}}(\beta_{0,l})d\beta_{0,l} \tag{4.24}$$

The characteristic function of $\hat{I}_{PAM}$ is the product of $\Phi_{\hat{I}_{PAM}^{(l)}}(\omega)$.

$$\Phi_{\hat{I}_{PAM}}(\omega) = \prod_{l=1}^{L-1} \Phi_{\hat{I}_{PAM}^{(l)}}(\omega) \tag{4.25}$$

C. CF of AWGN

The AWGN term $\hat{N}_{PAM}$ follows a Gaussian distribution with zero mean and variance of $N_0N_r/2$. Its characteristic function $\Phi_{\hat{N}_{PAM}}$ is given by

$$\Phi_{\hat{N}_{PAM}}(\omega) = \exp(-\frac{N_0N_r\omega^2}{4}) \tag{4.26}$$

D. CF of Total Noise

The total noise is defined as $\hat{\varsigma}_{PAM} = \hat{M}_{PAM} + \hat{I}_{PAM} + \hat{N}_{PAM}$. From the definitions in Eq. (4.18), it is found that $\hat{M}_{PAM}$, $\hat{I}_{PAM}$ and $\hat{N}_{PAM}$ are statistically independent random variables. The characteristic function of the total noise is calculated as

$$\Phi_{\hat{\varsigma}_{PAM}}(\omega) = \Phi_{\hat{M}_{PAM}}(\omega)\Phi_{\hat{I}_{PAM}}(\omega)\Phi_{\hat{N}_{PAM}}(\omega) \tag{4.27}$$

4.4 Characteristic Function Analysis of DS PPM UWB System

4.4.1 Decision Statistics

The characteristic function analysis of DS PPM UWB system is carried out similarly in this section. In detection of the 0^{th} symbol of the 0^{th} user, the output decision statistic Z_{PPM} is given by

$$\begin{aligned} Z_{PPM} &= \int_0^{T_r} r_{PPM}(t) v_{PPM}^{(0)}(t) dt \\ &= \underbrace{\int_0^{T_r} \alpha_{0,0} s_{PPM}^{(0)}(t) v_{PPM}^{(0)}(t) dt}_{Z_{PPM}^{(0)}} \\ &\quad + \underbrace{\int_0^{T_r} \sum_{l=1}^{L-1} \alpha_{0,l} s_{PPM}^{(0)}(t - lT_c) v_{PPM}^{(0)}(t) dt}_{I_{PPM}} \\ &\quad + \underbrace{\int_0^{T_r} \sum_{k=1}^{K-1} \sum_{l=0}^{L-1} \alpha_{k,l} s_{PPM}^{(k)}(t - \tau_k - lT_c) v_{PPM}^{(0)}(t) dt}_{M_{PPM}} \\ &\quad + \underbrace{\int_0^{T_r} n(t) v_{PPM}^{(0)}(t) dt}_{N_{PPM}} \end{aligned} \tag{4.28}$$

where $Z_{PPM}^{(0)}$ represents the desired signal, I_{PPM} is the SI due to the multipath propagation, M_{PPM} stands for MAI, and N_{PPM} is the contribution of AWGN. Though Z_{PPM} shares the similar format with Z_{PAM}, the different modulation scheme leads to different statistical property.

A. Desired Signal

The desired signal $Z_{PPM}^{(0)}$ is given by

$$Z_{PPM}^{(0)} = \int_0^{T_r} \alpha_{0,0} s_{PPM}^{(0)}(t) \alpha_{0,0} \sum_{n=0}^{N_r-1} a_n^0 q(t - T_c) dt = \alpha_{0,0}^2 (1 - 2b_0^0) \sqrt{P} N_r \tag{4.29}$$

B. Multiple Access Interference

The MAI term M_{PPM} is given by

$$M_{PPM} = \sum_{k=1}^{K-1} \sum_{l=0}^{L-1} \underbrace{\int_0^{T_r} \alpha_{k,l} s_{PPM}^{(k)}(t - \tau_k - lT_c)\alpha_{0,0} \sum_{n=0}^{N_r-1} a_n^0 q(t - T_c)dt}_{M_{PPM}^{(k,l)}} \quad (4.30)$$

where $M_{PPM}^{(k,l)}$ is the interference from the l^{th} path of the k^{th} user. $M_{PPM}^{(k,l)}$ is given by Eq. (4.31a) and Eq. (4.31b) for $\tau_{k,l} < T_r$ and $\tau_{k,l} \geq T_r$ respectively.

$$M_{PPM}^{(k,l)} = \int_{\tau_{k,l}}^{T_r} \alpha_{k,l}\sqrt{P} \sum_{n=0}^{N_r-1} a_n^k z(t - \tau_{k,l} - nT_c - b_0^k T_p) v_{PPM}^{(0)}(t)dt \quad (4.31a)$$

$$M_{PPM}^{(k,l)} = \int_0^{\tau_{k,l}-T_r} \alpha_{k,l}\sqrt{P} \sum_{n=0}^{N_r-1} a_n^k z(t - \tau_{k,l} + 2T_r - nT_c - b_{-1}^k T_p) v_{PPM}^{(0)}(t)dt \quad (4.31b)$$

To simplify $M_{PPM}^{(k,l)}$, following auxiliary definitions are introduced.

1. The asynchronous transmission delay τ_k is split as the summation of an integer multiple of T_c and a remaining part ΔT_k.

$$\tau_k = \gamma_k T_c + \Delta T_k \quad (4.32)$$

where $\gamma_k \in \{0, 1, \cdots, N_r - 1\}$ and $\Delta T_k \in [0, T_c)$, both with uniform distribution in their respective domains.

2. $R_{PPM}(\Delta T_k, b_i^k)$ and $\hat{R}_{PPM}(\Delta T_k, b_i^k)$ are the cross correlation functions of $z(t)$ and $q(t)$. They are related with b_i^k, which may bring additional shift of the UWB monocycles.

$$\begin{aligned} R_{PPM}(\Delta T_k, b_i^k) &= \int_0^{\Delta T_k} q(t) z(t + T_c - \Delta T_k - b_i^k T_p)dt \\ \hat{R}_{PPM}(\Delta T_k, b_i^k) &= \int_{\Delta T_k}^{T_c} q(t) z(t - \Delta T_k - b_i^k T_p)dt \end{aligned} \quad (4.33)$$

For any given value of ΔT_k, at least one of $R_{PPM}(\Delta T_k, b_i^k)$ and $\hat{R}_{PPM}(\Delta T_k, b_i^k)$ is zero. This property can be used to simplify the numerical computation.

3. $X_{PPM}(x)$ is defined as a Binomial random variable to represent the partial cross correlation of the spreading sequences of the desired user and the interfering user.

$$X_{PPM}(x) = \begin{cases} \sum_{n=1}^{x} c_n & x > 0 \\ 0 & \text{else} \end{cases} \tag{4.34}$$

where c_n takes value in $\{\pm 1\}$ with equal probability. In the analysis of the DS PAM UWB system, there are two random variables, $X_{PAM}^{(k,l)}$ and $Y_{PAM}^{(k,l)}$, defined in a similar way. The partial cross correlation of the spread sequences of the desired user and the interfering user can be regarded as summation of independent Bernoulli random variables because of the random property of a_n^k. The distribution of $X_{PPM}(x)$ is determined by x, which is the number of independent Bernoulli random variables in the summation.

With the help of these auxiliary definitions, $M_{PPM}^{(k,l)}$ is rewritten as Eq. (4.35a) and Eq. (4.35b) for $\tau_{k,l} < T_r$ and $\tau_{k,l} \geq T_r$ respectively.

$$\begin{aligned} M_{PPM}^{(k,l)} &= \alpha_{0,0}\alpha_{k,l}\sqrt{P}\Big[X_{PPM}(N_r - 1 - \gamma_k - l)R_{PPM}(\Delta T_k, b_0^k) \\ &\qquad + X_{PPM}(N_r - \gamma_k - l)\hat{R}_{PPM}(\Delta T_k, b_0^k)\Big] \end{aligned} \tag{4.35a}$$

$$\begin{aligned} M_{PPM}^{(k,l)} &= \alpha_{0,0}\alpha_{k,l}\sqrt{P}\Big[X_{PPM}(\gamma_k + l - N_r + 1)R_{PPM}(\Delta T_k, b_{-1}^k) \\ &\qquad + X_{PPM}(\gamma_k + l - N_r)\hat{R}_{PPM}(\Delta T_k, b_{-1}^k)\Big] \end{aligned} \tag{4.35b}$$

The interference from the k^{th} user, $M_{PPM}^{(k)}$, is the summation of $M_{PPM}^{(k,l)}$. It is expressed by Eq. (4.36a) and Eq. (4.36b) for $\tau_{k,L-1} < T_r$ and $\tau_{k,L-1} \geq T_r$ respectively.

$$\begin{aligned} M_{PPM}^{(k)} = \alpha_{0,0}\sqrt{P}\Big[&\sum_{l=0}^{L-1} \alpha_{k,l} X_{PPM}(N_r - 1 - \gamma_k - l)R_{PPM}(\Delta T_k, b_0^k) \\ &+ \sum_{l=0}^{L-1} \alpha_{k,l} X_{PPM}(N_r - \gamma_k - l)\hat{R}_{PPM}(\Delta T_k, b_0^k)\Big] \end{aligned} \tag{4.36a}$$

$$M_{PPM}^{(k)} = \alpha_{0,0}\sqrt{P}\Bigg[\sum_{l=0}^{N_r-\gamma_k-1} \alpha_{k,l} X_{PPM}(N_r-1-\gamma_k-l) R_{PPM}(\Delta T_k, b_0^k) + \sum_{l=0}^{N_r-\gamma_k-1} \alpha_{k,l} X_{PPM}(N_r-\gamma_k-l) \hat{R}_{PPM}(\Delta T_k, b_0^k) + \sum_{l=N_r-\gamma_k}^{L-1} \alpha_{k,l} X_{PPM}(\gamma_k+l-N_r+1) R_{PPM}(\Delta T_k, b_{-1}^k) + \sum_{l=N_r-\gamma_k}^{L-1} \alpha_{k,l} X_{PPM}(\gamma_k+l-N_r) \hat{R}_{PPM}(\Delta T_k, b_{-1}^k) \Bigg] \quad (4.36b)$$

C. Self Interference

The ISI does not exist due to the guarding interval T_r. And the SI contains only the current symbol b_0^0. The SI from the l^{th} path, $I_{PPM}^{(l)}$, is modeled as

$$I_{PPM}^{(l)} = \alpha_{0,0}\alpha_{0,l}\sqrt{P} \int_{lT_c}^{T_r} \sum_{m=0}^{N_r-1} a_m^0 z(t - lT_c - mT_c) \sum_{n=0}^{N_r-1} a_n^0 q(t - nT_c) dt \quad (4.37)$$

$I_{PPM}^{(l)}$ has a similar format with $M_{PPM}^{(k,l)}$ in Eq. (4.31a), where $\tau_{0,l} < T_r$. Hence $I_{PPM}^{(l)}$ is rewritten as below.

$$\begin{aligned} I_{PPM}^{(l)} &= \alpha_{0,0}\alpha_{0,l}\sqrt{P} X_{PPM}(N_r - l) \hat{R}(0, b_0^0) \\ &= \alpha_{0,0}\alpha_{0,l}(1 - 2b_0^0)\sqrt{P} X_{PPM}(N_r - l) \end{aligned} \quad (4.38)$$

Then I_{PPM} is given by

$$I_{PPM} = \sum_{l=1}^{L-1} I_{PPM}^{(l)} = \alpha_{0,0}\sqrt{P}(1 - 2b_0^0) \sum_{l=1}^{L-1} \alpha_{0,l} X_{PPM}(N_r - l) \quad (4.39)$$

D. AWGN

The AWGN term N_{PPM} is given by

$$N_{PPM} = \alpha_{0,0} \int_0^{T_r} n(t) \sum_{n=0}^{N_r-1} a_n^0 q(t - nT_c) dt \quad (4.40)$$

E. Decision Variables

Similar as the case in the DS PAM UWB system, $Z_{PPM}^{(0)}$, M_{PPM}, I_{PPM} and N_{PPM} contain a common factor $\alpha_{0,0}$ brought by the template waveform $v_{PPM}^{(0)}(t)$. Following decision variables are introduced by removing $\alpha_{0,0}$. Furthermore, we substitute $\beta_{k,l}X_{PPM}(x)$ for $\alpha_{k,l}X_{PPM}(x)$ as an equivalent random variable.

$$\begin{aligned}
\hat{Z}_{PPM}^{(0)} &= \alpha_{0,0}(1-2b_0^0)\sqrt{P}N_r \\
\hat{M}_{PPM}^{(k,l)} &= \begin{cases} \beta_{k,l}\sqrt{P}\Big[X_{PPM}(N_r-1-\gamma_k-l)R_{PPM}(\Delta T_k, b_0^k) \\ \qquad +X_{PPM}(N_r-\gamma_k-l)\hat{R}_{PPM}(\Delta T_k, b_0^k)\Big] & \text{if} \quad \tau_{k,l} < T_r \\ \beta_{k,l}\sqrt{P}\Big[X_{PPM}(\gamma_k+l-N_r+1)R_{PPM}(\Delta T_k, b_{-1}^k) \\ \qquad +X_{PPM}(\gamma_k+l-N_r)\hat{R}_{PPM}(\Delta T_k, b_{-1}^k)\Big] & \text{if} \quad \tau_{k,l} \geq T_r \end{cases} \\
\hat{M}_{PPM} &= \sum_{k=1}^{K-1}\hat{M}_{PPM}^{(k)} = \sum_{k=1}^{K-1}\sum_{l=0}^{L-1}\hat{M}_{PPM}^{(k,l)} \\
\hat{I}_{PPM} &= \sum_{l=1}^{L-1}\hat{I}_{PPM}^{(l)} = \sqrt{P}(1-2b_0^0)\sum_{l=1}^{L-1}\beta_{0,l}X_{PPM}(N_r-l) \\
\hat{N}_{PPM} &= \int_0^{T_r} n(t)\sum_{n=0}^{N_r-1}a_n^0 q(t-nT_c)dt
\end{aligned} \tag{4.41}$$

The decision statistic Z_{PPM} is rewritten as

$$Z_{PPM} = \alpha_{0,0}(\hat{Z}_{PPM}^{(0)} + \hat{M}_{PPM} + \hat{I}_{PPM} + \hat{N}_{PPM}) \tag{4.42}$$

4.4.2 Characteristic Function Analysis

A. CF of MAI

For given γ_k, ΔT_k, b_{-1}^k and b_0^k, the characteristic function of $\hat{M}_{PPM}^{(k,l)}$ is given by Eq. (4.43a) and Eq. (4.43b) for $\tau_{k,l} < T_r$ and $\tau_{k,l} \geq T_r$ respectively.

$$\begin{aligned}
\Phi_{\hat{M}_{PPM}^{(k,l)}|\gamma_k,\Delta T_k,b_{-1}^k,b_0^k}(\omega) &= \int_0^{\infty}\Big[\cos\Big(\beta_{k,l}\sqrt{P}R_{PPM}(\Delta T_k, b_0^k)\omega\Big)\Big]^{N_r-1-\gamma_k-l} \\
&\quad \cdot\Big[\cos\Big(\beta_{k,l}\sqrt{P}\hat{R}_{PPM}(\Delta T_k, b_0^k)\omega\Big)\Big]^{N_r-\gamma_k-l}
\end{aligned}$$

$$\cdot p_{\beta_{k,l}}(\beta_{k,l})d\beta_{k,l} \tag{4.43a}$$

$$\Phi_{\hat{M}_{PPM}^{(k,l)}|\gamma_k,\Delta T_k,b_{-1}^k,b_0^k}(\omega) = \int_0^\infty \left[\cos\left(\beta_{k,l}\sqrt{P}R_{PPM}(\Delta T_k, b_{-1}^k)\omega\right)\right]^{\gamma_k+l-N_r+1} \cdot \left[\cos\left(\beta_{k,l}\sqrt{P}\hat{R}_{PPM}(\Delta T_k, b_{-1}^k)\omega\right)\right]^{\gamma_k+l-N_r} \cdot p_{\beta_{k,l}}(\beta_{k,l})d\beta_{k,l} \tag{4.43b}$$

For different l, $\hat{M}_{PPM}^{(k,l)}$ conditioned on γ_k, ΔT_k, b_{-1}^k and b_0^k are independent. Thus the characteristic function of $\hat{M}_{PPM}^{(k)}$ is expressed in a product form.

$$\Phi_{\hat{M}_{PPM}^{(k)}|\gamma_k,\Delta T_k,b_{-1}^k,b_0^k}(\omega) = \prod_{l=0}^{L-1} \Phi_{\hat{M}_{PPM}^{(k,l)}|\gamma_k,\Delta T_k,b_{-1}^k,b_0^k}(\omega) \tag{4.44}$$

The unconditional characteristic function is obtained by averaging over the distributions of all conditional variables.

$$\Phi_{\hat{M}_{PPM}^{(k)}}(\omega) = \frac{1}{4N_rT_c}\sum_{\gamma_k=0}^{N_r-1}\int_0^{T_c}\Big[\Phi_{\hat{M}_{PPM}^{(k)}|\gamma_k,\Delta T_k,0,0}(\omega)+\Phi_{\hat{M}_{PPM}^{(k)}|\gamma_k,\Delta T_k,0,1}(\omega) +\Phi_{\hat{M}_{PPM}^{(k)}|\gamma_k,\Delta T_k,1,0}(\omega)+\Phi_{\hat{M}_{PPM}^{(k)}|\gamma_k,\Delta T_k,1,1}(\omega)\Big]d\Delta T_k \tag{4.45}$$

Since the $K-1$ interfering users are transmitting data independently, the characteristic function of $\hat{M}_{PPM}$ is in the following product form.

$$\Phi_{\hat{M}_{PPM}}(\omega) = \prod_{k=1}^{K-1} \Phi_{\hat{M}_{PPM}^{(k)}}(\omega) \tag{4.46}$$

B. CF of Self Interference

The self interference $\hat{I}_{PPM}$ comes from the 1^{st} to the $L-1^{th}$ paths of the desired user. The characteristic function of $\hat{I}_{PPM}^{(l)}$ is given by

$$\begin{aligned}\Phi_{\hat{I}_{PPM}^{(l)}}(\omega) &= \int_0^\infty \left[\cos(\sqrt{P}(1-2b_0^0)\beta_{0,l}\omega)\right]^{N_r-l} p_{\beta_{0,l}}(\beta_{0,l})d\beta_{0,l} \\ &= \int_0^\infty \left[\cos(\sqrt{P}\beta_{0,l}\omega)\right]^{N_r-l} p_{\beta_{0,l}}(\beta_{0,l})d\beta_{0,l}\end{aligned} \tag{4.47}$$

The characteristic function of $\hat{I}_{PPM}$ is expressed as follows.

$$\Phi_{\hat{I}_{PPM}}(\omega) = \prod_{l=1}^{L-1} \Phi_{\hat{I}_{PPM}^{(l)}}(\omega) \tag{4.48}$$

C. CF of AWGN

The AWGN term $\hat{N}_{PPM}$ follows a Gaussian distribution with zero mean and variance of $N_0 N_r$. Its characteristic function $\Phi_{\hat{N}_{PPM}}$ is given by

$$\Phi_{\hat{N}_{PPM}}(\omega) = \exp(-\frac{N_0 N_r \omega^2}{2}) \tag{4.49}$$

D. CF of Total Noise

The total noise is denoted as $\hat{\varsigma}_{PPM} = \hat{M}_{PPM} + \hat{I}_{PPM} + \hat{N}_{PPM}$. By removing the common factor $\alpha_{0,0}$, $\hat{M}_{PPM}$,$\hat{I}_{PPM}$ and $\hat{N}_{PPM}$ are independent. Thus the characteristic function of $\hat{\varsigma}_{PPM}$ is given by

$$\Phi_{\hat{\varsigma}_{PPM}}(\omega) = \Phi_{\hat{M}_{PPM}}(\omega)\Phi_{\hat{I}_{PPM}}(\omega)\Phi_{\hat{N}_{PPM}}(\omega) \tag{4.50}$$

4.5 BER Formula

The characteristic function of the total noise $\hat{\varsigma}_{PAM/PPM}$ is derived in the previous sections. The PDF of $\hat{\varsigma}_{PAM/PPM}$ is obtained by performing an inverse Fourier transform on Eq. (4.27) and Eq. (4.50).

$$p_{\hat{\varsigma}_{PAM/PPM}}(x) = \frac{1}{2\pi}\int_{-\infty}^{\infty} \Phi_{\hat{\varsigma}_{PAM/PPM}}(\omega)\exp(-j\omega x)d\omega \tag{4.51}$$

The decision rule for the DS UWB system is giving by

$$\begin{cases} Z_{PAM/PPM} > 0 \Rightarrow b_0^0 = 1/0 \\ Z_{PAM/PPM} \leq 0 \Rightarrow b_0^0 = -1/1 \end{cases} \tag{4.52}$$

By taking into account the symmetrical property of PDF of $\hat{\varsigma}_{PAM/PPM}$, we simplify the expression of BER as below.

$$\begin{aligned} P_e &= \frac{1}{2}\text{Prob}(Z_{PAM/PPM} \leq 0 | b_0^0 = 1/0) + \frac{1}{2}\text{Prob}(Z_{PAM/PPM} > 0 | b_0^0 = -1/1) \\ &= \text{Prob}\left(\alpha_{0,0}(\alpha_{0,0}\sqrt{P}N_r + \hat{\varsigma}_{PAM/PPM}) \leq 0\right) \\ &= \text{Prob}\left(\hat{\varsigma}_{PAM/PPM} \leq -\beta_{0,0}\sqrt{P}N_r\right) \end{aligned} \tag{4.53}$$

The exact BER can be obtained by two fold integral of the PDF of $\hat{\varsigma}_{PAM/PPM}$ over the error region.

$$\begin{aligned} P_e &= \int_0^{\infty} \int_{-\infty}^{-\beta_{0,0}\sqrt{P}N_r} p_{\hat{\varsigma}_{PAM/PPM}}(x)dx p_{\beta_{0,0}}(\beta_{0,0})d\beta_{0,0} \\ &= \frac{1}{2} - \frac{1}{\pi}\int_0^{\infty}\int_0^{\infty} \Phi_{\hat{\varsigma}_{PAM/PPM}}(\omega)\frac{\sin(\beta_{0,0}\sqrt{P}N_r\omega)}{\omega}d\omega p_{\beta_{0,0}}(\beta_{0,0})d\beta_{0,0} \end{aligned} \quad (4.54)$$

Though we restrict our consideration on the lognormal multipath fading channels, the analysis method is applicable to arbitrary multipath fading channels.

4.6 BER Derivation Using the GA Method

For completeness and comparison, we also present the BER calculation using the GA method. In this method, the total noise $\hat{\varsigma}_{PAM/PPM}$ is assumed to be Gaussian distributed. Since $\hat{M}_{PAM/PPM}$, $\hat{I}_{PAM/PPM}$ and $\hat{N}_{PAM/PPM}$ are statistically independent, the variance of $\hat{\varsigma}_{PAM/PPM}$ is given by

$$\begin{aligned} \sigma^2_{\hat{\varsigma}_{PAM/PPM}} &= \sigma^2_{\hat{M}_{PAM/PPM}} + \sigma^2_{\hat{I}_{PAM/PPM}} + \sigma^2_{\hat{N}_{PAM/PPM}} \\ &= \sum_{k=1}^{K-1} \sigma^2_{\hat{M}^{(k)}_{PAM/PPM}} + \sigma^2_{\hat{I}_{PAM/PPM}} + \sigma^2_{\hat{N}_{PAM/PPM}} \end{aligned} \quad (4.55)$$

The mean of $\sigma^2_{\hat{M}^{(k)}_{PAM/PPM}}$ is zero and its variance is derived as

$$\sigma^2_{\hat{M}^{(k)}_{PAM/PPM}} = \mathrm{E}\left[\left(\hat{M}^{(k)}_{PAM/PPM}\right)^2\right] = \sum_{l=0}^{L-1}\mathrm{E}\left[\left(\hat{M}^{(k,l)}_{PAM/PPM}\right)^2\right] \quad (4.56)$$

The variance of $\sigma^2_{\hat{I}_{PAM/PPM}}$ is the summation of $L-1$ terms.

$$\sigma^2_{\hat{I}_{PAM/PPM}} = \mathrm{E}\left[\left(\hat{I}_{PAM/PPM}\right)^2\right] = \sum_{l=1}^{L-1}\mathrm{E}\left[\left(\hat{I}^{(l)}_{PAM/PPM}\right)^2\right] \quad (4.57)$$

$\gamma_{PAM/PPM}$ is defined as the instantaneous output SINR depending on the instantaneous channel conditions.

$$\gamma_{PAM/PPM} = \frac{\left(\hat{Z}^{(0)}_{PAM/PPM}\right)^2}{\sigma^2_{\hat{\varsigma}_{PAM/PPM}}}$$

$$= \frac{\alpha_{0,0}^2 P N_r^2}{\sum_{k=1}^{K-1}\sum_{l=0}^{L-1} \mathrm{E}\left[(\hat{M}_{PAM/PPM}^{(k,l)})^2\right] + \sum_{l=1}^{L-1} \mathrm{E}\left[(\hat{I}_{PAM/PPM}^{(l)})^2\right] + \sigma_{\hat{N}_{PAM/PPM}}^2} \quad (4.58)$$

The instantaneous BER of the DS UWB systems is given by the following expression.

$$P_{\text{Instant}}(\gamma_{PAM/PPM}) = \frac{1}{2}\text{erfc}\left(\sqrt{\frac{\gamma_{PAM/PPM}}{2}}\right) \quad (4.59)$$

The average BER is obtained by averaging the conditional BER in Eq. (4.59) over the distribution of the instantaneous SINR.

$$P_{\text{Average}} = \int_0^\infty P_{\text{Instant}}(\gamma) p_{\gamma_{PAM/PPM}}(\gamma) d\gamma \quad (4.60)$$

where $p_{\gamma_{PAM/PPM}}(\gamma)$ is the PDF of the instantaneous SINR at the output of the correlation receiver. The average BER in the lognormal multipath fading channels is computed using the Monte Carlo method.

4.7 Numerical Results and Comparison

In this section, we evaluate the BER performance for the DS PAM UWB and the DS PPM UWB systems using both the CF method and the GA method. Simulation results are also presented for comparison.

4.7.1 System Parameters Setting

The analysis in this work is applicable for any UWB monocycle waveform. Here a commonly used Gaussian monocycle is adopted in the numerical study.

$$z(t) = A \exp\left[-0.5\left(\frac{t}{\sigma} - 3.5\right)^2\right] \quad (4.61)$$

The duration of $z(t)$ is $T_p = 7\sigma$ to contain more than 99% of the energy of the Gaussian waveform [80], and $z(t)$ is energy normalized as $\int_0^{T_p} z^2(t)dt = 1$. The

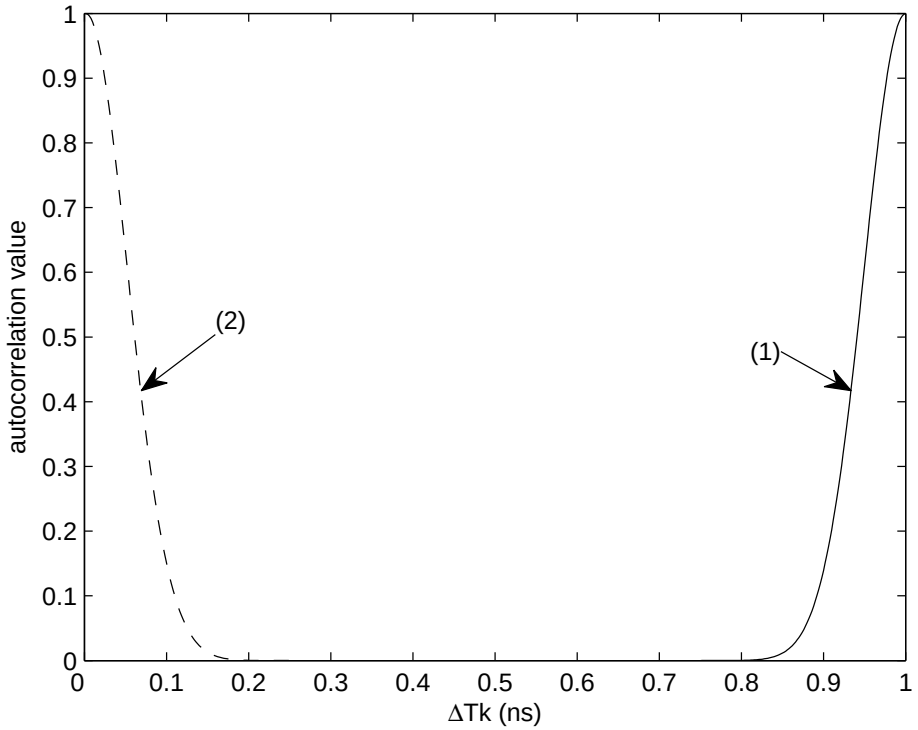

Figure 4.1: The autocorrelation functions of $z(t)$: (1) is $R_{PAM}(\Delta T_k)$, (2) is $\hat{R}_{PAM}(\Delta T_k)$.

amplitude of the monocycle is $A = 1.25687 \times 10^5$. The other parameters are set as $T_c = 1$ns, $T_p = 0.25$ns and $\sigma = T_p/7 \approx 0.035714$ns.

The autocorrelation function of $z(t)$ defined in Eq. (4.10), $\hat{R}_{PAM}(x)$, has a closed form as in Eq. (4.62). In Fig. 4.1, $R_{PAM}(x)$ and $\hat{R}_{PAM}(x)$ are plotted. The cross correlation function of $z(t)$ and $q(t)$ defined in Eq. (4.33), $R_{PPM}(x, b_i^k)$ and $\hat{R}_{PPM}(x, b_i^k)$ are plotted in Fig. 4.2.

$$\hat{R}_{PAM}(x) = \frac{T_c\sqrt{\pi}A^2}{56} \exp\left(-\left(\frac{x}{2\sigma}\right)^2\right) \operatorname{erfc}\left(\sqrt{2}\left(\frac{x}{\sigma} - 3.5\right) - \frac{x}{\sqrt{2}\sigma}\right) \quad (4.62)$$

The lognormal multipath fading channel parameters are chosen according to the reference values given in [54]. The decay factor $\Gamma = 4.3$, and the standard deviation of lognormal fading gain is $\sigma = 3.4$dB.

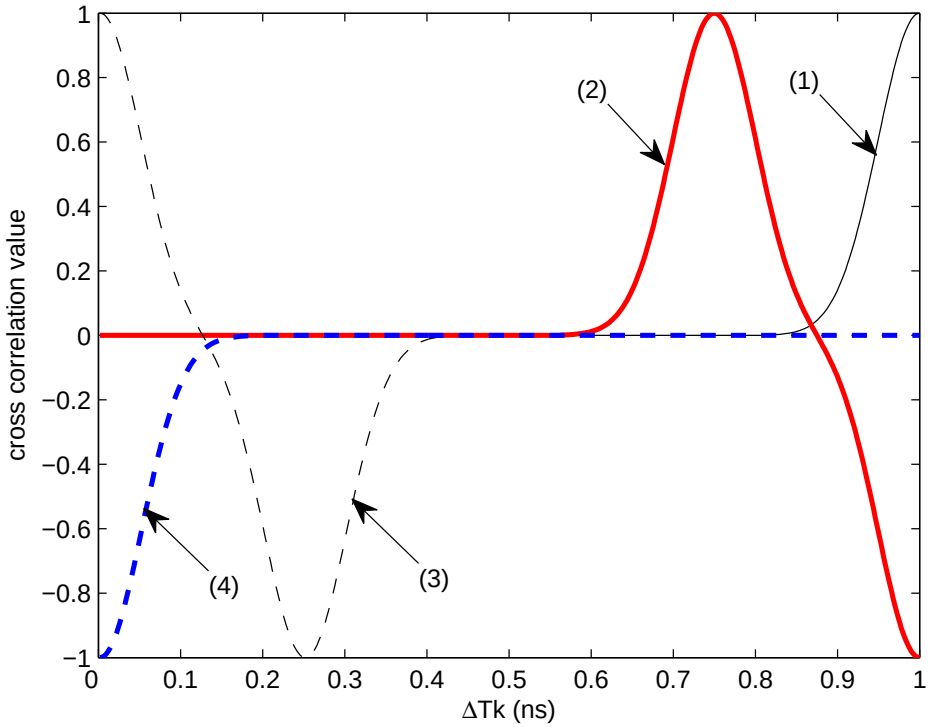

Figure 4.2: The cross correlation functions of $z(t)$ and $q(t)$: (1) is $R_{PPM}(\Delta T_k, 0)$, (2) is $R_{PPM}(\Delta T_k, 1)$, (3) is $\hat{R}_{PPM}(\Delta T_k, 0)$, (4) is $\hat{R}_{PPM}(\Delta T_k, 1)$.

The exact BER formula Eq. (4.54) is applicable for DS UWB systems with any number of users in arbitrary multipath fading channels. In the numerical study, we consider systems with small number of users for the purpose of illustration. It should be noted that the UWB applications are limited in a short range of about 4 to 10 meters. Therefore the number of users could possibly be small. Though the transmitted power P of all users is set to be the same, the random channel fading gain $\alpha_{k,l}$ leads to the imperfect power control at the receiver side.

Since the main purpose of the numerical analysis is to verify the BER expressions derived, we restrict our consideration on cases with small number of

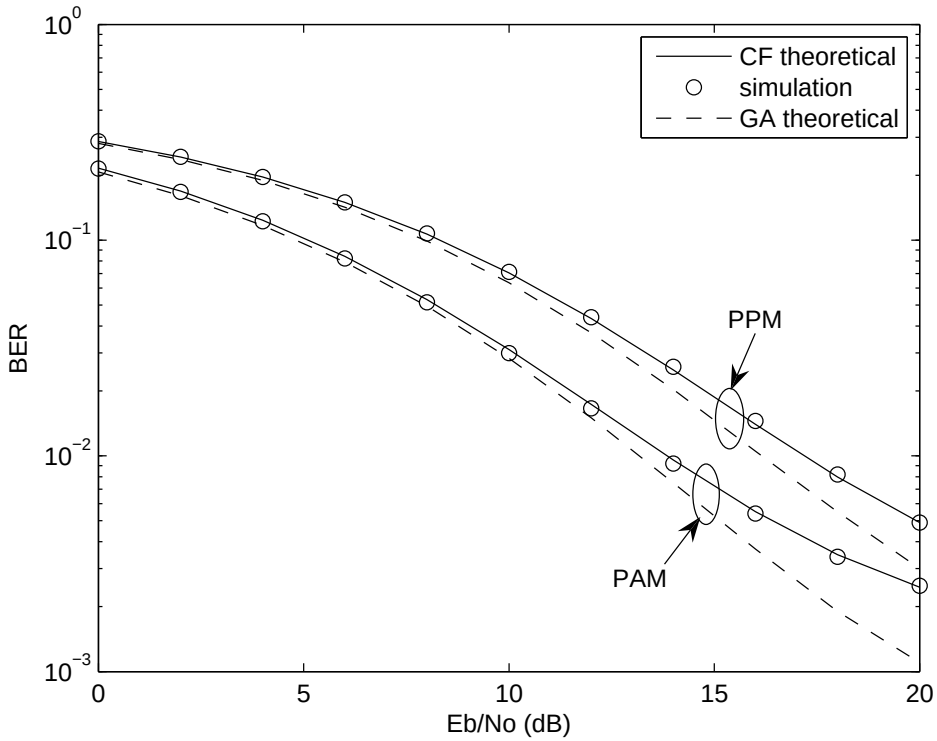

Figure 4.3: Comparison of the GA and CF methods for the DS UWB systems: 2 users, 3 paths, Nr=64

paths in the numerical examples, which is useful in some UWB applications. For example, two UWB devices very near each other probably employ a channel with a strong LOS path and a few weaker paths. In Fig. 3 of [15], the measurement gives an example of this kind. On the other hand, the utilization of polarization and smart antenna with high directivity can effectively reduce the multipath effects [81], which makes small number of paths possible for certain UWB applications.

4.7.2 BER Results and Comparison

We consider a DS PAM/PPM UWB system with 2 users, where each user has 3 paths. The length of the spread sequence takes 4 different values: $N_r =$

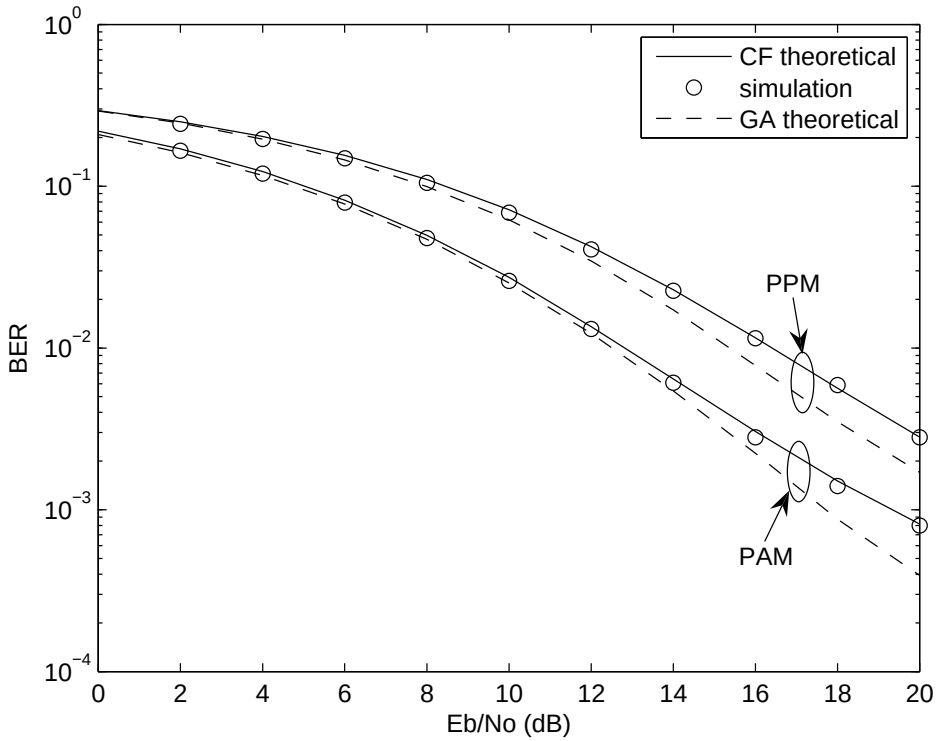

Figure 4.4: Comparison of the GA and CF methods for the DS UWB systems: 2 users, 3 paths, Nr=128

$64, 128, 256, 512$ in Fig. 4.3, 4.4, 4.5 and 4.6 respectively. In these figures, we show the accurate BER curves computed using the CF method (solid line), the BER theoretical curves obtained by the GA method (dashed line) and simulation results(circle marked) for both systems.

Observing Fig. 4.3, 4.4, 4.5 and 4.6, we have three main findings:

1. The theoretical curves generated by the CF method and the simulation results are in excellent agreement. The GA theoretical curves are in good agreement with simulation results for small SNR values. However, the GA evaluation is not so accurate for medium and high SNR values (from 10dB and above).

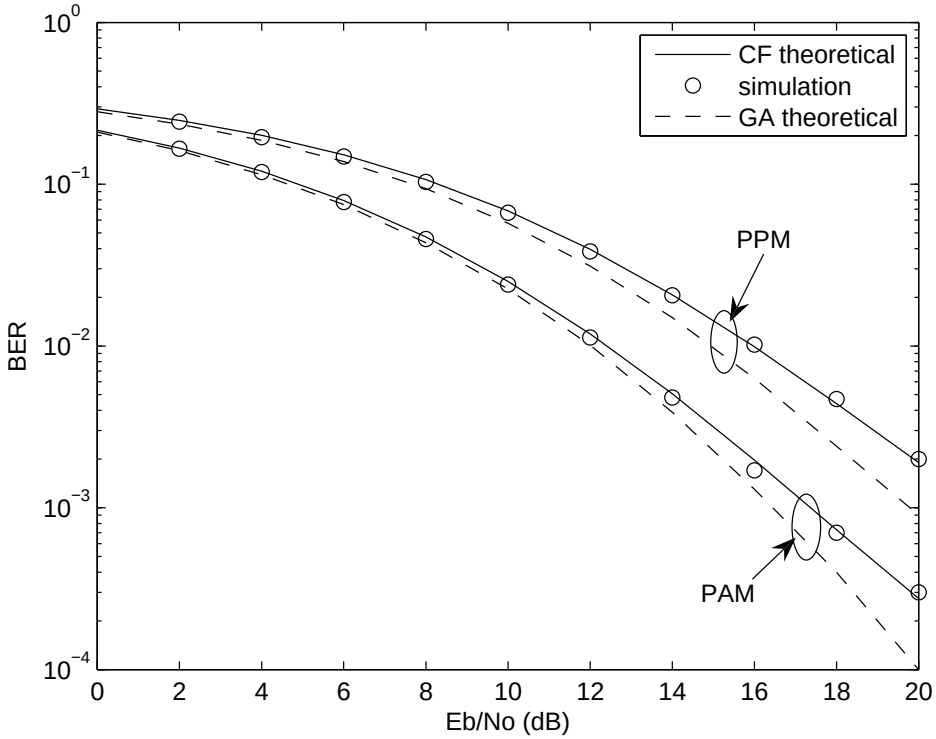

Figure 4.5: Comparison of the GA and CF methods for the DS UWB systems: 2 users, 3 paths, Nr=256

2. Comparing the BER performance of the DS PAM UWB and the DS PPM UWB systems, we observe that the DS PAM UWB system significantly outperforms the DS PPM UWB system in all SNR range. Similar results were reported on the comparison of the TH PAM UWB and the TH PPM UWB systems in AWGN channels [82]. Thus PAM is generally a better modulation option compared with PPM for UWB communications.

3. The larger N_r values bring the better overall BER performance as expected. However, the increase of N_r does not bring so much advantage to the BER performance of the DS PPM UWB system compared with the DS PAM UWB system. For example, we fix the SNR value as 20dB to examine the

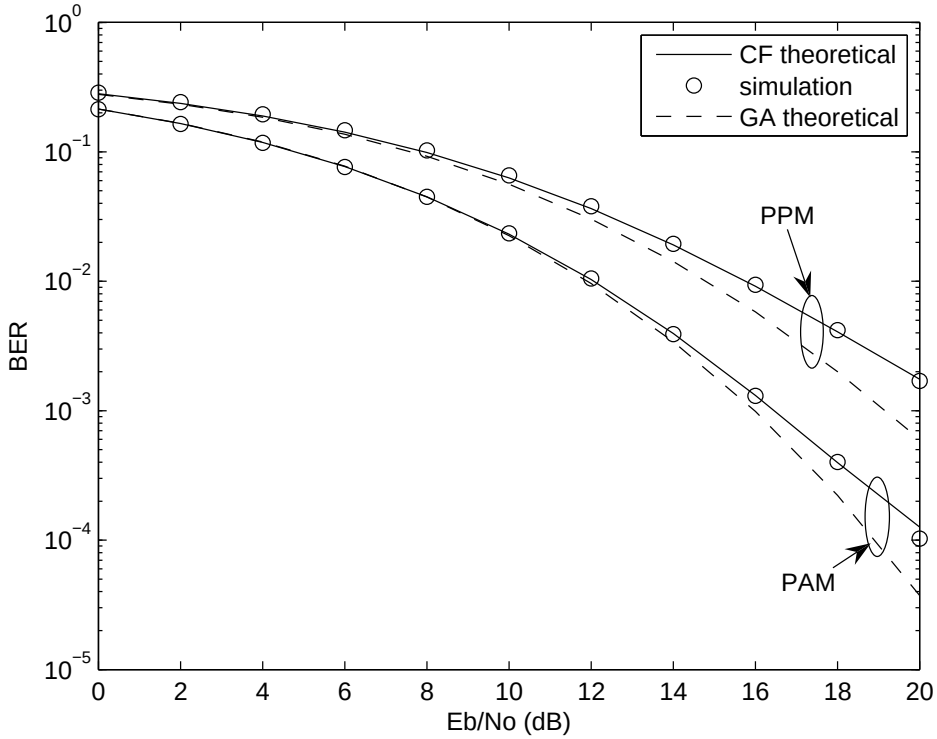

Figure 4.6: Comparison of the GA and CF methods for the DS UWB systems: 2 users, 3 paths, Nr=512

effect of N_r. In the DS PAM UWB system, the simulation BER value is 2.5×10^{-3} for $N_r = 64$ and it reduces by more than one order to 1.027×10^{-4} for $N_r = 512$. On the other hand, in the DS PPM UWB system, the simulation BER values are 4.9×10^{-3} and 1.7×10^{-3} for $N_r = 64$ and $N_r = 512$ respectively, which are still in the same order.

4.7.3 Explanation Based on Characteristic Functions

We plot the characteristic functions of the DS PAM UWB and the DS PPM UWB systems in Fig. 4.7, 4.8, 4.9 and 4.10. In these figures, different N_r and SNR values are used, which help interpreting the numerical results.

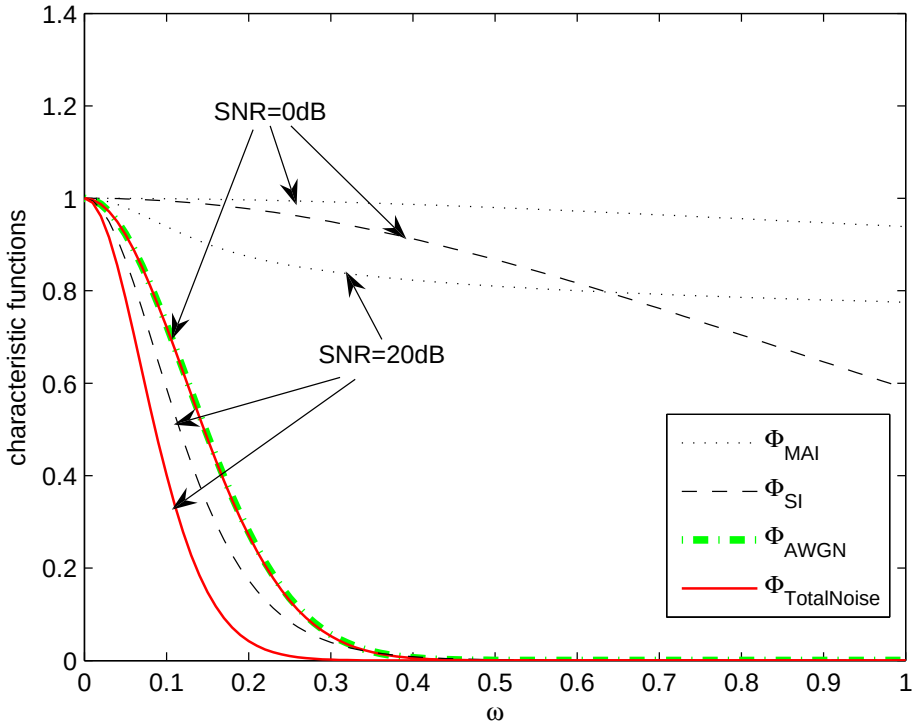

Figure 4.7: The characteristic functions of the DS PAM UWB system: 2 users, 3 paths, Nr=64

1. The BER results obtained by the CF method are more accurate than the GA method in large SNR range since the CF method deals with the exact PDF of the total noise. In the GA method, MAI and SI are modeled as Gaussian random variables. Actually in small SNR range, AWGN dominates the total noise. As a result, the total noise can be approximated as Gaussian distributed. However, in high SNR range, MAI and SI place more influence on the total noise, which generally does not follow Gaussian distribution in a multipath fading environment [9]. Accordingly the GA method does not work well in high SNR range. It is observed in Fig. 4.7, 4.8, 4.9 and 4.10 that when SNR=0dB, $\Phi_{\text{TotalNoise}}$, the characteristic function of the total noise, almost overlaps with the characteristic function of AWGN Φ_{AWGN}.

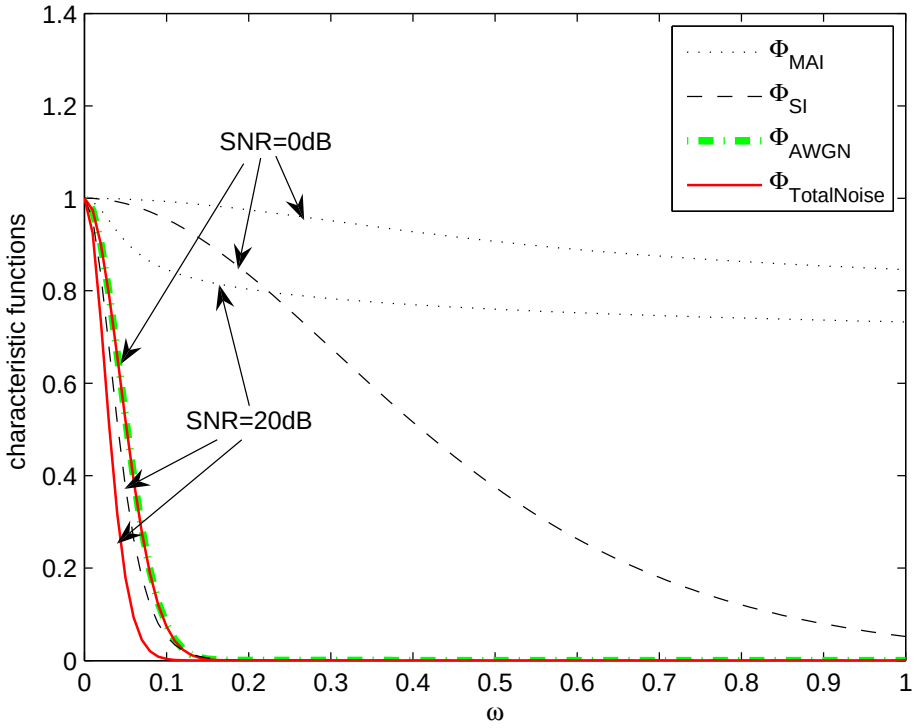

Figure 4.8: The characteristic functions of the DS PAM UWB system: 2 users, 3 paths, Nr=512

This is an intuitive illustration that in small SNR range, the total noise is dominated by AWGN. When SNR=20dB, $\Phi_{\text{TotalNoise}}$ comes under the influence of MAI and SI and it is apparently different from Φ_{AWGN}.

2. The DS PAM UWB system has better overall BER performance than the DS PPM UWB system. This conclusion is consistent with the properties hiding in the characteristic function figures. If we examine $\Phi_{\text{TotalNoise}}$ of the DS PAM UWB and the DS PPM UWB systems under the same parameters, for example, SNR=20dB and $N_r = 64$ as in Fig. 4.7 and 4.9, it is found that $\Phi_{\text{TotalNoise}}$ in the DS PPM UWB system is more peaked than $\Phi_{\text{TotalNoise}}$ in the DS PAM UWB system. This implies that the PDF of the total noise

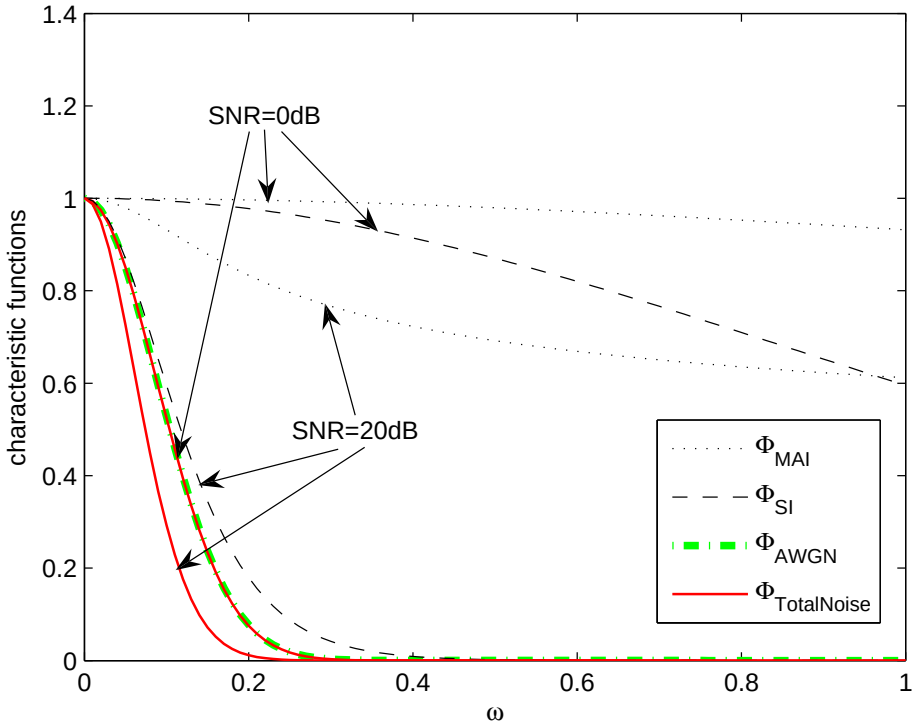

Figure 4.9: The characteristic functions of the DS PPM UWB system: 2 users, 3 paths, Nr=64

in the DS PPM UWB system would be flatter than that of the DS PAM UWB system. Since the BER is obtained by a tail integral on the PDF of the total noise, the BER performance of the DS PPM UWB system would worse than that of the DS PAM UWB system.

3. The larger N_r values bring less advantage to the BER performance of the DS PPM UWB system compared with the DS PAM UWB system. This could be explained from the total noise properties shown in Fig. 4.9 and 4.10. It is observed in these two figures that AWGN is the most important noise component in the DS PPM UWB system: Φ_{AWGN} is the nearest curve to $\Phi_{\text{TotalNoise}}$. In other words, the performance of the DS PPM UWB system

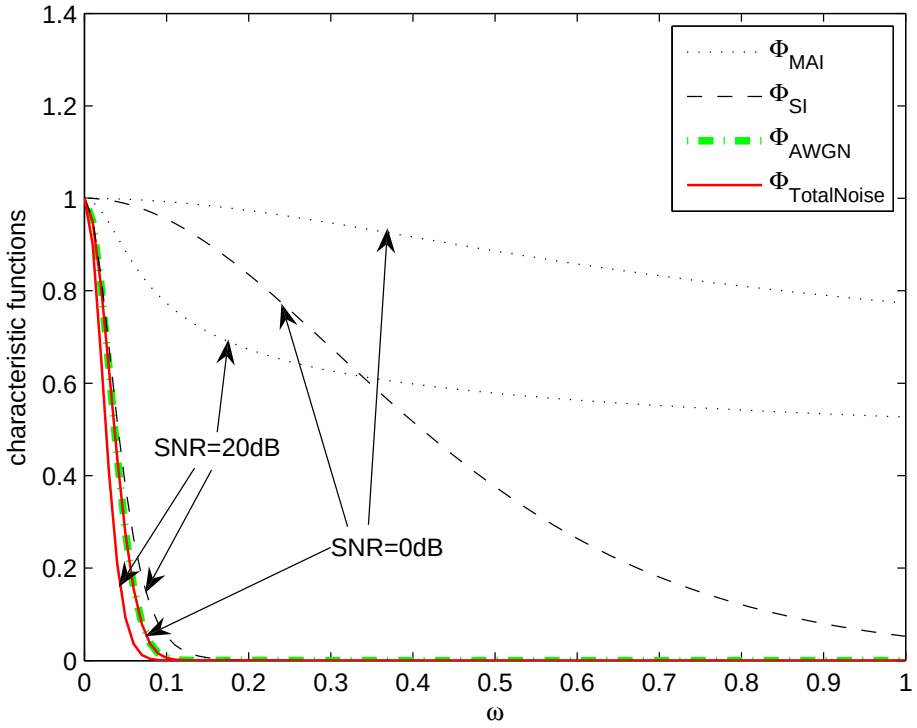

Figure 4.10: The characteristic functions of the DS PPM UWB system: 2 users, 3 paths, Nr=512

is mainly restricted by AWGN. The growth of the spreading sequence length N_r leads to both pros and cons: The variance of the AWGN term increases, and the spreading gain also increases. The impact of the former is more significant in the DS PPM UWB system, and this is the reason why the BER performance does not improve much with larger N_r values.

4.8 Conclusions

We present the exact BER analysis for the DS PAM UWB and the DS PPM UWB multiple access systems using the CF method in the lognormal multipath fading channels. Instead of approximating the total noise (including MAI, SI and

AWGN) as Gaussian random variable, we derive the characteristic function of the total noise and then use this result to derive the exact BER formula. For both the DS PAM UWB and the DS PPM UWB systems with small number of interfering sources, the theoretical BER obtained by the CF method is in good agreement with simulation results, while the GA method underestimates the BER values in high SNR range. The Gaussian distribution assumption on MAI and SI is questionable in case of small number of interfering sources and under imperfect power control. In such cases, the CF method is a good alternative to evaluate the BER performance for the DS UWB systems. The BER performance of the DS PAM UWB and the DS PPM UWB systems are accurately compared for different lengths of spreading sequence. And the plotting of the characteristic functions is used to further interpret our findings.

Chapter 5

Design and Analysis of Prerake DS UWB Multiple Access Systems Under Imperfect Channel Estimation

In this chapter, a Prerake DS UWB multiple access system is proposed to effectively capture signal energy in multipath fading channels. Prior research on various Prerake UWB systems is summarized in Section 5.1. The system model and signal structure design is presented in Section 5.2. Then signal model of the Prerake DS UWB multiple access system is elaborated in Section 5.3. Next, analysis of BER performance and multiple access performance is presented in Section 5.4 and Section 5.5 respectively. Numerical analysis in Section 5.6 provides verification of our derivations, and further discussions are given. In Section 5.7, conclusions are drawn according to our findings.

5.1 Introduction

One of the main advantages of the UWB communications is the super fine time resolution property, which significantly reduces the channel fading effects even in a dense multipath environment [11][56]. However, how to utilize the fine time resolution and effectively capture the signal energy in dense multipath channels is still a challenging task.

If the conventional Rake receiver is used to combine multipath components in a typical UWB channel, a large number of Rake fingers are generally needed to capture enough signal energy [56]. In addition, channel estimation at the receiver significantly increases the complexity and cost of the system. In those UWB systems with a centralized topology (including a few fixed access points and a lot of portable receivers), low complexity receivers are desirable to reduce the whole system cost. This is the key motivation for us to study the Prerake DS UWB multiple access systems.

The Prerake combining (also called Time Reversal) is originally used in underwater wideband transmission with acoustic signals [67][83] and TDD CDMA systems [30][84]. The principle of the Prerake combining is that the transmitter prefilters the original signal using the temporal reverse channel impulse response before transmission. When the "preraked" transmitted signal convolves with the channel impulse response, a strong peak is produced at the output of the channel. The main attraction of the Prerake combining is that equivalent performance of Rake MRC can be achieved using a simple receiver with only one finger. Besides, channel estimation is not necessary at the receiver, which is very desirable for low cost/complexity system design. Another notable benefit of the Prerake combining is that the signal energy focuses in both time and space domains at the output of the channel. This property not only helps to reduce ISI and MAI, but also allows

higher data rate transmission in those channels with very large delay spread. Moreover, the temporal/spatial focusing to some extent provides low probability of detection and location related security in multiple access systems [85].

Recently the Prerake combining has been considered for the UWB communications in some literature. The preliminary performance comparison of the Prerake combining and the Rake combining in the absence of ISI is reported in [25][26] based on Monte Carlo simulations. The results show that these two combining schemes achieve almost the same BER performance when the number of taps in the Prerake filter equals to the number of fingers in the Rake receiver. Later, the Prerake combining has been found to outperform the Rake combining in the presence of NBI [27]. The effect of other kinds of interference in the Prerake UWB systems, such as ISI [28][29] and IPI [27], is also an important topic in the performance analysis and improvement. Commonly used equalization techniques including zero-forcing [27] and MMSE [28][29] have been applied in the Prerake UWB systems to combat the malign impact of IPI and ISI. In all these works [25][26][27][28][29], the Prerake combining for UWB systems is studied in single user scenario and the effect of MAI is not addressed. Since MAI is one of the major difference between the Prerake and the Rake systems [30], it is of interest to study the Prerake UWB multiple access systems. The TH Prerake UWB multiple access system has been investigated in [86], where a semi-analytical method is used to study the effect of ISI and MAI.

A common assumption in these works [25][26][27][28][29][86] is the perfect channel estimation. However, it is found that the channel estimation error largely degrades the performance of the Prerake TDD CDMA systems, especially in a multiple access environment [31]. Hence the effect of imperfect channel estimation should be considered with carefulness in the study of the Prerake UWB systems. Though the channel estimation methods have been addressed in

some publications [85][87] for the Prerake UWB systems, no work has been done on the effect of imperfect channel estimation in a multiple access Prerake UWB system. Furthermore, to the best of our knowledge, the analytical signal model for the Prerake UWB multiple access systems has not been presented yet.

In this chapter, we propose a Prerake DS UWB multiple access system and explore its performance under imperfect channel estimation. For the first time, the analytical signal model of the Prerake UWB multiple access system is presented. Next, the BER formula is derived based on this signal model. In numerical analysis, the BER formula is validated by simulations. The effect of imperfect channel estimation on the system performance is discussed in detail. By defining a degradation factor (DF), we derive the expression of the maximum number of users as a function of DF. And the multiple access performance is evaluated in terms of maximum number of users supported for a desired BER.

5.2 System Model

5.2.1 Channel Model

According to [54], the channel impulse response of the k^{th} user is modeled as

$$h^{(k)}(t) = \sum_{l=0}^{L-1} \alpha_{l,k} \delta(t - \tau_{l,k}) \tag{5.1}$$

where L is the number of paths in the channel. The path gain $\alpha_{l,k} = \theta_{l,k}\beta_{l,k}$, where $\theta_{l,k}$ is equiprobable ± 1 to account for pulse inversion due to reflection and $\beta_{l,k}$ is the lognormal fading amplitude. For different k and l, $\alpha_{l,k}$ are independent random variables. We consider the resolvable multipath channel [88] with $\tau_{l,k} = \tau_{0,k} + lT_p$, where T_p is the width of UWB monocycle $z(t)$. Since multipath components tend to arrive in clusters [54], the l^{th} path can be expressed as the j^{th} ray in the i^{th} cluster. Therefore, delay of the l^{th} path $\tau_{l,k} = \mu_{i,k} + \nu_{j,i,k}$,

where $\mu_{i,k}$ is delay of the i^{th} cluster and $\nu_{j,i,k}$ is delay of the j^{th} ray in the i^{th} cluster relative to $\mu_{i,k}$. The power delay profile of the channel is double exponential decaying by rays and clusters. The sum of the mean square value of the channel gains is normalized as $\sum_{l=0}^{L-1} \mathrm{E}\left[\alpha_{l,k}^2\right] = 1$. Since the transmitter and receiver are stationary in most WPAN applications [54][23], the channel is assumed to remain constant over a block of symbols. This quasi-static property is the basis for the Prerake combining. The transmitter in the fixed access points obtains the channel information by utilizing the symmetrical channel impulse response on the up/down links [30].

5.2.2 Transmitted Signal

The transmitted signal of the k^{th} user is

$$\tilde{s}^{(k)}(t) = A_k \sum_{i=-\infty}^{\infty} b_i^k x^{(k)}(t - iT_r) \tag{5.2}$$

where T_r is the symbol duration, A_k denotes the amplitude, $b_i^k \in \{\pm 1\}$ is the i^{th} symbol. In a DS UWB multiple access system with K users, the symbol waveform of the k^{th} user is given by

$$x^{(k)}(t) = \sum_{n=0}^{N_r-1} a_n^k g^{(k)}(t - nT_c) \tag{5.3}$$

where $\{a_n^k\}_{n=0}^{N_r-1}$ is the DS signature assigned to the k^{th} user and $T_c = T_r/N_r$ is the chip duration. The chip waveform $g^{(k)}(t)$ is formed by passing the UWB monocycle $z(t)$ through a Prerake filter $\tilde{h}^{(k)}(t)$.

$$g^{(k)}(t) = z(t) * \tilde{h}^{(k)}(t) = \sum_{l=0}^{L_p-1} \tilde{\alpha}_{L_p-1-l,k} z(t - lT_p) \tag{5.4}$$

where $*$ represents the convolution operation, $z(t)$ is the UWB monocycle of duration T_p with normalized energy. The Prerake filter $\tilde{h}^{(k)}(t) = \sum_{l=0}^{L_p-1} \tilde{\alpha}_{L_p-1-l,k}\delta(t - lT_p)$ contains L_p taps and the chip duration $T_c = L_p T_p$.

Following the concept of All-Prerake and Partial-Prerake schemes introduced in [26], a data rate increasing factor N_c is defined as a submultiple of L, i.e., $L = N_c L_p$. In the All-Prerake scheme, $N_c = 1$ and data rate is $R_b = 1/(N_r L T_p)$. In the Partial-Prerake scheme, $N_c > 1$ and the data rate is $R_b = N_c/(N_r L T_p)$, which is N_c times of the data rate in All-Prerake scheme. In $\tilde{h}^{(k)}(t)$, $\{\tilde{\alpha}_{l,k}\}_{l=0}^{L_p-1}$ is the estimated value of channel gain $\{\alpha_{l,k}\}_{l=0}^{L_p-1}$. The amplitude $A_k = \sqrt{E_p \Big/ \sum_{l=0}^{L_p-1} \mathrm{E}\left[\tilde{\alpha}_{l,k}^2\right]}$ is to keep the average transmitted symbol energy constant as $E_b = N_r E_p$.

5.2.3 Received Signal

The received signal due to the k^{th} user is given by

$$\begin{aligned} r^{(k)}(t) &= \tilde{s}^{(k)}(t) * h^{(k)}(t) \\ &= A_k \sum_{i=-\infty}^{\infty} b_i^k \underbrace{\left[x^{(k)}(t - iT_r) * h^{(k)}(t)\right]}_{\tilde{x}^{(k)}(t-iT_r)} \end{aligned} \tag{5.5}$$

where $\tilde{x}^{(k)}(t)$ is obtained using Eq. (5.3) as

$$\begin{aligned} \tilde{x}^{(k)}(t) &\triangleq x^{(k)}(t) * h^{(k)}(t) \\ &= \sum_{n=0}^{N_r-1} a_n^k \underbrace{\left[g^{(k)}(t - nT_c) * h^{(k)}(t)\right]}_{\tilde{g}^{(k)}(t-nT_c)} \end{aligned} \tag{5.6}$$

where $\tilde{g}^{(k)}(t) \triangleq g^{(k)}(t) * h^{(k)}(t)$ is the channel response of a chip waveform $g^{(k)}(t)$.

The total received signal in the Prerake DS UWB system with K asynchronous users is given by

$$r(t) = \sum_{k=0}^{K-1} r^{(k)}(t - \tau_{0,k}) + n(t) \tag{5.7}$$

where $n(t)$ is AWGN with double sided PSD of $N_0/2$ and $\tau_{0,k}$ serves as the transmission delay of the k^{th} user. Since random antipodal DS sequences/data symbols are assumed, the interfering users appear to the desired user as essentially

transmitting random $\{\pm 1\}$ sequences and the boundaries of interfering symbols do not matter in asynchronous transmission. This property allows us to assume that $\tau_{0,k}$ is uniformly distributed in $[0, T_c)$.

5.2.4 Channel Estimation

The estimated channel gains $\{\tilde{\alpha}_{l,k}\}_{l=0}^{L_p-1}$ are obtained by a time domain channel estimation scheme. We assume all other users keep silent during channel estimation period of the k^{th} user. The k^{th} user sends N_t training UWB monocycles $z(t)$. The training monocycle repetition interval is larger than the maximum delay spread of the channel to avoid interference between training monocycles. Assuming perfect synchronization, the base station correlates and samples at the tap rate on the i^{th} received training monocycle to get the estimated channel gain on the first L_p paths.

$$\tilde{\alpha}_{l,k}(i)=\int_{lT_p}^{(l+1)T_p}\left(\sum_{l'=0}^{L-1}\alpha_{l',k}z(t-l'T_p)+n_i(t)\right)z(t-lT_p)dt \tag{5.8}$$

where $i = 0, 1, \cdots, N_t-1$ is the index of training monocycles. Then N_t estimation results are averaged to obtain the estimated channel gain as follows.

$$\tilde{\alpha}_{l,k} = \frac{1}{N_t}\sum_{i=0}^{N_t-1}\tilde{\alpha}_{l,k}(i) = \alpha_{l,k} + n_{l,k} \tag{5.9}$$

where $n_{l,k}$ is the noise brought by imperfect channel estimation on the l^{th} path, and it follows Gaussian distribution with zero mean and variance of $N_0/(2N_t)$. Since total L_p paths are to be estimated, larger L_p will lead to stronger impact of imperfect channel estimation.

In the time domain channel estimation, larger number or higher power of the training monocycles would lead to more accurate channel estimation and improve the system performance. Besides the time domain channel estimation,

the combined frequency domain channel estimation/equalization [89] could be a promising candidate to achieve better system performance.

5.3 Signal Modeling and Decision Statistics

5.3.1 Signal Modeling

The channel gain and the estimated channel gain used in the Prerake filter for the k^{th} user are defined as vectors $\boldsymbol{\alpha}_k$ and $\tilde{\boldsymbol{\alpha}}_k$ respectively.

$$\begin{aligned} \boldsymbol{\alpha}_k &= \begin{pmatrix} \alpha_{0,k} & \alpha_{1,k} & \cdots & \alpha_{L-1,k} \end{pmatrix}^T \\ \tilde{\boldsymbol{\alpha}}_k &= \begin{pmatrix} \tilde{\alpha}_{L_p-1,k} & \tilde{\alpha}_{L_p-2,k} & \cdots & \tilde{\alpha}_{0,k} \end{pmatrix}^T \end{aligned} \tag{5.10}$$

$\tilde{g}^{(k)}(t)$ in Eq. (5.6) can be discretized by sampling on the tap rate, i.e., $\tilde{g}_{j,k} = \int_{jT_p}^{(j+1)T_p} \tilde{g}^{(k)}(t) z(t - jT_p) dt$. And $\tilde{g}^{(k)}(t)$ is expressed as vector $\tilde{\mathbf{g}}_k$.

$$\tilde{\mathbf{g}}_k = \mathbf{T}_{\boldsymbol{\alpha}_k} \tilde{\boldsymbol{\alpha}}_k = \begin{pmatrix} \tilde{g}_{0,k} & \tilde{g}_{1,k} & \cdots & \tilde{g}_{L+L_p-2,k} \end{pmatrix}^T \tag{5.11}$$

where $\mathbf{T}_{\boldsymbol{\alpha}_k}$ is a $(L + L_p - 1) \times L_p$ Toeplitz matrix with $\boldsymbol{\alpha}_k$ as the first L elements in its 0^{th} column and zero elsewhere. The effect of imperfect channel estimation is included in $\tilde{\mathbf{g}}_k$, which is brought by $\tilde{\boldsymbol{\alpha}}_k$. And the element $\tilde{g}_{L_p-1,k} = \sum_{l=0}^{L_p-1} \alpha_{l,k} \tilde{\alpha}_{l,k}$ is the desired peak.

Another Toeplitz matrix $\mathbf{T}_{\mathbf{a}_k}$ of size $(2N_r L_p) \times (L + L_p - 1)$ is defined using the DS signature $\{a_n^k\}_{n=0}^{N_r-1}$. The 0^{th} column of $\mathbf{T}_{\mathbf{a}_k}$ contains $\begin{pmatrix} a_0^k & \mathbf{0}_{L_p-1} & a_1^k & \mathbf{0}_{L_p-1} & \cdots & a_{N_r-1}^k & \mathbf{0}_{L_p-1} \end{pmatrix}^T$ as the first $N_r L_p$ elements and zero elsewhere, where $\mathbf{0}_{L_p-1}$ denotes the zero vector with $L_p - 1$ elements. Next, $\mathbf{T}_{\mathbf{a}_k}$ is split into two $(N_r L_p) \times (L + L_p - 1)$ matrices: $\mathbf{T}_{\mathbf{a}_{k,0}}$ consists of the upper half of $\mathbf{T}_{\mathbf{a}_k}$ from the 0^{th} row to the $(N_r L_p - 1)^{th}$ row, and $\mathbf{T}_{\mathbf{a}_{k,1}}$ consists of the lower half of $\mathbf{T}_{\mathbf{a}_k}$ from the the $(N_r L_p)^{th}$ row to the $(2N_r L_p - 1)^{th}$ row.

In order to convert the continuous-time signal $r^{(k)}(t)$ into a discrete format, $r^{(k)}(t)$ is filtered by a tap-matched filter $z(t)$ and then sampled at the tap rate. Therefore each symbol consists of $N_r L_p$ samples. Without loss of generality, we assume that the 0^{th} symbol is the desired symbol. The received discrete symbol can be expressed as

$$\begin{aligned} \mathbf{r}_k &= \begin{pmatrix} r_0^k & r_1^k & \cdots & r_{N_r L_p - 1}^k \end{pmatrix}^T \\ &= A_k \mathbf{T}_{\mathbf{a}_{k,0}} \tilde{\mathbf{g}}_k b_0^k + A_k \mathbf{T}_{\mathbf{a}_{k,1}} \tilde{\mathbf{g}}_k b_{-1}^k \end{aligned} \tag{5.12}$$

5.3.2 Decision Statistics

We assume that the 0^{th} user is the desired user. To detect the 0^{th} symbol, the 0^{th} receiver performs correlation on the N_r peaks in the received signal $r(t)$. The output decision statistic Z is given by

$$\begin{aligned} Z &= \int_0^{T_r} r(t) v^{(0)}(t) dt \\ &= \underbrace{\int_0^{T_r} r^{(0)}(t) v^{(0)}(t) dt}_{S+I_C+I_S} + \underbrace{\sum_{k=1}^{K-1} \int_0^{T_r} r^{(k)}(t-\tau_{0,k}) v^{(0)}(t) dt}_{I_M} + \underbrace{\int_0^{T_r} n(t) v^{(0)}(t) dt}_{N} \end{aligned} \tag{5.13}$$

where $v^{(0)}(t) = \sum_{n=0}^{N_r-1} a_n^0 z(t - nT_c - (L_p - 1)T_p)$ is the template waveform in the 0^{th} receiver. The decision statistic Z can be decomposed as desired signal S, inter-chip interference (ICI) I_C, inter-symbol interference I_S, multiple access interference I_M and AWGN term N.

A. Desired Signal, Inter-Chip Interference and Inter-Symbol Interference

Similar to $r^{(k)}(t)$, the template waveform $v^{(0)}(t)$ can be expressed in a discrete format of $\mathbf{v}_0 = \begin{pmatrix} \mathbf{0}_{L_p-1} & a_0^0 & \mathbf{0}_{L_p-1} & a_1^0 & \cdots & \mathbf{0}_{L_p-1} & a_{N_r-1}^0 \end{pmatrix}$. Then the first

term in the second line of Eq. (5.13) is rewritten as

$$\begin{aligned} S + I_C + I_S &= \mathbf{v}_0 \mathbf{r}_0 \\ &= \underbrace{A_0 \mathbf{v}_0 \mathbf{T}_{\mathbf{a}_{0,0}} \tilde{\mathbf{g}}_0 b_0^0}_{S+I_C} + \underbrace{A_0 \mathbf{v}_0 \mathbf{T}_{\mathbf{a}_{0,1}} \tilde{\mathbf{g}}_0 b_{-1}^0}_{I_S} \end{aligned} \tag{5.14}$$

Recall the fact that $\tilde{g}_{L_p-1,0}$ is the peak containing the desired signal energy. S and I_C are expressed as below, and both terms contain the imperfect channel estimation effect brought by $\tilde{\mathbf{g}}_0$.

$$\begin{aligned} S &= A_0 \mathbf{v}_0 \mathbf{T}_{\mathbf{a}_{0,0}} \tilde{\mathbf{g}}_0' b_0^0 \\ I_C &= A_0 \mathbf{v}_0 \mathbf{T}_{\mathbf{a}_{0,0}} (\tilde{\mathbf{g}}_0 - \tilde{\mathbf{g}}_0') b_0^0 \end{aligned} \tag{5.15}$$

where $\tilde{\mathbf{g}}_0'$ is obtained by setting all elements in $\tilde{\mathbf{g}}_0$ as zeros except the element $\tilde{g}_{L_p-1,0}$.

B. Multiple Access Interference

In pervious work on Prerake TDD CDMA systems [90], the imperfect channel estimation in MAI is ignored to avoid computational complexity. However, the imperfect channel estimation should not be neglected because it leads to interference energy distraction and changes the statistical property of MAI. Therefore we take the imperfect channel estimation effect into account in the analysis of I_M. From Eq. (5.13), $I_M = \sum_{k=1}^{K-1} I_{M,k}$, where $I_{M,k}$ is the interference from the k^{th} interfering user. $I_{M,k}$ comes from either one or two adjacent symbols. We add the index i in Eq. (5.12) to indicate the i^{th} symbol of the k^{th} user.

$$\begin{aligned} \mathbf{r}_k(i) &= \begin{pmatrix} r_0^k(i) & r_1^k(i) & \cdots & r_{N_r L_p - 1}^k(i) \end{pmatrix}^T \\ &= A_k \mathbf{T}_{\mathbf{a}_{k,0}} \tilde{\mathbf{g}}_k b_i^k + A_k \mathbf{T}_{\mathbf{a}_{k,1}} \tilde{\mathbf{g}}_k b_{i-1}^k \end{aligned} \tag{5.16}$$

The asynchronous delay $\tau_{0,k}$ can be split as $\tau_{0,k} = \gamma_k T_p + \Delta T_k$, where $\gamma_k \in \{0, 1, \cdots, L_p - 1\}$ and $\Delta T_k \in [0, T_p)$, both with uniform distribution. The

autocorrelation functions of $z(t)$ is defined as $P(x) = \int_0^x z(t)z(t+T_p-x)\,dt$. Then $I_{M,k}$ is given by

$$I_{M,k} = \mathbf{v}_0\mathbf{R}_{k,0}P(\Delta T_k) + \mathbf{v}_0\mathbf{R}_{k,1}P(T_p - \Delta T_k) \tag{5.17}$$

where

$$\mathbf{R}_{k,x} = \left(r^k_{N_rL_p-\gamma_k-1+x}(-1)\ \cdots\ r^k_{N_rL_p-1}(-1)\quad r^k_0(0)\ \cdots\ r^k_{N_rL_p-\gamma_k-2+x}(0)\right)^T \tag{5.18}$$

5.4 BER Performance Analysis

Since the number of multipaths is large, we use the GA method to calculate the BER value. Set the total noise $\varsigma = I_C + I_S + I_M + N$. It is easy to prove that all terms in ς have zero mean and are independent conditioned on $\boldsymbol{\alpha}_0$ and $\tilde{\boldsymbol{\alpha}}_0$. The instantaneous SINR is defined as

$$\gamma = \frac{S^2}{\sigma^2_\varsigma} = \frac{S^2}{\sigma^2_{I_C} + \sigma^2_{I_S} + \sigma^2_{I_M} + N_0N_r/2} \tag{5.19}$$

where S^2, $\sigma^2_{I_C} + \sigma^2_{I_S}$ and $\sigma^2_{I_M}$ are derived as below.

$$\begin{aligned} S^2 &= A_0^2\mathbf{v}_0\mathbf{T}_{\mathbf{a}_{0,0}}\tilde{\mathbf{g}}_0'\tilde{\mathbf{g}}_0'^T\mathbf{T}^T_{\mathbf{a}_{0,0}}\mathbf{v}_0^T \\ &= A_0^2N_r^2\tilde{g}^2_{L_p-1,0} \end{aligned} \tag{5.20}$$

$$\begin{aligned} \sigma^2_{I_C}+\sigma^2_{I_S} &= A_0^2\mathrm{E}\left[\mathbf{v}_0\mathbf{T}_{\mathbf{a}_{0,0}}(\tilde{\mathbf{g}}_0-\tilde{\mathbf{g}}_0')(\tilde{\mathbf{g}}_0-\tilde{\mathbf{g}}_0')^T\mathbf{T}^T_{\mathbf{a}_{0,0}}\mathbf{v}_0^T\right]+A_0^2\mathrm{E}\left[\mathbf{v}_0\mathbf{T}_{\mathbf{a}_{0,1}}\tilde{\mathbf{g}}_0\tilde{\mathbf{g}}_0^T\mathbf{T}^T_{\mathbf{a}_{0,1}}\mathbf{v}_0^T\right] \\ &= A_0^2N_r\sum_{j=2}^{N_c}\tilde{g}^2_{jL_p-1,0} \end{aligned} \tag{5.21}$$

$$\begin{aligned} \sigma^2_{I_M} &= (K-1)\sigma^2_{I_{M,k}} \\ &= \frac{2(K-1)}{L_p}\mathrm{E}\left[P^2(\Delta T_k)\right]\mathrm{E}\left[\mathbf{r}_k^T\mathbf{r}_k\right] \\ &= \frac{2(K-1)}{L_p}\mathrm{E}\left[P^2(\Delta T_k)\right]A_k^2N_r\sum_{j=0}^{L+L_p-2}\mathrm{E}\left[\tilde{g}^2_{j,k}\right] \end{aligned} \tag{5.22}$$

The expectations of $\tilde{g}_{j,k}^2$ are given as follows.

$$\begin{aligned}
\mathrm{E}\left[\tilde{g}_{j,k}^2\right]_{j\neq L_p-1} &= \sum_{n=\max[0,j-L+1]}^{\min[j,\,L_p-1]} \mathrm{E}\left[\alpha_{j-n,k}^2\right] \mathrm{E}\left[\alpha_{L_p-1-n,k}^2\right] \\
&\quad + \frac{N_0}{2N_t} \sum_{n=\max[0,j-L+1]}^{\min[j,\,L_p-1]} \mathrm{E}\left[\alpha_{j-n,k}^2\right] \qquad (5.23a) \\
\mathrm{E}\left[\tilde{g}_{L_p-1,k}^2\right] &= \sum_{n=0}^{L_p-1} \mathrm{E}\left[\alpha_{n,k}^4\right] + \sum_{n=0}^{L_p-1} \sum_{\substack{n'=0 \\ n'\neq n}}^{L_p-1} \mathrm{E}\left[\alpha_{n,k}^2\right] \mathrm{E}\left[\alpha_{n',k}^2\right] \\
&\quad + \frac{N_0}{2N_t} \sum_{n=0}^{L_p-1} \mathrm{E}\left[\alpha_{n,k}^2\right] \qquad (5.23b)
\end{aligned}$$

The x^{th} moment (where x is an even number) of $\alpha_{l,k}$ can be obtained by the x^{th} moment of $\beta_{l,k}$, i.e., $\mathrm{E}[(\beta_{l,k})^x] = \exp(x\eta_{y_{l,k}} + x^2\sigma_{y_{l,k}}^2/2)$, where $\beta_{l,k} = \exp(y_{l,k})$ and $y_{l,k}$ follows a Gaussian distribution with mean of $\eta_{y_{l,k}}$ and variance of $\sigma_{y_{l,k}}^2$.

The average BER P_{Average} is obtained by averaging the instantaneous BER $P_{\text{Instant}}(\gamma)$ over the distribution of the instantaneous SINR γ.

$$\begin{aligned}
P_{\text{Instant}}(\gamma) &= \frac{1}{2}\mathrm{erfc}\left(\sqrt{\frac{\gamma}{2}}\right) \\
P_{\text{Average}} &= \int_0^\infty P_{\text{Instant}}(\gamma) p_\gamma(\gamma)\, d\gamma \qquad (5.24)
\end{aligned}$$

where $p_\gamma(\gamma)$ is the PDF of the instantaneous SINR at the output of the receiver. In Section V, we compute the average BER using the Monte Carlo method.

5.5 Multiple Access Performance Analysis

5.5.1 Definition of Degradation Factor

The output SINR γ in Eq. (5.19) is rewritten as follows to give more insight into the multiple access performance of the system.

$$\gamma = \left(\left(\underbrace{\frac{S^2}{\sigma_{I_C}^2 + \sigma_{I_S}^2 + N_0 N_r/2}}_{\mathrm{SINR}_1} \right)^{-1} + \left(\underbrace{\frac{S^2}{\sigma_{I_M}^2}}_{\mathrm{SINR}_\mathrm{K}} \right)^{-1} \right)^{-1} \tag{5.25}$$

After some straightforward manipulations, we get the following expression.

$$\mathrm{SINR}_1 = \frac{\gamma}{1 - \gamma/\mathrm{SINR}_\mathrm{K}} \tag{5.26}$$

where SINR_1 is the SINR in a single user scenario, SINR_K is the signal to MAI ratio in a system of K users.

Let's define γ_r to be the specific received SINR to achieve a desired BER value. According to Eq. (5.26), we get $\mathrm{SINR}_1 = \gamma_r$ when there is only one user in the system. On the other hand, in a system with K users, we have

$$\mathrm{SINR}_1 = \frac{\gamma_r}{1 - \gamma_r/\mathrm{SINR}_\mathrm{K}} \tag{5.27}$$

To study the multiple access performance, we define a DF as in [69][91]. DF measures the additional amount of SINR required by the desired user to overcome the negative effect of MAI caused by the other $K-1$ interfering users.

$$\begin{aligned} \mathrm{DF} &= \frac{\mathrm{SINR}_1 \text{ in a } K\text{-user system}}{\mathrm{SINR}_1 \text{ in a single user system}} \\ &= \frac{1}{1 - \gamma_r/\mathrm{SINR}_\mathrm{K}} \\ &= \frac{1}{1 - \frac{(K-1)\gamma_r}{S^2/\sigma_{I_{M,k}}^2}} \end{aligned} \tag{5.28}$$

5.5.2 Degradation Factor and Number of Users

The number of users K is expressed as a function of DF.

$$K = 1 + \frac{1 - 1/\mathrm{DF}}{\gamma_r} \cdot \frac{S^2}{\sigma^2_{I_{M,k}}} \tag{5.29}$$

where S depends on the instantaneous channel conditions. Therefore K is the number of users can be accommodated under the instantaneous channel conditions. By taking the expectation of K, we get rid of the effect of random channel conditions and get the average number of users.

$$K_{\mathrm{Average}} = \mathrm{E}[K] = 1 + \frac{C_1(1 - 1/\mathrm{DF})}{\gamma_r} \tag{5.30}$$

where $C_1 = \frac{\mathrm{E}[S^2]}{\sigma^2_{I_{M,k}}} = \frac{N_r L_p \mathrm{E}\left[\tilde{g}^2_{L_p-1,0}\right]}{\mathrm{E}[P^2(\Delta T_k)] \sum_{j=0}^{L+L_p-2} \mathrm{E}\left[\tilde{g}^2_{j,k}\right]}$ is a constant for given system parameters.

It is observed in Eq. (5.30) that K_{Average} increases with the growth of DF. However, the number of users is capped with a maximum value when DF tends to infinity, which suggests that the system has its limited capacity for multiple access. From Eq. (5.30), the maximum number of users is

$$K_{\mathrm{Max}} = \lim_{\mathrm{DF}\to\infty} K_{\mathrm{Average}} = 1 + \frac{C_1}{\gamma_r} \tag{5.31}$$

5.6 Numerical Results and Discussion

In Table 5.1, the channel parameters are listed according to [54]. The UWB monocycle is a 2^{nd} derivative of Gaussian with normalized energy, i.e., $z(t) = \varepsilon\left(1 - 4\pi\left(\frac{t-T_p/2}{\tau_p}\right)^2\right)\exp\left(-2\pi\left(\frac{t-T_p/2}{\tau_p}\right)^2\right)$, where $T_p = 0.25$ns, $\tau_p = 0.10275$ns and $\varepsilon = 1.6111 \times 10^5$. The length of the DS sequence is $N_r = 16$. Different values of the data rate increasing factor $N_c = 1, 4, 8, 20$ are used. With the growth of N_c, the data rate R_b increases. For the same N_c value, R_b in CM1 is larger than in CM3 because of the smaller maximum delay spread of CM1.

Table 5.1: The system parameters used in numerical study

System Parameters	CM1	CM3
Γ_1 (cluster power decay factor)	7.1	14
Γ_2 (ray power decay factor)	4.3	7.9
σ_1 (stand. dev. of cluster lognormal fading in dB)	3.3941	3.3941
σ_2 (stand. dev. of ray lognormal fading in dB)	3.3941	3.3941
L (path number)	200	400
R_b (Mbps) when $N_c = 1$	1.25	0.625
R_b (Mbps) when $N_c = 4$	5	2.5
R_b (Mbps) when $N_c = 8$	10	5
R_b (Mbps) when $N_c = 20$	25	12.5

In Fig. 5.1, the theoretical and simulation BER results are shown for a single user scenario in CM1. It is found that the BER value is a concave function of N_c because of the imperfect channel estimation effect. When N_c is small (e.g. $N_c = 1, 4$), AWGN dominates the total noise and SINR can be approximated as $\gamma \approx 2A_0^2 N_r \tilde{g}_{L_p-1,0}^2 / N_0$. The growth of N_c makes A_0^2 grows faster than the decrease of $\tilde{g}_{L_p-1,0}^2$, which results in larger γ and better BER performance. However, the sum of ICI and ISI becomes dominant when N_c is large (e.g. $N_c = 8, 20$). Then SINR can be approximated as $\gamma \approx N_r \tilde{g}_{L_p-1,0}^2 / \sum_{j=2}^{N_c} \tilde{g}_{jL_p-1,0}^2$, and the growth of N_c leads to less desired signal energy and larger ICI and ISI. Therefore BER performance degrades with the growth of N_c.

In Fig. 5.2, the BER performance in multiple user scenario is shown in CM1. In low SNR (E_b/N_0) range, the BER performance of $N_c = 1$ is worse than $N_c = 8$ for both $K = 10, 50$. With the increase of SNR, the BER performance of $N_c = 1$ gets better than $N_c = 8$. This reflects the impact of imperfect channel estimation

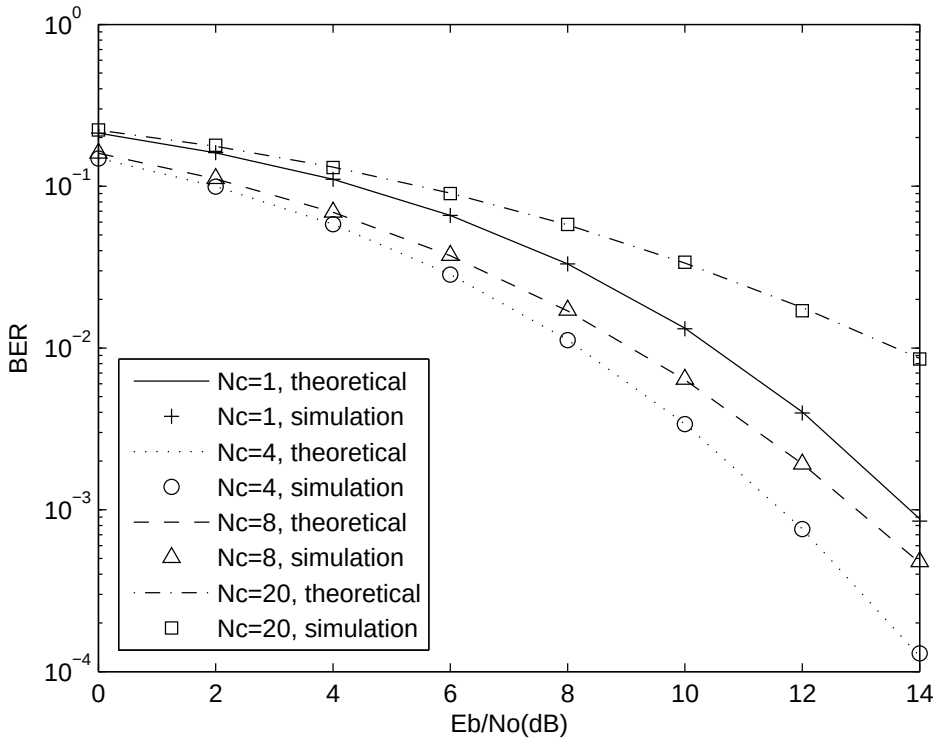

Figure 5.1: BER performance of the Prerake DS UWB system in UWB channel model CM1 under imperfect channel estimation, the data rate increasing factor $N_c = 1, 4, 8, 20$, the number of users $K = 1$, the number of training monocycles $N_t = 100$.

under different SNR. In low SNR range, AWGN dominates the total noise so that the growth of N_c brings better BER performance by decreasing the effect of imperfect channel estimation. On the other hand, the dominating factor in the total noise becomes the sum of ICI, ISI and MAI in high SNR range, so the BER performance of $N_c = 8$ is worse than $N_c = 1$ because of stronger interference brought by larger N_c value. The BER curves of $N_c = 1$ and $N_c = 8$ intersect at about $E_b/N_0 = 12$dB and 8dB for $K = 10$ and 50 respectively. This shows that the growth of SNR brings larger MAI increment when the number of users is larger.

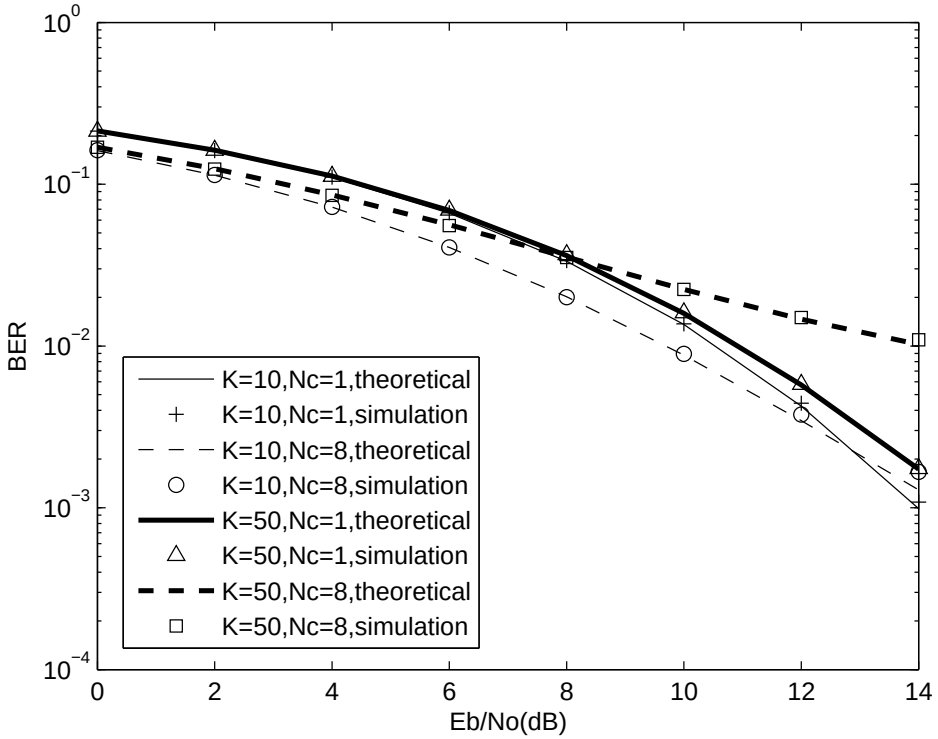

Figure 5.2: BER performance of the Prerake DS UWB system in UWB channel model CM1 under imperfect channel estimation, the data rate increasing factor $N_c = 1, 8$, the number of users $K = 10, 50$, the number of training monocycles $N_t = 100$.

In Fig. 5.3, the BER curves for $K = 50$ in CM1 are plotted under perfect and imperfect channel estimation. As expected, larger N_t brings better BER performance because that the variance of $n_{l,k}$ in Eq. (5.9) gets smaller as N_t increases. For a desired BER of 10^{-3}, the SNR gain between $N_t = 200$ and $N_t = \infty$ is around 3.5dB when $N_c = 1$. Another finding is that when N_c is larger, the BER gap between imperfect and perfect channel estimation becomes smaller. The reason is that larger N_c corresponds to smaller L_p and the impact of imperfect channel estimation is in proportion to L_p.

In Fig. 5.4, the BER performance is depicted as a function of the number

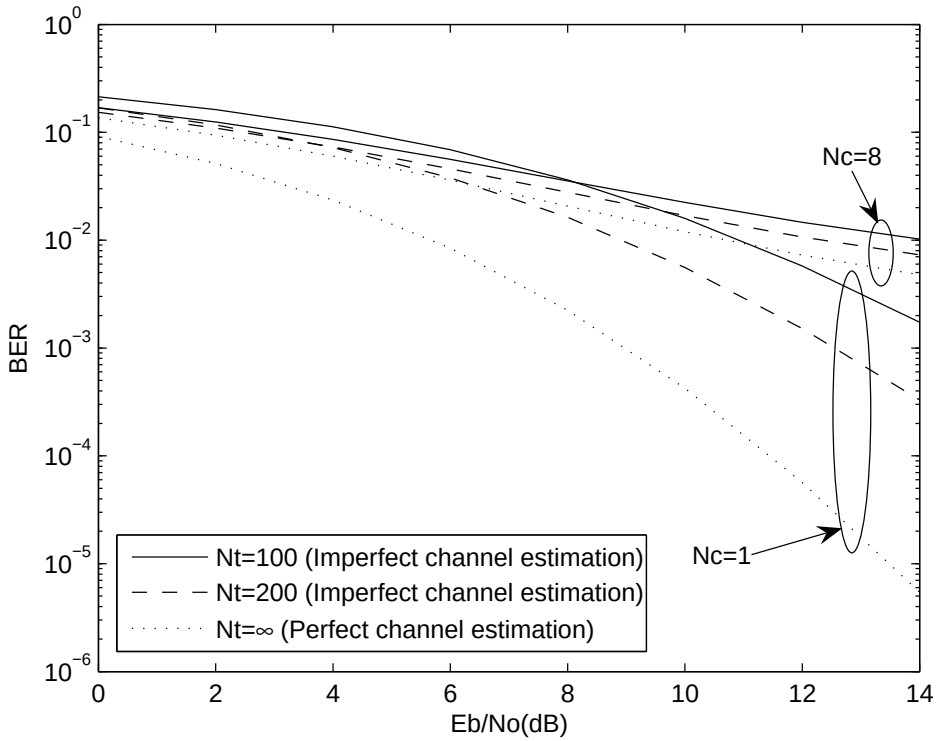

Figure 5.3: BER performance of the Prerake DS UWB system in UWB channel model CM1 under imperfect and perfect channel estimation, the data rate increasing factor $N_c = 1, 8$, the number of users $K = 50$, the number of training monocycles $N_t = 100, 200, \infty$.

of multiple access users under perfect and imperfect channel estimation. The SNR value is fixed as 14dB. With the increase of number of users, the BER value increases as expected. The BER performance in CM3 is better than in CM1 under perfect channel estimation, which is consistent with the results in [92]. When the number of training monocycles in channel estimation $N_t = 100$, the BER performance in CM1 is better than in CM3. This indicates that imperfect channel estimation exerts more unfavorable influence on the BER performance in CM3 due to the larger number of multipaths.

In Fig. 5.5, the number of users K is plotted as a function of DF when

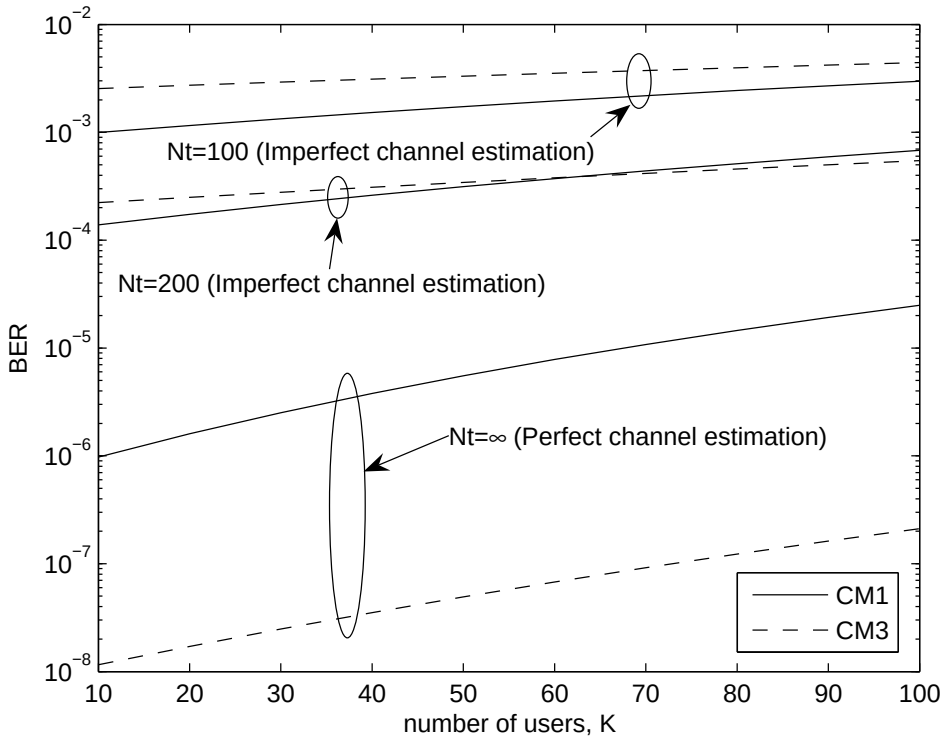

Figure 5.4: BER performance of the Prerake DS UWB system in UWB channel model CM1 and CM3 with different number of users, the data rate increasing factor $N_c = 1$, the number of training monocycles $N_t = 100, 200, \infty$.

the desired BER value is set as 10^{-3}. When $N_c = 1$, the data rate in CM1 is $R_b = 1.25$Mbps, which is twice of the data rate ($R_b = 0.625$Mbps) in CM3. And the maximum number of users that can be supported in CM1 is $K_{\text{Max}} \approx 1655$, which is half of the value in CM3 ($K_{\text{Max}} \approx 3218$). This shows the tradeoff between the data rate per user R_b and number of users K when the system capacity is fully used. Further, we compare the maximum number of users in CM1 and CM3 when the data rate is fixed as $R_b = 5$Mbps. It is found that the maximum number of users in CM1 ($K_{\text{Max}} \approx 400$) is slightly larger than that in CM3 ($K_{\text{Max}} \approx 307$). This could be explained from the viewpoint of the signal energy captured. When $R_b = 5$Mbps, the signal energy on the first $L_p = 50$ paths is combined. In CM1,

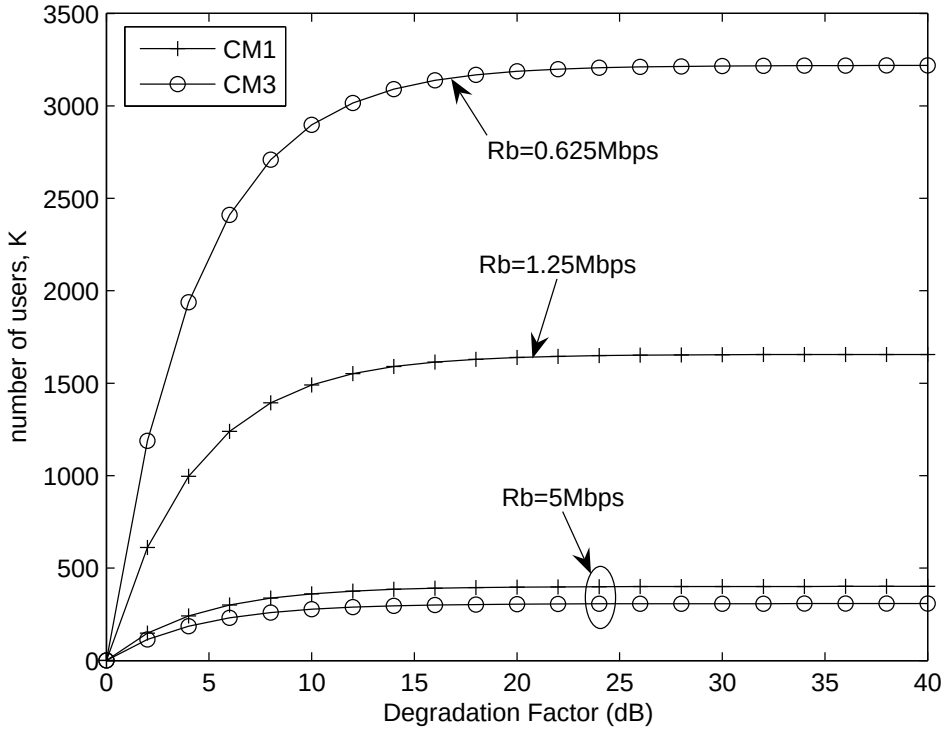

Figure 5.5: The number of users K as a function of degradation factor in CM1 and CM3 under perfect channel estimation. The desired BER is set as 10^{-3}. The data rate increasing factor $N_c = 1, 4, 8$.

the first 50 paths carry around 93% of the total energy. However, the signal energy carried by the first 50 paths in CM3 is only 60% of the total energy.

5.7 Conclusions

We study the performance of Prerake DS UWB multiple access systems under imperfect channel estimation. The analytical signal model of the system is derived, which clearly presents the components of ICI, ISI and MAI. The BER formula is derived based on the signal model and verified by numerical results. Under perfect channel estimation, the BER performance degrades with

the growth of data rate. However, the BER performance does not decrease monotonically with the increase of data rate under imperfect channel estimation. The BER performance depends on the dominant factor in the output SINR, which is a combined result of SNR, channel estimation noise and number of users. Generally, the imperfect channel estimation exerts more unfavorable influence on the BER performance when the data rate is lower or in a channel with larger number of multipaths. By defining a degradation factor, the maximum number of users that can be supported by the systems is derived. And the tradeoff between the data rate and the maximum number of users is illustrated and discussed in detail.

Chapter 6

Design and Analysis of High Data Rate Prerake DS UWB Multiple Access Systems

In this chapter, we propose a novel high data rate Prerake DS UWB multiple access system and analyze its performance. Section 6.1 introduces relevant research and briefly describes principle of the HDR Prerake DS UWB system. The system model is depicted in Section 6.2. In Section 6.3, signal model of the HDR Prerake DS UWB system is elaborated. Distribution of different interference is discussed in Section 6.4. Based on the distribution of interference, the BER formula is derived using the CF method in Section 6.5. Then our analytical derivations are validated by numerical examples in Section 6.6. Finally, conclusions are drawn in Section 6.7.

6.1 Introduction

Using the Prerake combining, the signal energy at the output of the channel focuses in the time domain, which largely reduces the delay spread of the

composite channel (including the prefilter and the actual channel). Though it is claimed by many researchers that the temporal focusing greatly alleviates ISI [85][93][94] and allows high data rate transmission [29] in the UWB communications, little research has been done on the high data rate Prerake UWB systems.

The data rate issue is explicitly discussed only in [28] and [94]. In [94], the conventional TH UWB system and the Prerake TH UWB system is compared under different data rates. And simulation results show that the amount of ISI in the conventional TH UWB system increases much more rapidly than that in the Prerake TH UWB system with the growth of the data rate. Furthermore, the tradeoff between the data rate and system complexity is studied in [28]. It is shown that any required performance of a Prerake UWB system can be achieved by either transmitting with lower data rate or using more transmit antennas. In both [28] and [94], the Prerake UWB system is studied in single user scenario and the performance analysis is done under perfect channel estimation.

In Chapter 5, the tradeoff between the data rate and the BER performance is studied for a Prerake DS UWB multiple access system under imperfect channel estimation. Since the number of paths combined equals to the number of taps in the Prerake filter in this Prerake DS UWB system, we rename it as "Partial-Prerake DS UWB system" to distinguish it from the HDR DS UWB system proposed in this chapter. To increase the data rate of the Partial-Prerake DS UWB system, the number of taps in the Prerake filter is decreased. As a result, the BER performance degrades quickly with the growth of the data rate due to less signal energy captured. In this chapter, we propose a novel HDR Prerake DS UWB system, in which high data rate can be achieved by superposition of chip waveforms. Though the superposed chip waveforms introduce ICI, signal energy focusing helps to keep ICI sufficiently small and guarantees good BER

performance. We analyze the statistical property of ICI and MAI. Then a generalized Gaussian distribution is adopted to well model the distribution of MAI. The BER formula is derived using the CF method described in Chapter 3 and Chapter 4. The accuracy of the BER formula is verified by simulations. Numerical results are provided to compare the performance of the HDR Prerake DS UWB system and the Partial-Prerake DS UWB system. Furthermore, the effect of imperfect channel estimation is discussed in detail.

6.2 System Model

6.2.1 Channel Model

According to [54], the channel impulse response of the k^{th} user is modeled as

$$h^{(k)}(t) = \sum_{l=0}^{L-1} \alpha_{l,k} \delta(t - \tau_{l,k}) \tag{6.1}$$

where L denotes the number of multipaths, $\alpha_{l,k}$ is the lognormal path gain with random phase of ± 1 and $\tau_{l,k}$ stands for the delay of the l^{th} path. For different k and l, $\alpha_{l,k}$ are independent random variables. We consider the resolvable multipath channel [88] with $\tau_{l,k} = \tau_{0,k} + lT_p$, where T_p is the width of the UWB monocycle $z(t)$. Since the multipath components arrive in clusters rather than in a continuum [54], the l^{th} path can be expressed as the j^{th} ray in the i^{th} cluster. Therefore $\tau_{l,k} = \mu_{i,k} + \nu_{j,i,k}$, where $\mu_{i,k}$ is delay of the i^{th} cluster and $\nu_{j,i,k}$ is delay of the j^{th} ray in the i^{th} cluster relative to $\mu_{i,k}$. The power delay profile of the channel is double exponential decaying by rays and clusters. Since the transmitter and receiver are stationary in most PAN applications [54], we assume that the channel remains invariant over a block of symbols.

6.2.2 Transmitted Signal

The transmitted signal due to the k^{th} user is

$$\tilde{s}^{(k)}(t) = A_k \sum_{i=-\infty}^{\infty} b_i^k x_i^{(k)}(t - iT_r) \tag{6.2}$$

where T_r is the symbol duration, A_k denotes the amplitude, $b_i^k \in \{\pm 1\}$ is the i^{th} symbol. The i^{th} symbol waveform of the k^{th} user is

$$x_i^{(k)}(t) = \sum_{n=0}^{N_r-1} a_{i,n}^k g^{(k)}(t - nT_c) \tag{6.3}$$

where N_r is the number of chips in one symbol, $T_c = T_r/N_r$ is the chip duration. Long code is used in this HDR Prerake DS UWB system, and $\{a_{i,n}^k\}_{n=0}^{N_r-1}$ is the random DS signature assigned to the i^{th} symbol of the k^{th} user. The chip waveform $g^{(k)}(t)$ is formed by passing $z(t)$ through a Prerake filter $\tilde{h}^{(k)}(t)$.

$$g^{(k)}(t) = z(t) * \tilde{h}^{(k)}(t) = \sum_{l=0}^{L_p-1} \tilde{\alpha}_{L_p-1-l,k} z(t - lT_p) \tag{6.4}$$

where $z(t)$ is the energy-normalized UWB monocycle of duration T_p. The Prerake filter $\tilde{h}^{(k)}(t) = \sum_{l=0}^{L_p-1} \tilde{\alpha}_{L_p-1-l,k}\delta(t - lT_p)$ contains L_p taps. In $\tilde{h}^{(k)}(t)$, $\{\tilde{\alpha}_{l,k}\}_{l=0}^{L_p-1}$ is the estimated value of path gain $\{\alpha_{l,k}\}_{l=0}^{L_p-1}$. The amplitude $A_k = \sqrt{E_p \Big/ \sum_{l=0}^{L_p-1} \mathrm{E}\left[\tilde{\alpha}_{l,k}^2\right]}$ to keep the average transmitted symbol energy constant as $E_b = N_r E_p$.

6.2.3 Received Signal

The received signal due to the k^{th} user is given by

$$r^{(k)}(t) = \tilde{s}^{(k)}(t) * h^{(k)}(t) = A_k \sum_{i=-\infty}^{\infty} b_i^k \underbrace{\left[x_i^{(k)}(t - iT_r) * h^{(k)}(t)\right]}_{\tilde{x}_i^{(k)}(t-iT_r)} \tag{6.5}$$

where $\tilde{x}_i^{(k)}(t)$ is obtained using Eq. (6.3) as

$$\tilde{x}_i^{(k)}(t) \triangleq x_i^{(k)}(t) * h^{(k)}(t) = \sum_{n=0}^{N_r-1} a_{i,n}^k \underbrace{\left[g^{(k)}(t - nT_c) * h^{(k)}(t)\right]}_{\tilde{g}^{(k)}(t-nT_c)} \tag{6.6}$$

As shown in Eq. (6.6), $\tilde{g}^{(k)}(t) \triangleq g^{(k)}(t) * h^{(k)}(t)$ is the channel response of a chip waveform $g^{(k)}(t)$.

The total received signal in a K-user system is given by

$$r(t) = \sum_{k=0}^{K-1} r^{(k)}(t - \tau_{0,k}) + n(t) \tag{6.7}$$

where $n(t)$ is AWGN with double-sided PSD $N_0/2$ and $\tau_{0,k}$ denotes the transmission delay of the k^{th} user. Since random DS sequences/data symbols of ± 1 are assumed, the interfering users appear to the desired user as essentially transmitting random ± 1 sequences and the boundaries of interfering symbols do not matter in asynchronous transmission. This property allows us to assume that $\tau_{0,k}$ is uniformly distributed in $[0, T_c)$.

6.2.4 Channel Estimation

The estimated path gain $\{\tilde{\alpha}_{l,k}\}_{l=0}^{L_p-1}$ is obtained by sending N_t pilot UWB monocycles $z(t)$. The repetition interval of the pilot monocycles is larger than the maximum delay spread of the channel to avoid interference between pilot pulses. During the channel estimation period of the k^{th} user, all other users keep silent. Assuming perfect synchronization, the base station correlates and samples at the tap rate on the i^{th} received pilot monocycle to get the estimated path gain on the first L_p paths.

$$\tilde{\alpha}_{l,k}(i) = \int_{lT_p}^{(l+1)T_p} \left(\sum_{l'=0}^{L-1} \alpha_{l',k} z(t - l'T_p) + n_i(t) \right) z(t - lT_p) dt \tag{6.8}$$

Then N_t estimation results are averaged to obtain the estimated path gain.

$$\tilde{\alpha}_{l,k} = \frac{1}{N_t} \sum_{i=0}^{N_t-1} \tilde{\alpha}_{l,k}(i) = \alpha_{l,k} + n_{l,k} \tag{6.9}$$

where $n_{l,k}$ is the channel estimation noise on the l^{th} path and it follows Gaussian distribution with zero mean and variance of $N_0/(2N_t)$. When $N_t \to \infty$, the variance of $n_{l,k} \to 0$ and the channel estimation tends to the perfect estimation.

6.3 Signal Modeling and Decision Statistics

6.3.1 Signal Structure

Let one chip contain L_c taps, i.e., $T_c = L_c T_p$. The data rate is $R_b = 1/(N_r L_c T_p)$. For given N_r and T_p, higher data rate R_b can be achieved by decreasing L_c.

In the Partial-Prerake DS UWB system discussed in Chapter 5, L_c equals the number of taps in the Prerake filter L_p, and the signal energy captured equals the maximal ratio combining on the first L_p paths. So the captured signal energy in the Partial-Prerake DS UWB system is reduced with the decrease of L_c (or the increase of R_b). As shown in [92], the BER performance of the Partial-Prerake DS UWB system degrades rapidly with the increase of the data rate.

In this chapter, we propose to set L_p to a large value while keeping L_c sufficiently small, i.e., $L_p > L_c$. With a large L_p, more signal energy is captured to guarantee satisfying BER performance. With a small L_c, higher data rate R_b is achieved via superposition of chip waveforms. Comparison of the chip structure in the HDR Prerake and Partial-Prerake schemes is shown in Fig. 6.1, where the chip duration in the unit of taps is $L_c = 4$. As shown, $g^{(k)}(t)$ in the HDR Prerake scheme contains more taps ($L_p = 6$) than in the Partial-Prerake scheme ($L_p = 4$). The difference between the two schemes is: In the HDR Prerake scheme, the chip waveforms overlap with each other to shorten the chip duration, while in the Partial-Prerake scheme, the chip waveform is tailored to fit the chip duration.

6.3.2 Signal Modeling

For the k^{th} user, the path gain and the estimated path gain used in the Prerake filter are defined as vectors $\boldsymbol{\alpha}_k$ and $\tilde{\boldsymbol{\alpha}}_k$ respectively.

$$\boldsymbol{\alpha}_k = \begin{pmatrix} \alpha_{0,k} & \alpha_{1,k} & \cdots & \alpha_{L-1,k} \end{pmatrix}^T$$

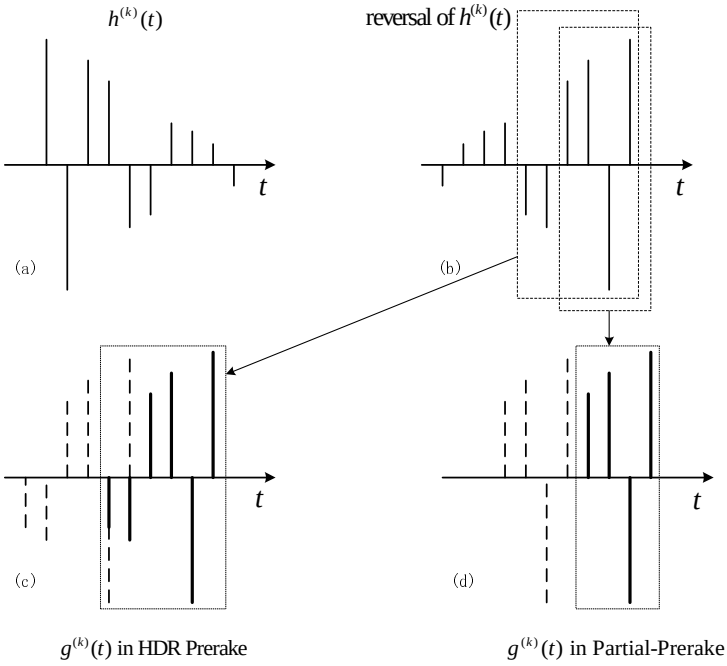

Figure 6.1: Comparison of HDR Prerake and Partial-Prerake schemes, (a) is the channel impulse response $h^{(k)}(t)$ with $L = 10$, (b) is the reversal of $h^{(k)}(t)$, (c) is the structure of two chips (one in dashed lines, the other in solid lines) in the HDR Prerake scheme, with $L_c = 4$, $L_p = 6$, (d) is the structure of two chips (one in dashed lines, the other in solid lines) in the Partial-Prerake scheme, with $L_c = L_p = 4$.

$$\tilde{\boldsymbol{\alpha}}_k = \begin{pmatrix} \tilde{\alpha}_{L_p-1,k} & \tilde{\alpha}_{L_p-2,k} & \cdots & \tilde{\alpha}_{0,k} \end{pmatrix}^T \tag{6.10}$$

$\tilde{g}^{(k)}(t)$ in Eq. (6.6) is discretized by $\tilde{g}_{j,k} = \int_{jT_p}^{(j+1)T_p} \tilde{g}^{(k)}(t) z(t - jT_p) dt$ and expressed as

$$\tilde{\mathbf{g}}_k = \mathbf{T}_{\boldsymbol{\alpha}_k} \tilde{\boldsymbol{\alpha}}_k = \begin{pmatrix} \tilde{g}_{0,k} & \tilde{g}_{1,k} & \cdots & \tilde{g}_{L+L_p-2,k} \end{pmatrix}^T \tag{6.11}$$

where $\mathbf{T}_{\boldsymbol{\alpha}_k}$ is a $(L + L_p - 1) \times L_p$ Toeplitz matrix with $\boldsymbol{\alpha}_k$ as the first L elements in its 0^{th} column and zero elsewhere.

The effect of imperfect channel estimation is included in $\tilde{\mathbf{g}}_k$ due to the channel

estimation noise brought by $\tilde{\boldsymbol{\alpha}}_k$. The element $\tilde{g}_{L_p-1,k} = \sum_{l=0}^{L_p-1} \alpha_{l,k}\tilde{\alpha}_{l,k}$ is the desired peak, which is equivalent to the maximal ratio combining on the first L_p paths. Obviously, larger L_p leads to more signal energy captured. However, overall channel estimation noise increases with the growth of L_p, since total L_p paths are to be estimated.

We first consider the signal model on the chip level and then extend the results to the symbol level. In the HDR Prerake scheme, any chip is interfered by its following n_1 chips and its previous n_2 chips, where $n_1 \triangleq \lfloor \frac{L_p-1}{L_c} \rfloor$ and $n_2 \triangleq \lfloor \frac{L-2}{L_c} \rfloor + 1$. Assume the n^{th} chip of the i^{th} symbol from the k^{th} user is the desired chip, which has a phase of $a_{i,n}^k b_i^k$. Similarly, we write the phase of each interfering chip into a sequence $\{c_{i,n}^k(0), c_{i,n}^k(1), \cdots, c_{i,n}^k(n_1+n_2)\}$. In this sequence, $c_{i,n}^k(n_2) = a_{i,n}^k b_i^k$ is the phase of the desired chip. $\{c_{i,n}^k(0), \cdots, c_{i,n}^k(n_2-1)\}$ and $\{c_{i,n}^k(n_2+1), \cdots, c_{i,n}^k(n_1+n_2)\}$ stand for the phases of the n_2 and n_1 interfering chips before and after the desired chip respectively.

The desired chip is expressed by a vector $\mathbf{r}_{i,n}^k$ as below. Each chip consists of L_c taps, and the peak is included in the last tap r_{i,n,L_c-1}^k.

$$\mathbf{r}_{i,n}^k = \begin{pmatrix} r_{i,n,0}^k & r_{i,n,1}^k & \cdots & r_{i,n,L_c-1}^k \end{pmatrix}^T = A_k \mathbf{T}_{\mathbf{C}_{i,n}^k} \hat{\mathbf{g}}_k \tag{6.12}$$

where $\mathbf{T}_{\mathbf{C}_{i,n}^k} = \mathbf{C}_{i,n}^k \otimes \mathbf{I}_{L_c}$ is a $L_c \times (n_1+n_2+1)L_c$ Toeplitz matrix, $\otimes$ means Kronecker product, $\mathbf{I}_x$ is the identity matrix of size $x \times x$. $\mathbf{C}_{i,n}^k$ is a $1 \times (n_1+n_2+1)$ vector built by reversing the phase sequence related to the desired chip as $\mathbf{C}_{i,n}^k = \begin{pmatrix} c_{i,n}^k(n_1+n_2) & c_{i,n}^k(n_1+n_2-1) & \cdots & c_{i,n}^k(0) \end{pmatrix}$. $\hat{\mathbf{g}}_k$ is a $(n_1+n_2+1)L_c \times 1$ vector obtained by extending $\tilde{\mathbf{g}}_k$ as $\hat{\mathbf{g}}_k = \begin{pmatrix} \mathbf{0}_{|L_p-(n_1+1)L_c|}^T & \tilde{\mathbf{g}}_k^T & \mathbf{0}_{n_2L_c-L+1}^T \end{pmatrix}^T$, where $\mathbf{0}_x$ denotes the zero row vector with x elements.

6.3.3 Decision Statistics

Assume the desired symbol is the 0^{th} symbol of the 0^{th} user. With perfect synchronization, the 0^{th} receiver performs correlation on the N_r peaks in the received signal $r(t)$. The output decision statistic is expressed as

$$\begin{aligned} Z &= \underbrace{\int_{(L_p-L_c)T_p}^{(L_p-L_c)T_p+N_rT_c} r^{(0)}(t)v^{(0)}(t)dt}_{S+I_C} \\ &\quad + \underbrace{\int_{(L_p-L_c)T_p}^{(L_p-L_c)T_p+N_rT_c} \sum_{k=1}^{K-1} r^{(k)}(t-\tau_{0,k})v^{(0)}(t)dt}_{I_M} \\ &\quad + \underbrace{\int_{(L_p-L_c)T_p}^{(L_p-L_c)T_p+N_rT_c} n(t)v^{(0)}(t)dt}_{N} \end{aligned} \tag{6.13}$$

where $v^{(0)}(t) = \sum_{n=0}^{N_r-1} a_{0,n}^0 z(t-nT_c-(L_p-1)T_p)$ is the template waveform used in the 0^{th} receiver. Z is decomposed as desired signal S, inter-chip interference I_C, multiple access interference I_M and AWGN term N.

A. Desired Signal and Inter-Chip Interference

The sum of S and I_C is given by

$$S+I_C = \sum_{n=0}^{N_r-1} \underbrace{\int_{(L_p-L_c)T_p+nT_c}^{(L_p-L_c)T_p+(n+1)T_c} r^{(0)}(t)a_{0,n}^0 z(t-nT_c-(L_p-1)T_p)dt}_{S(n)+I_C(n)} \tag{6.14}$$

As shown in Eq. (6.14), the detection of a symbol is decomposed as the detection of N_r chips. In the n^{th} chip detection, $S(n)$ and $I_C(n)$ is expressed as

$$\begin{aligned} S(n)+I_C(n) &= \mathbf{v}_{0,n}^0 \mathbf{r}_{0,n}^0 \\ &= \underbrace{A_0 \mathbf{v}_{0,n}^0 \mathbf{T}_{\mathbf{C}_{0,n}^0} \hat{\mathbf{g}}_0'}_{S(n)} + \underbrace{A_0 \mathbf{v}_{0,n}^0 \mathbf{T}_{\mathbf{C}_{0,n}^0} (\hat{\mathbf{g}}_0 - \hat{\mathbf{g}}_0')}_{I_C(n)} \end{aligned} \tag{6.15}$$

where $\mathbf{v}_{0,n}^0 = \begin{pmatrix} \mathbf{0}_{L_c-1} & a_{0,n}^0 \end{pmatrix}$ is the discrete format of the template waveform in the n^{th} chip detection. Since $\tilde{g}_{L_p-1,0}$ is the peak containing the desired signal

energy, $\hat{\mathbf{g}}_0'$ is obtained by setting all elements in $\hat{\mathbf{g}}_0$ as zeros except the element $\tilde{g}_{L_p-1,0}$.

B. Multiple Access Interference

Similar to the analysis of MAI in Chapter 5, we consider the effect of imperfect channel estimation in I_M for completeness. From Eq. (6.13), I_M is given by

$$I_M = \sum_{k=1}^{K-1} \sum_{n=0}^{N_r-1} \underbrace{\int_{(L_p-L_c)T_p+nT_c}^{(L_p-L_c)T_p+(n+1)T_c} r^{(k)}(t-\tau_{0,k}) a_{0,n}^0 z(t-nT_c-(L_p-1)T_p) dt}_{I_M^k(n)} \quad (6.16)$$

where $I_M^k(n)$ is the interference from the k^{th} interfering user in the n^{th} chip detection.

The asynchronous delay $\tau_{0,k}$ is split as $\tau_{0,k} = \gamma_k T_p + \Delta T_k$, where $\gamma_k \in \{0, 1, \cdots, L_c - 1\}$ and $\Delta T_k \in [0, T_p)$, both with uniform distribution. The autocorrelation functions of $z(t)$ is defined as $P(x) = \int_0^x z(t) z(t + T_p - x)\, dt$. Then $I_M^k(n)$ is expressed as

$$I_M^k(n) = \mathbf{v}_{0,n}^0 \mathbf{r}_{0,n}^k(\gamma_k + 1) P(\Delta T_k) + \mathbf{v}_{0,n}^0 \mathbf{r}_{0,n}^k(\gamma_k) P(T_p - \Delta T_k) \quad (6.17)$$

where

$$\mathbf{r}_{0,n}^k(x) = \begin{cases} \begin{pmatrix} r_{0,n-1,L_c-x}^k & \cdots & r_{0,n-1,L_c-1}^k & r_{0,n,0}^k & \cdots & r_{0,n,L_c-1-x}^k \end{pmatrix}^T & n \neq 0 \\ \begin{pmatrix} r_{-1,N_r-1,L_c-x}^k & \cdots & r_{-1,N_r-1,L_c-1}^k & r_{0,0,0}^k & \cdots & r_{0,0,L_c-1-x}^k \end{pmatrix}^T & n = 0 \end{cases} \quad (6.18)$$

6.4 Distribution of Interference

In Eq. (6.15), we observe that $I_C(n)$ is the summation of $\tilde{g}_{j,0}$ with random phases, where $j = L_p - 1 + xL_c$, $x \in \{-n_1, \cdots, n_2\}$ and $x \neq 0$ (which means the peak $\tilde{g}_{L_p-1,0}$ is not contained). Similarly, it is observed from Eq. (6.17) and Eq. (6.18) that $I_M^k(n)$ can be decomposed as summation of elements in $\tilde{\mathbf{g}}_k$, which are sampled

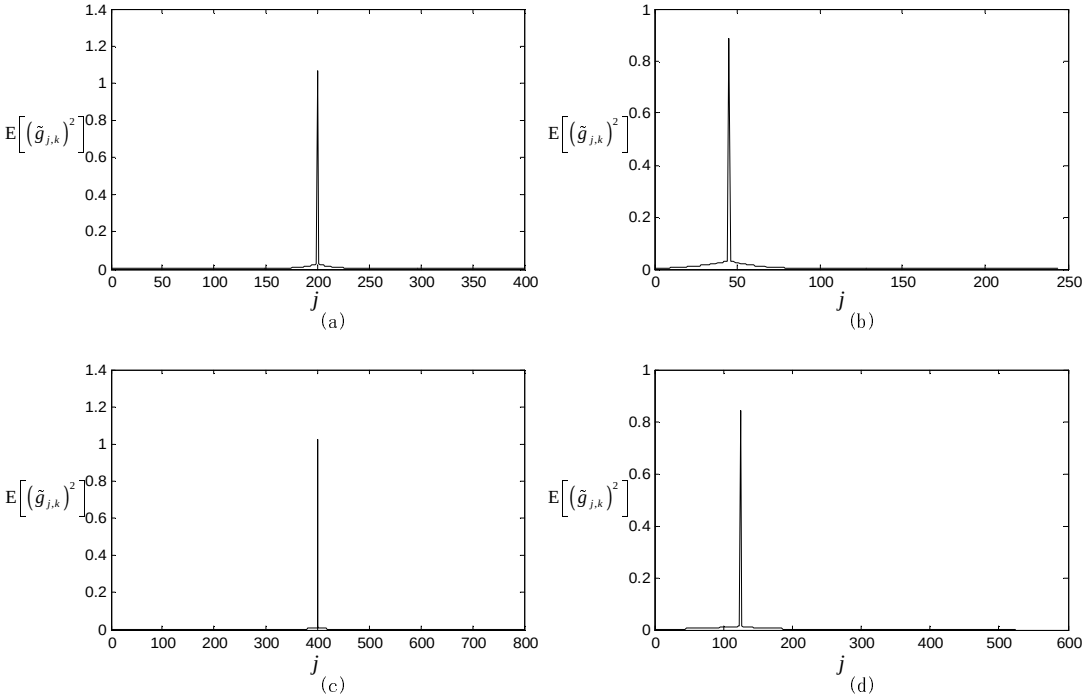

Figure 6.2: The variance of $\tilde{g}_{j,k}$, (a) is in CM1, $L_p = 200$ with perfect channel estimation ($N_t = \infty$), (b) is in CM1, $L_p = 45$ with imperfect channel estimation ($N_t = 200$), (c) is in CM3, $L_p = 400$ with perfect channel estimation ($N_t = \infty$), (d) is in CM3, $L_p = 125$ with imperfect channel estimation ($N_t = 200$).

by the interval of L_c with random phases and the autocorrelation effect added. Because of the random asynchronous delay $\tau_{0,k}$, $I_M^k(n)$ contains the peak $\tilde{g}_{L_p-1,k}$. Then I_C and I_M are obtained by summation of $I_C(n)$ and $I_M^k(n)$ respectively.

The distribution of I_C and I_M depends on the distribution of $\tilde{g}_{j,k}$. The variance of $\tilde{g}_{j,k}$ in several cases is plotted in Fig. 6.2, which reflects the energy focusing in received Prerake UWB signals. In all cases, the peak $\tilde{g}_{L_p-1,k}$ has a remarkably large variance, while the variance of the non-peaks $\tilde{g}_{j,k}$ with $j \neq L_p - 1$ is much smaller.

Since I_C does not contain the peak, the terms in the summation are with relatively similar variance. Therefore we can use the central limit theorem (CLT) to approximate I_C as a Gaussian random variable. In contrast, I_M contains the peak $\tilde{g}_{L_p-1,k}$, which is a dominant term in the summation because of its distinguishing variance. Thus the basis of the CLT is violated, and the Gaussian distribution may not fit the distribution of I_M well. Therefore, we propose to use a generalized Gaussian distribution to fit the distribution of I_M.

In Appendix A, the evaluation of the expectation values related to $\tilde{g}_{j,k}$ is provided, which will be used in the derivation of variance and higher order moment of I_C and I_M.

6.4.1 Inter-Chip Interference

Since I_C is modeled as a Gaussian random variable, we need to evaluate the mean and variance of I_C. It is easy to show the mean of $\{I_C(n)\}_{n=0}^{N_r-1}$ is zero and for different n, $I_C(n)$ are independent conditioned on $\boldsymbol{\alpha}_0$ and $\tilde{\boldsymbol{\alpha}}_0$. Therefore the mean of I_C is zero. The variance of I_C conditioned on $\boldsymbol{\alpha}_0$ and $\tilde{\boldsymbol{\alpha}}_0$ is given by

$$\begin{aligned}
\sigma_{I_C}^2 &= N_r \sigma_{I_C(n)}^2 \\
&= N_r A_0^2 \mathrm{E}\left[\mathbf{v}_{0,n}^0 \mathbf{T}_{\mathbf{C}_{0,n}^0}(\hat{\mathbf{g}}_0 - \hat{\mathbf{g}}_0')(\hat{\mathbf{g}}_0 - \hat{\mathbf{g}}_0')^T \mathbf{T}_{\mathbf{C}_{0,n}^0}^T (\mathbf{v}_{0,n}^0)^T\right] \\
&= N_r A_0^2 \sum_{\substack{x=-n_2 \\ x\neq 0}}^{n_1} \tilde{g}_{L_p-1-xL_c}^2
\end{aligned} \tag{6.19}$$

6.4.2 Multiple Access Interference

As well as I_C, it is easy to find that I_M is a zero mean random variable. Since the peak $\tilde{g}_{L_p-1,k}$ is a dominant term in $I_M^k(n)$, we use a generalized Gaussian distribution [95] to fit the distribution of I_M instead of the conventionally used Gaussian distribution. The generalize Gaussian distribution is a general

distribution that encompasses many important distributions (e.g., Gaussian and Laplace distribution). The PDF of a zero mean generalized Gaussian random variable x is

$$f_X(x) = a\exp(-b^\zeta|x|^\zeta), \quad -\infty < x < \infty, \quad \zeta > 0 \tag{6.20}$$

where $a = \sqrt{\frac{b\zeta}{2\Gamma(1/\zeta)}}$, $b = \frac{1}{\sigma}\sqrt{\frac{\Gamma(3/\zeta)}{\Gamma(1/\zeta)}}$, σ^2 is the variance, ζ denotes the shape parameter, the gamma function is defined as $\Gamma(z) = \int_0^\infty t^{z-1}e^{-t}dt$. Note that $\zeta = 1$ and 2 yields Laplace and Gaussian PDF respectively.

There are several methods to evaluate the parameter ζ in the generalized Gaussian distribution [96]. We adopt the moment matching method with kurtosis ratio in our analysis. The n^{th} moment of the zero mean generalized Gaussian distribution is given by

$$\mathrm{E}\left[x^n\right] = \begin{cases} 0 & n = 1, 3, 5, \cdots \\ \sigma^n \frac{\Gamma((n+1)/\zeta)}{\Gamma^{n/2}(3/\zeta)\Gamma^{1-n/2}(1/\zeta)} & n = 2, 4, 6, \cdots \end{cases} \tag{6.21}$$

Substitute Eq. (6.21) into the definition of kurtosis, we get

$$\mathcal{K}(\zeta) = \frac{\mathrm{E}[x^4]}{(\mathrm{E}[x^2])^2} = \frac{\Gamma(5/\zeta)\Gamma(1/\zeta)}{\Gamma^2(3/\zeta)} \tag{6.22}$$

To determine the distribution of I_M, we calculate the variance and 4^{th} moment of I_M and substitute them into Eq. (6.22) to find the generalized Gaussian distribution parameter ζ. We compute the variance and 4^{th} moment of $I_M^k(n)$ first, and then extend the results to obtain the variance and 4^{th} moment of I_M.

The variance of $I_M^k(n)$ is evaluated as

$$\begin{aligned} \sigma^2_{I_M^k(n)} &= \frac{2}{L_c}\mathrm{E}\left[P^2(\Delta T_k)\right]\mathrm{E}\left[(\mathbf{r}_{i,n}^k)^T\mathbf{r}_{i,n}^k\right] \\ &= \frac{2A_k^2}{L_c}\mathrm{E}\left[P^2(\Delta T_k)\right]\sum_{j=0}^{L+L_p-2}\mathrm{E}\left[\tilde{g}_{j,k}^2\right] \end{aligned} \tag{6.23}$$

The variance of I_M is given by

$$\sigma^2_{I_M} = (K-1)\sigma^2_{I^k_M} = (K-1)N_r\sigma^2_{I^k_M(n)} \tag{6.24}$$

The 4^{th} moment of $I^k_M(n)$ is evaluated by

$$\begin{aligned}
\mathrm{E}\left[\left(I^k_M(n)\right)^4\right] &= \frac{2}{L_c}\mathrm{E}\left[P^4(\Delta T_k)\right]\mathrm{E}\left[\sum_{m=0}^{L_c-1}(r^k_{i,n,m})^4\right] \\
&= \frac{2A^4_k}{L_c}\mathrm{E}\left[P^4(\Delta T_k)\right]\sum_{j=0}^{L+L_p-2}\mathrm{E}\left[\tilde{g}^4_{j,k}\right] \\
&\quad + \frac{6A^4_k}{L_c}\mathrm{E}\left[P^4(\Delta T_k)\right]\sum_{m=0}^{L_c-1}\sum_{x=-(n_1+1)}^{n_2-1}\sum_{\substack{x'=-(n_1+1)\\x'\neq x}}^{n_2-1}\mathrm{E}\left[\tilde{g}^2_{L_p+xL_c+m}\tilde{g}^2_{L_p+x'L_c+m}\right]
\end{aligned}$$

The 4^{th} moment of I^k_M is calculated as

$$\begin{aligned}
\mathrm{E}\left[\left(I^k_M\right)^4\right] &= \frac{2A^4_k\left(N_r+3N_r(N_r-1)\right)}{L_c}\mathrm{E}\left[P^4(\Delta T_k)\right]\mathrm{E}\left[\tilde{g}^4_{j,k}\right] \\
&\quad + \frac{6A^4_kN^2_r}{L_c}\mathrm{E}\left[P^4(\Delta T_k)\right]\sum_{m=0}^{L_c-1}\sum_{x=-(n_1+1)}^{n_2-1}\sum_{\substack{x'=-(n_1+1)\\x'\neq x}}^{n_2-1}\mathrm{E}\left[\tilde{g}^2_{L_p+xL_c+m}\tilde{g}^2_{L_p+x'L_c+m}\right]
\end{aligned}$$

The 4^{th} moment of I_M is obtained by

$$\mathrm{E}\left[(I_M)^4\right] = (K-1)\mathrm{E}\left[\left(I^k_M\right)^4\right] + 3(K-1)(K-2)N_r\sigma^2_{I^k_M(n)} \tag{6.25}$$

6.5 BER Performance Analysis

Denote the total noise $\varsigma = I_C + I_M + N$, where I_C, I_M and N are independent zero mean random variables. As mentioned in Section 6.4, I_C is assumed to be Gaussian distributed and I_M is modeled as a generalized Gaussian random variable. Then we use the CF method to derive the BER formula.

The characteristic function of the sum of $I_C + N$ is given by

$$\Phi_{I_C+N}(\omega) = \exp\left(-\frac{\omega^2(\sigma^2_{I_C}+\sigma^2_N)}{2}\right) \tag{6.26}$$

The characteristic function of I_M is obtained by taking a Fourier transform on the generalized Gaussian PDF as below.

$$\begin{aligned}\Phi_{I_M}(\omega) &= \int_{-\infty}^{\infty} a\exp\left(-b^{\zeta}|m|^{\zeta}\right)\exp(j\omega m)dm \\ &= 2\int_{0}^{\infty} a\exp\left(-b^{\zeta}m^{\zeta}\right)\cos(\omega m)dm \end{aligned} \tag{6.27}$$

The characteristic function of ς equals to the product of $\Phi_{I_C+N}(\omega)$ and $\Phi_{I_M}(\omega)$ because I_C, I_M and N are independent.

$$\Phi_{\varsigma}(\omega) = \Phi_{I_C+N}(\omega)\Phi_{I_M}(\omega) \tag{6.28}$$

The distribution of ς is obtained by performing an inverse Fourier transform on $\Phi_{\varsigma}(\omega)$.

$$\begin{aligned} f_{\varsigma}(x) &= \frac{1}{2\pi}\int_{-\infty}^{\infty}\Phi_{\varsigma}(\omega)\exp(-j\omega x)d\omega \\ &= \int_{0}^{\infty}\frac{a\exp\left(-b^{\zeta}m^{\zeta}\right)}{\sqrt{2\pi(\sigma_{I_C}^2+\sigma_N^2)}}\left[\exp\left(-\frac{(m+x)^2}{2(\sigma_{I_C}^2+\sigma_N^2)}\right)+\exp\left(-\frac{(m-x)^2}{2(\sigma_{I_C}^2+\sigma_N^2)}\right)\right]dm \end{aligned} \tag{6.29}$$

The instantaneous desired signal S is given by

$$S = N_r S(n) = N_r A_0 \mathbf{v}_0 \mathbf{T}_{\mathbf{a}_{0,0}}\tilde{\mathbf{g}}_0' = N_r A_0 b_0^0 \tilde{g}_{L_p-1,0} \tag{6.30}$$

The instantaneous BER is derived by substituting Eq. (6.29) into the following integration.

$$\begin{aligned} P_{\text{Instant}} &= \frac{1}{2} - \int_0^{|S|} f_{\varsigma}(x)dx \\ &= \frac{1}{2} - \frac{a}{2}\int_0^{\infty}\exp\left(-b^{\zeta}m^{\zeta}\right)\text{erf}\left(\frac{m+|S|}{\sqrt{2(\sigma_{I_C}^2+\sigma_N^2)}}\right)dm \\ &\quad -\frac{a}{2}\int_0^{|S|}\exp\left(-b^{\zeta}m^{\zeta}\right)\text{erf}\left(\frac{|S|-m}{\sqrt{2(\sigma_{I_C}^2+\sigma_N^2)}}\right)dm \\ &\quad +\frac{a}{2}\int_{|S|}^{\infty}\exp\left(-b^{\zeta}m^{\zeta}\right)\text{erf}\left(\frac{m-|S|}{\sqrt{2(\sigma_{I_C}^2+\sigma_N^2)}}\right)dm \end{aligned} \tag{6.31}$$

The average BER is obtained by averaging P_{Instant} over the lognormal fading channel. In the numerical analysis, we compute the average BER in the lognormal multipath fading channels using the Monte Carlo method.

6.6 Numerical Results and Discussion

According to [54], the channel parameters are listed in Table 6.1. We adopt a commonly used 2^{nd} Gaussian derivative UWB monocycle $z(t) = \varepsilon\left[1-4\pi\left(\frac{t-T_p/2}{\tau_p}\right)^2\right]\exp\left[-2\pi\left(\frac{t-T_p/2}{\tau_p}\right)^2\right]$ with normalized energy, where $T_p = 0.25$ns, $\tau_p = 0.10275$ns and $\varepsilon = 1.6111 \times 10^5$. The length of the DS sequence is set as $N_r = 16$. We study the system performance under two high data rate settings: $R_b = 25$Mbps (i.e., $L_c = 10$) and $R_b = 50$Mbps (i.e., $L_c = 5$).

Table 6.1: The system parameters used in numerical study

System Parameters	CM1	CM3
Γ_1 (cluster power decay factor)	7.1	14
Γ_2 (ray power decay factor)	4.3	7.9
σ_1 (stand. dev. of cluster lognormal fading term in dB)	3.3941	3.3941
σ_2 (stand. dev. of ray lognormal fading term in dB)	3.3941	3.3941
L (path number)	200	400

6.6.1 Distribution of Interference

In Fig. 6.3, the distribution of MAI is examined in CM1 under perfect channel estimation ($N_t = \infty$), where number of users $K = 4$, $R_b = 50$Mbps and $L_p = 200$ (100% of the total signal energy captured). The PDF of I_M obtained by simulation data is marked as "simulation PDF". The theoretical PDF of

the Gaussian distribution obtained by $\sigma^2_{I_M}$ is plotted for comparison. Similarly, the theoretical PDF of the generalized Gaussian distribution is also plotted, where $\sigma^2_{I_M}$ and $\mathrm{E}\left[(I_M)^4\right]$ are calculated to obtain the parameter ζ. It is clearly shown that the generalized Gaussian distribution fits the simulation PDF of I_M much more accurately than the Gaussian distribution in most of the value range. Though the generalized Gaussian distribution does not match well with the simulation PDF at the center (i.e., around 0), it should be emphasized that the tail of the interference distribution is of the most important interest in BER calculation (involving the tail integral) especially when SNR is medium or high. Therefore the mismatch around the center does not affect much in the BER performance evaluation.

Similarly, the distribution of MAI in CM3 under imperfect channel estimation ($N_t = 200$) with number of users $K = 4$, $R_b = 25$Mbps and $L_p = 125$ (around 90% of the total signal energy captured) is plotted in Fig. 6.4. Under imperfect channel estimation, the generalized Gaussian distribution also provides good fitting to the distribution of I_M, while the Gaussian distribution does not match well with the simulation PDF again.

In Fig. 6.5, the distribution of ICI is plotted in CM3 under imperfect channel estimation ($N_t = 200$) with number of users $K = 4$, $R_b = 25$Mbps and $L_p = 125$ (around 90% of the total signal energy captured). This figure shows that the PDF of I_C obtained by the simulation almost fits well with the theoretical Gaussian distribution obtained using $\sigma^2_{I_C}$. Under perfect channel estimation, we can get similar results to show that I_C is well approximated as Gaussian distributed.

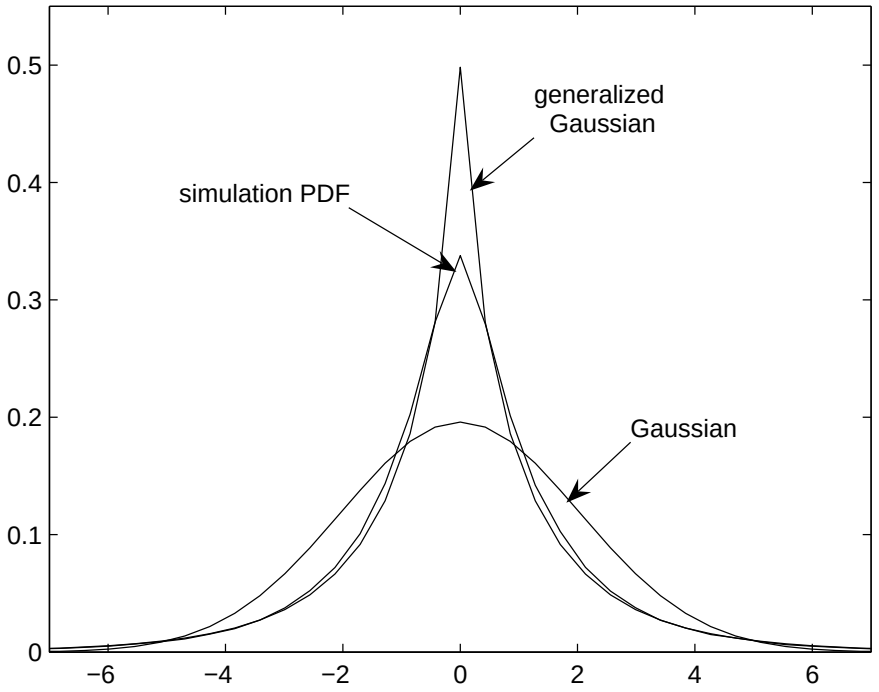

Figure 6.3: Comparison of the simulation PDF of I_M and its generalized Gaussian fitting and Gaussian fitting in CM1, $R_b = 50$Mbps, $L_p = 200$, $L_c = 5$, perfect channel estimation ($N_t = \infty$), 4 users.

6.6.2 BER Performance

In Fig. 6.6, the BER performance comparison of the HDR Prerake DS UWB system and the Partial-Prerake DS UWB system is provided. The data rate is set as $R_b = 25$Mbps, i.e., $L_c = 10$. It is shown that the HDR Prerake DS UWB system achieves much better BER performance than the Partial-Prerake DS UWB system under both perfect and imperfect channel estimation. The reason lies in the different amount of signal energy captured in these two systems. In the Partial-Prerake DS UWB system, $L_p = L_c = 10$ means that the signal energy on the first 10 paths are captured only (around 43% of the total signal energy).

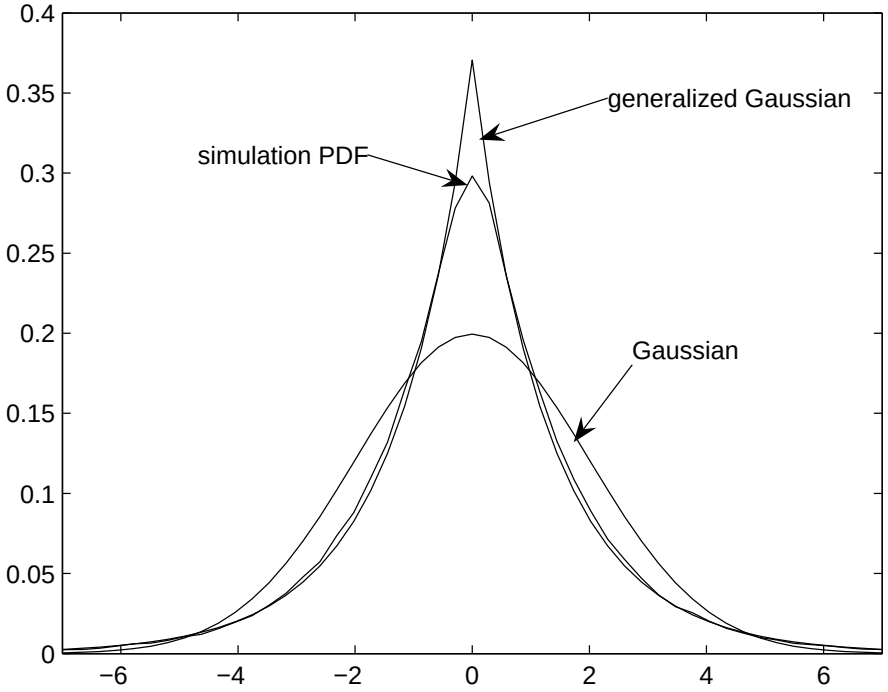

Figure 6.4: Comparison of the simulation PDF I_M and its generalized Gaussian fitting and Gaussian fitting in CM3, $R_b = 25$Mbps, $L_p = 125$, $L_c = 10$, imperfect channel estimation ($N_t = 200$), 4 users.

In contrast, we set $L_p = 45 > L_c$ in the HDR Prerake DS UWB system. So the signal energy on the first 45 paths are captured (around 90% of the total signal energy) while keeping the same data rate as 25Mbps.

In Fig. 6.7 and Fig. 6.8, the comparison of the accuracy of the CF and GA methods in the theoretical BER calculation is provided. In Fig. 6.7, the theoretical BER calculated using Eq. (6.31) (derived using the CF method) matches well with the simulation results in CM1 under perfect channel estimation when $R_b = 50$Mbps. In contrast, the theoretical BER computed using the GA method (where I_M is approximated as Gaussian distributed random variable) deviates from the simulation results in medium and high E_b/N_0 range. Similar

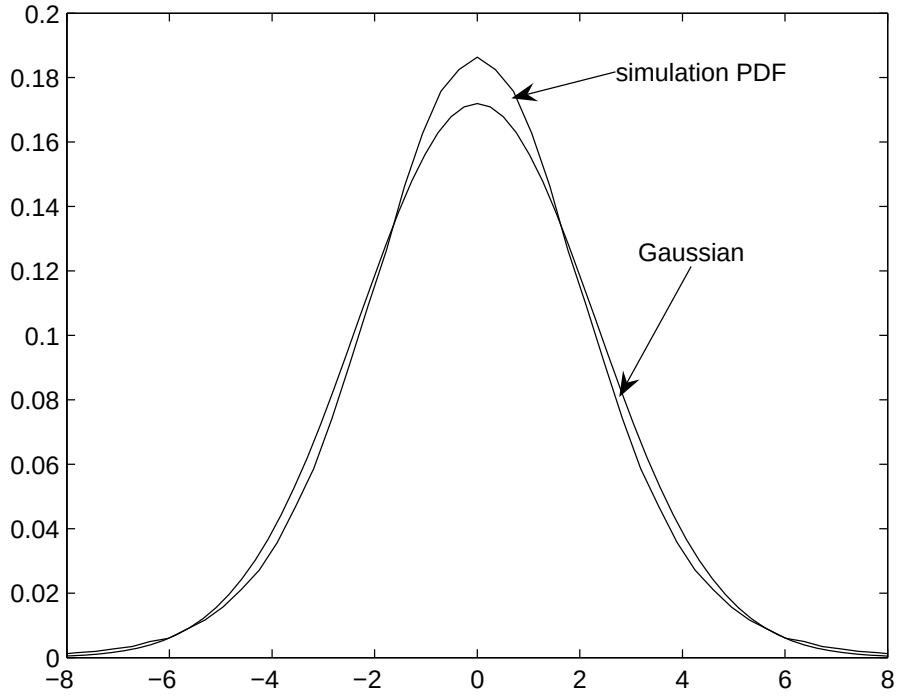

Figure 6.5: Comparison of the simulation PDF of I_C and its Gaussian fitting in CM3, $R_b = 25$Mbps, $L_p = 125$, $L_c = 10$, imperfect channel estimation ($N_t = 200$), 4 users.

results are observed in Fig. 6.8, where data rate is set as $R_b = 25$Mbps in CM3 under imperfect channel estimation. Fig. 6.7 and Fig. 6.8 justify the rationality of the generalized Gaussian distribution assumption for the distribution of MAI from another viewpoint, which is consistent with Fig. 6.3 and Fig. 6.4.

6.6.3 Effect of Imperfect Channel Estimation

In Fig. 6.9, the effect of imperfect channel estimation is illustrated in CM1. The number of taps in the Prerake filter takes two values: $L_p = 45$ means around 90% of the total signal energy is captured, while $L_p = 200$ means signal energy

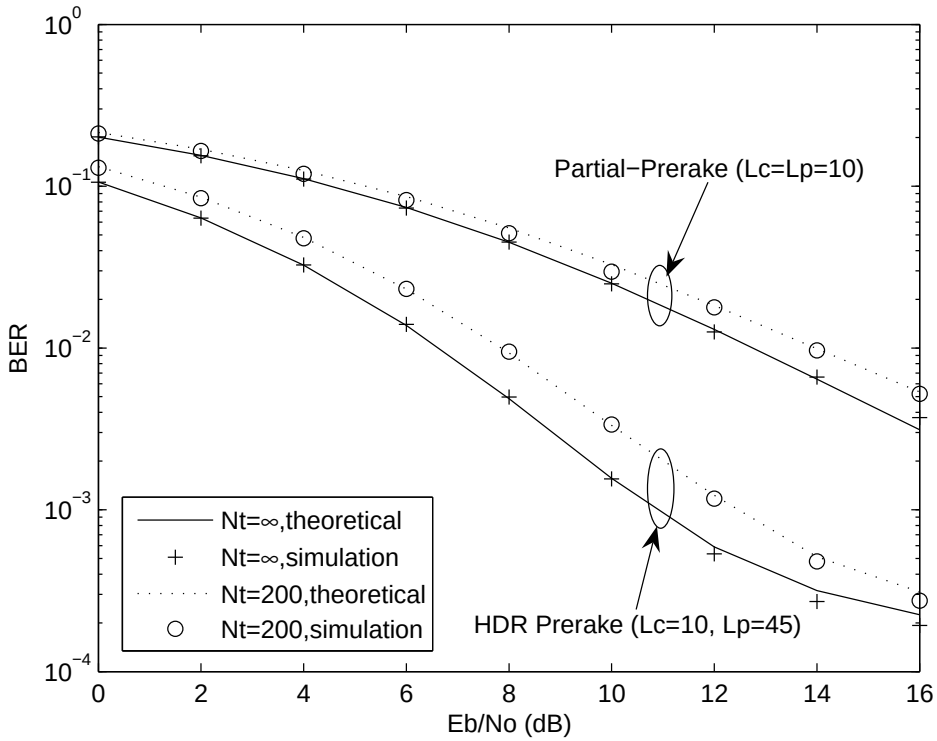

Figure 6.6: BER performance comparison of the HDR Prerake DS UWB system and the Partial-Prerake DS UWB system in CM1, $R_b = 25$Mbps, under both perfect ($N_t = \infty$) and imperfect channel estimation ($N_t = 200$).

on all paths (100%) is combined. Under perfect channel estimation ($N_t = \infty$), the larger L_p gives better BER performance. Conversely, the smaller L_p yields better BER performance when the channel estimation is imperfect ($N_t = 200$). This observation can be explained by the channel estimation noise $n_{l,k}$ in Eq. (6.9). When the channel estimation is perfect, larger L_p brings better BER performance because of more signal energy captured. However, under imperfect channel estimation, channel estimation noise $n_{l,k}$ is added to each estimated path (as shown in Eq. (6.9)), therefore larger L_p brings more channel estimation noise.

In Fig. 6.10, the multiple access performance of the HDR Prerake and Partial-Prerake DS UWB systems is plotted. The transmission SNR is $E_b/N_0 =$

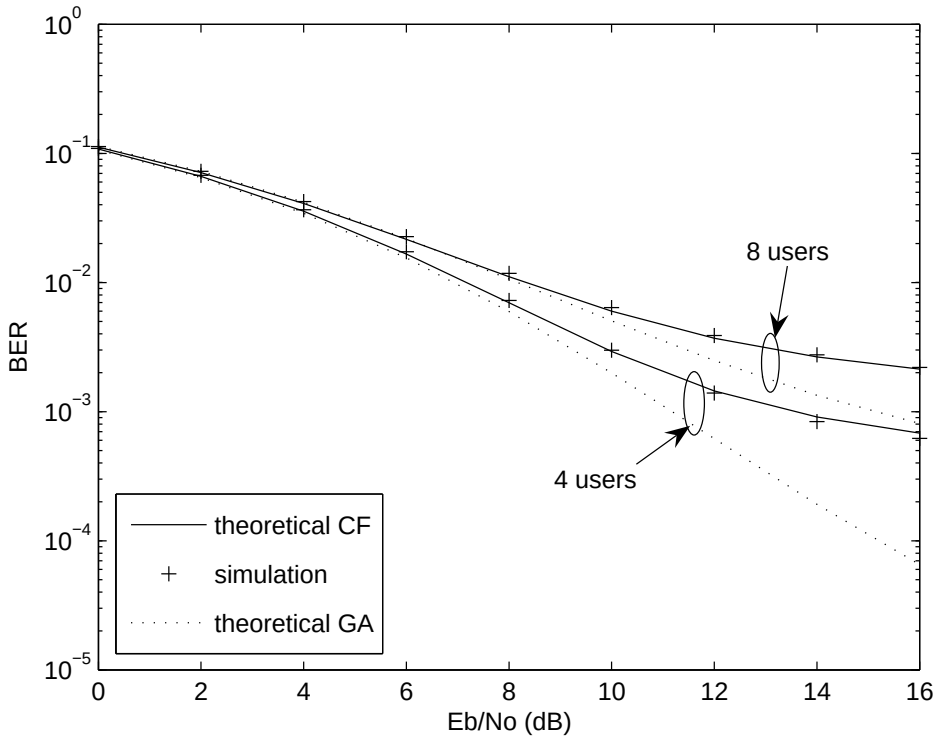

Figure 6.7: Comparison of the accuracy of the GA and the CF methods in BER calculation under perfect channel estimation ($N_t = \infty$) in CM1, $R_b = 50$Mbps, $L_p = 45$, the number of users $K = 4$ and 8 respectively.

16dB. The data rate is $R_b = 25$Mbps. The multiple access performance of the Partial-Prerake DS UWB system is unacceptable because of too small amount of the signal energy captured. For the HDR Prerake DS UWB system, the overall BER performance in an acceptable range (BER$\leq 10^{-3}$) in CM3 is better than in CM1, which is consistent with the results in [92]. Under perfect channel estimation and with a fixed BER value of 10^{-3}, 35 users can be supported in CM3, while only 22 users can be supported in CM1 by the HDR Prerake DS UWB system. This implies that better multiple access performance can be achieved in a denser multipath environment because of the higher degree of the multipath diversity. When the channel estimation is imperfect ($N_t = 200$), the number of

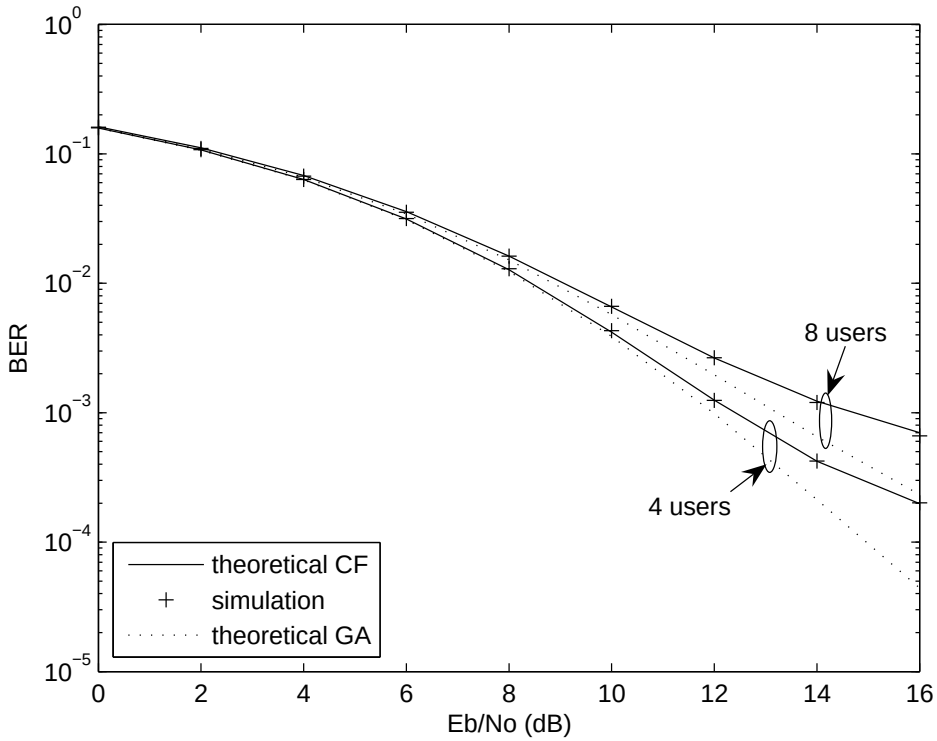

Figure 6.8: Comparison of the accuracy of the GA and the CF methods in BER calculation under imperfect channel estimation ($N_t = 200$) in CM3, $R_b = 25$Mbps, $L_p = 125$, the number of users $K = 4$ and 8 respectively.

users that can be supported by the HDR Prerake DS UWB system at the BER value of 10^{-3} is 16 and 19 for CM1 and CM3 respectively. It is observed that in the HDR Prerake DS UWB system, the performance degradation brought by the imperfect channel estimation is greater in CM3 than in CM1. The reason is that the channel estimation noise is proportional to the number of taps in Prerake filter L_p (or the number of paths to be combined).

In Fig. 6.11, the output SNIR $S^2/\left(\sigma_{I_C}^2 + \sigma_{I_M}^2 + \sigma_N^2\right)$ is plotted versus the number of taps L_p in the Prerake filter. Four different values of N_t are used: $N_t = 200, 500, 1000, \infty$. The larger value of N_t means that the smaller channel estimation noise $n_{l,k}$ is added to each estimated path (refer to Eq. (6.9)). As a

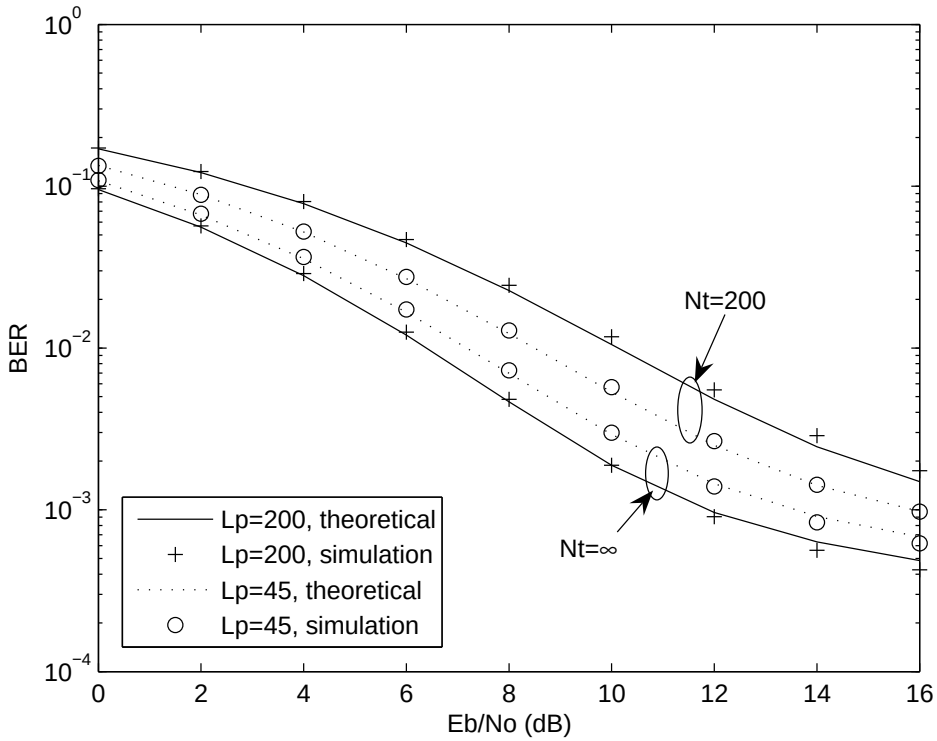

Figure 6.9: The effect of imperfect channel estimation ($N_t = 200$) with different number of taps L_p in Prerake filter in CM1, $R_b = 50$Mbps, $L_c = 5$, 4 users.

result, larger N_t brings overall higher output SNIR. One important finding is that the output SNIR is a convex function of L_p under imperfect channel estimation ($N_t \neq \infty$) and an optimal L_p exists. This can be explained by the tradeoff between the signal energy captured and the channel estimation noise introduced. Since the power decay profile of UWB channels is double exponential decaying by rays and clusters, the signal energy captured does not increase linearly with the growth of L_p. On the other hand, the channel estimation noise is linearly proportional to L_p. Therefore in practical system design, appropriate value of L_p should be chosen to capture enough signal energy while keeping the effect of imperfect channel estimation tolerable. Though the theoretical derivation of

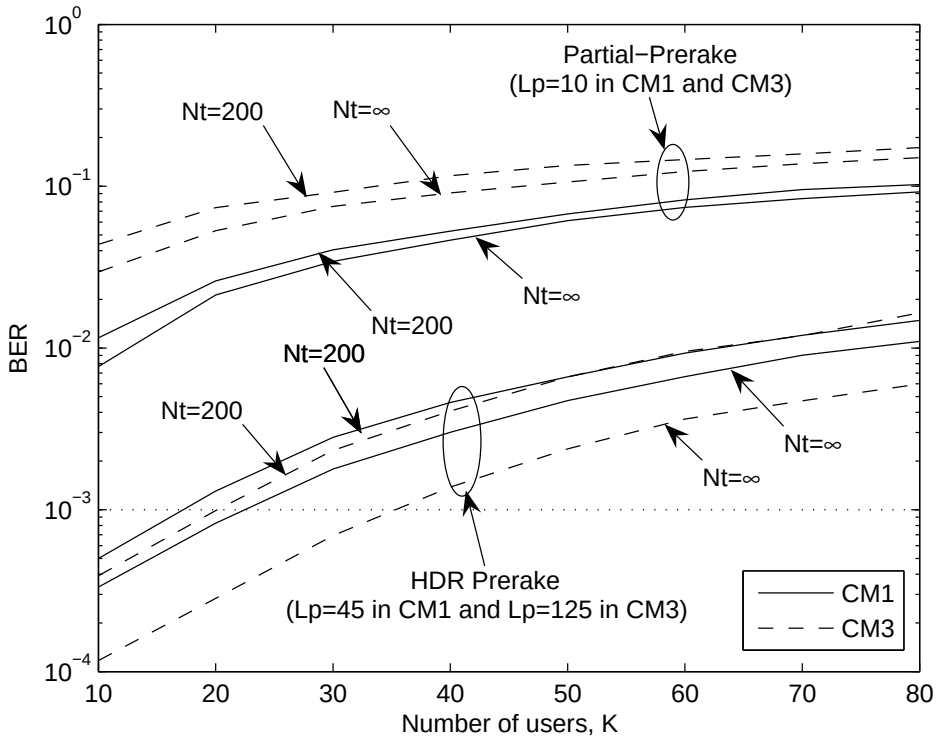

Figure 6.10: Multiple access performance of the HDR Prerake DS UWB system and the Partial-Prerake DS UWB system under perfect ($N_t = \infty$) **and imperfect channel estimation** ($N_t = 200$)**,** $R_b = 25$**Mbps,** $L_c = 10$**,** $E_b/N_0 = 16dB$**.**

optimal L_p is intractable, it is found that 90% signal energy capturing is a good choice for Prerake filter design in our extensive experiments.

6.7 Conclusions

A novel HDR Prerake DS UWB multiple access system is proposed. Its main advantage is that high data rate can be achieved without much degradation of the BER performance. We present simulation results to show that the HDR Prerake DS UWB system significantly outperforms the conventional Partial-Prerake DS

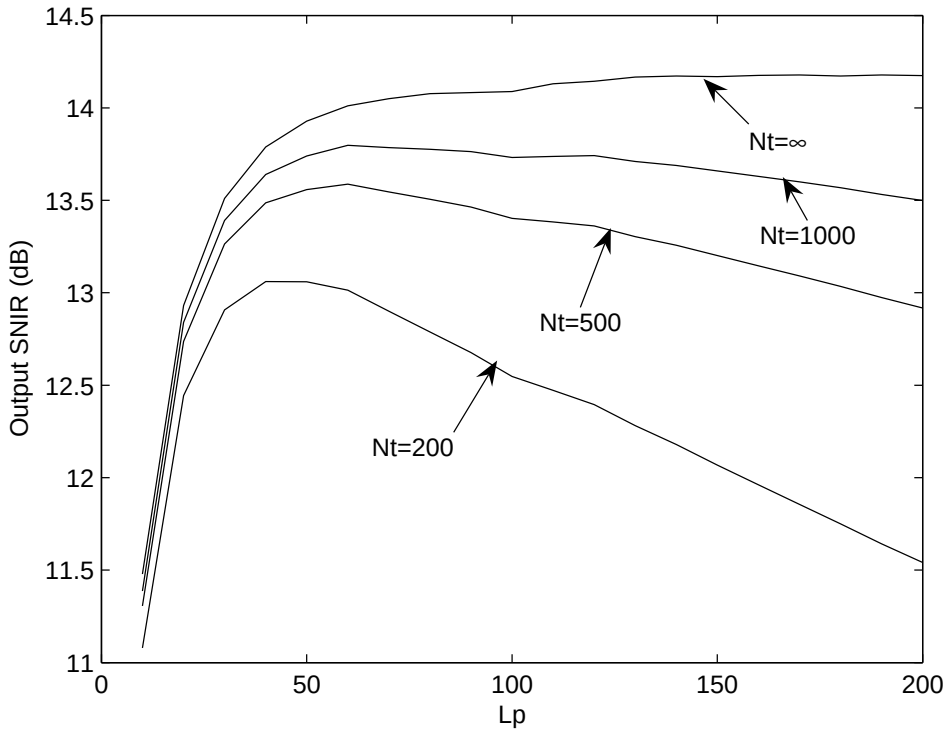

Figure 6.11: The output SNIR as a function of number of taps L_p in the Prerake filter under perfect ($N_t = \infty$) and imperfect channel estimation ($N_t = 200, 500, 1000$) with $E_b/N_0 = 16$dB in CM1, $R_b = 50$Mbps, 4 users.

UWB system in high data rate scenario. We study the statistical property of the interference and use the generalized Gaussian distribution to fit the distribution of MAI more accurately. Then the BER formula is derived using the CF method. Numerical results verify that our BER formula is more accurate compared with the BER evaluation using the GA method. The effect of imperfect channel estimation is illustrated to show the tradeoff between signal energy captured and channel estimation noise introduced, which implies that the Prerake filter should contain only those taps carrying most of the energy under imperfect channel estimation.

Chapter 7

Conclusions and Future Work

In this thesis, we study two important topics in DS UWB communication systems. Firstly, we derive the accurate BER formula using the CF method. Secondly, we design two DS UWB multiple access systems using Prerake combining for medium/high data rate transmission.

A novel BER evaluation method based on the characteristic function is proposed for the DS UWB multiple access systems using PAM/PPM schemes. Instead of approximating the total noise, including MAI, SI and AWGN, as Gaussian distributed, we derive the characteristic function of each term and find the exact PDF of the total noise. Then accurate BER formula is obtained based on exact PDF of the total noise. We carry out the comparison on accuracy of the CF method and the GA method under both perfect and imperfect power control in AWGN channels at first. The analytical and simulation results show that the CF method yields accurate BER values in both cases. In contrast, the GA method does not work well in medium and high SNR range. Accuracy of the GA method largely depends on the dominant component in the total noise. Next, we extend the exact BER analysis to the more practical lognormal multipath fading channels. Similarly, the CF method outperforms the GA method with more

accurate BER calculation. Furthermore, BER performance of DS PAM UWB and DS PPM UWB systems are accurately compared using the BER formula derived. It is found that DS PAM UWB system steadily outperforms DS PPM UWB system.

We design two Prerake DS UWB multiple access systems for medium and high data rate transmission respectively. In both Prerake DS UWB systems, the temporal reverse channel impulse response is used as a prefilter at the transmitter. In the first proposed Prerake DS UWB system, we cut the temporal reverse channel impulse response to fit the duration of the chip. The analytical signal model of the system is derived, which clearly presents the components of ICI, ISI and MAI. We derive the BER formula and verify it by numerical results. It is found that the BER performance does not decrease monotonically with the increase of data rate under imperfect channel estimation. And the BER performance depends on the dominant factor in the output SINR, which is a combined result of SNR, channel estimation noise and number of users. We derive the maximum number of users using the degradation factor. The numerical results further show the tradeoff between the data rate and the maximum number of users supported by the systems. In the second proposed HDR Prerake DS UWB system, we remove the constraint between the data rate and energy capture existing in the first proposed Prerake DS UWB system and largely improve the system performance in high data rate transmission. We investigate the statistical property of the interference and use a generalized Gaussian distribution to fit the distribution of MAI more accurately. Based on the CF method, an accurate BER formula is derived. Further, the effect of imperfect channel estimation is studied. It is found that the Prerake filter should contain only those taps carrying most of the energy to avoid the malign effect of channel estimation noise.

The following issues are to be studied in the future.

Firstly, though the exact PDF of the total noise in DS UWB systems can be expressed using the characteristic functions, there is no closed form for its exact distribution. Some preliminary study on the asymptotic distribution of the correlation receiver output has been conducted for TH UWB systems in [9]. More effort could be made in interference modeling for DS UWB systems, which provides curial theoretical basis for interference suppression.

Secondly, it is found that channel estimation plays an important role in Prerake DS UWB systems performance. Therefore, a good channel estimation method deserves further exploration. Besides the time domain channel estimation, the combined frequency domain channel estimation/equalization [89] could be a promising candidate to achieve better system performance.

Thirdly, channel information feedback from the transmitter to the receiver could be an expensive overhead in Prerake DS UWB systems. To overcome this problem, a study [87] suggests to use the channel phase information to build the Prerake filter. However, less energy is combined in this scheme, which leads to performance degradation. Therefore, how to decrease the feedback workload without sacrifice system performance is an interesting open question.

Bibliography

[1] "Revision of part 15 of the commission's rules regarding ultra-wideband transmission systems: First report and order," Federal Communications Commission, ET-Docket 98-153, FCC 02-8, Tech. Rep., Apr 2002.

[2] I. F. Akyildiz, W. Su, Y. Sankarasubramaniam, and E. Cayirci, "A survey on sensor networks," *IEEE Communications Magazine*, vol. 40, no. 8, pp. 102–114, 2002.

[3] R. A. Scholtz, "Multiple access with time-hopping impulse modulation," in *IEEE Military Communications Conference*, 1993, pp. 447–450.

[4] L. Zhao, A. M. Haimovich, and H. Grebel, "Performance of ultra-wideband communications in the presence of interference," in *IEEE International Conference on Communications*, Jun 2001, pp. 2948–2952.

[5] L. Piazzo, "Performance analysis and optimization for impulse radio and direct-sequence impulse radio in multiuser interference," *IEEE Transaction on Communications*, vol. 52, no. 5, pp. 801–810, May 2004.

[6] N. Boubaker and K. B. Letaief, "Ultra wideband DSSS for multiple access communications using antipodal signaling," in *IEEE International Conference on Communications*, May 2003, pp. 2197–2201.

[7] ——, "Performance analysis of DS-UWB multiple access under imperfect power control," *IEEE Transactions on Communications*, vol. 52, no. 9, pp. 1459–1463, Sep 2004.

[8] G. Durisi and G. Romano, "On the validity of gaussian approximation to characterize the multiuser capacity of UWB TH PPM," in *IEEE Conference on Ultra Wideband Systems and Technologies*, May 2002, pp. 157–161.

[9] J. Fiorina and W. Hachem, "On the asymptotic distribution of the correlation receiver output for time-hopped UWB signals," *IEEE Transactions on Signal Processing*, vol. 54, no. 7, pp. 2529–2545, July 2006.

[10] T. W. Barrett, "History of ultra wideband (UWB) radar and communications: Pioneers and innovators," in *Proceedings of Progress in Electromagnetics Symposium*, 2000.

[11] M. Z. Win and R. A. Scholtz, "Ultra-wide bandwidth time-hopping spread-spectrum impulse radio for wireless multiple-access communications," *IEEE Transactions on Communications*, vol. 48, no. 4, pp. 679–689, Apr 2000.

[12] M. Z. Win, G. Chrisikos, and N. R. Sollenberger, "Performance of RAKE reception in dense multipath channels: implications of spreading bandwidth and selection diversity order," *IEEE Journal on Selected Areas in Communications*, vol. 18, no. 8, pp. 1516–1525, Aug 2000.

[13] J. D. Choi and W. E. Stark, "performance of ultra-wideband communications with suboptimal receivers in multipath channels," *IEEE Journal on Selected Areas in Communications*, vol. 20, no. 9, pp. 1754–1766, Dec 2002.

[14] V. Lottici, A. D'Andrea, and U. Mengali, "Channel estimation for ultra-wideband communications," *IEEE Journal on Selected Areas in Communications*, vol. 20, pp. 1638–1645, 2002.

[15] M. Z. Win and R. A. Scholtz, "Characterization of ultra-wide bandwidth wireless indoor channels: a communication-theoretic view," *IEEE Journal on Selected Areas in Communications*, vol. 20, no. 9, pp. 1613–1627, Dec 2002.

[16] R. T. Hoctor and H. W. Tomlinson, "Delay-hopped transmitted-reference RF communications," in *IEEE Conference on Ultra Wideband Systems and Technologies*, 2002, pp. 265–270.

[17] Z. Xu and B. M. Sadler, "Multiuser transmitted reference ultra-wideband communication systems," *IEEE Journal on Selected Areas in Communications*, vol. 24, no. 4, pp. 766–772, Apr 2006.

[18] R. Fleming, C. Kushner, G. Roberts, and U. Nandiwada, "Rapid acquisition for Ultra-wideband localizers," in *IEEE Conference on Ultra Wideband Systems and Technologies*, 2002, pp. 245–250.

[19] B. M. Sadler and A. Swami, "On the performance of episodic UWB and direct-sequence communication systems," *IEEE Transactions on Wireless Communications*, vol. 3, no. 6, pp. 2246–2255, Nov 2004.

[20] V. Venkatesan, H. Liu, C. Nilsen, R. Kyker, and M. E. Magana, "Performance of an optimally spaced PPM ultra-wideband system with direct sequence spreading for multiple access," in *IEEE Vehicular Technology Conference*, Oct 2003, pp. 602–606.

[21] J. R. Foerster, "The performance of a direct-sequence spread ultra-wideband system in the presence of multipath, narrowband interference, and

multiuser interference," in *IEEE Conference on Ultra Wideband Systems and Technologies*, May 2002, pp. 87–91.

[22] G. Durisi and S. Benedetto, "Performance evaluation of TH-PPM UWB systems in the presence of multiuser interference," *IEEE Communications Letters*, vol. 7, no. 5, pp. 224–226, May 2003.

[23] A. F. Molisch and J. R. Foerster, "Channel models for ultrawideband personal area networks," *IEEE Wireless Communications*, pp. 14–21, Dec 2003.

[24] D. Cassioli, M. Z. Win, and A. F. Molisch, "The ultra-wide bandwidth indoor channel: from statistical model to simulations," *IEEE Journal on Selected Areas in Communications*, vol. 20, no. 6, pp. 1247–1257, Aug 2002.

[25] K. Usuda, H. Zhang, and M. Nakagawa, "Pre-RAKE diversity combining for UWB systems in IEEE 802.15 UWB multipath channel," in *IEEE Wireless Communications and Networking Conference*, May 2004, pp. 236–240.

[26] S. Imada and T. Ohtsuki, "Pre-RAKE diversity combining for UWB systems in IEEE 802.15 UWB multipath channel," in *Conference on Ultrawideband Systems and Technologies Joint with International Workshop on Ultra Wideband Systems*, May 2004, pp. 236–240.

[27] S. Zhao and H. Liu, "Prerake diversity combining for pulsed UWB systems considering realistic channels with pulse overlapping and narrow-band interference," in *IEEE Global Telecommunications Conference*, Nov 2005, pp. 3784–3788.

[28] M. Emami, M. Vu, J. Hansen, A. J. Paulraj, and G. Papanicolaou, "Matched filtering with rate back-off for low complexity communications in very large delay spread channels," in *Asilomar Conference on Signals, Systems and Computers*, Nov 2004, pp. 218–222.

[29] T. Strohmer, M. Emami, J. Hansen, G. Papanicolaou, and A. J. Paulraj, "Application of time-reversal with MMSE equalizer to UWB communications," in *IEEE Global Telecommunications Conference*, Nov 2004, pp. 3123–3127.

[30] R. Esmailzadeh, E. Sourour, and M. Nakagawa, "PreRAKE diversity combining in time-division duplex CDMA mobile communications," *IEEE Transactions on Vehicular Technology*, vol. 48, no. 3, pp. 795–801, May 1999.

[31] N. B. Harum, Y. Tamura, S. P. W. Jarot, R. Esmailzadeh, and M. Nakagawa, "Analysis of performance degradation due to channel estimation error in Pre-Rake TDD/CDMA," in *IEEE International Symposium on Personal, Indoor and Mobile Radio Communications*, Sep 2003, pp. 921–925.

[32] M. Z. Win and R. A. Scholtz, "Impulse radio: how it works," *IEEE Communications Letters*, vol. 2, no. 2, pp. 36–38, Feb 1998.

[33] D. C. Laney, G. M. Maggio, F. Lehmann, and L. Larson, "Multiple access for UWB impulse radio with pseudochaotic time hopping," *IEEE Journal on Selected Areas in Communications*, vol. 20, no. 9, pp. 1692–1700, Dec 2002.

[34] A. Rajeswaran, V. S. Somayazulu, and J. R. Foerster, "RAKE performance for a pulse based UWB system in a realistic UWB indoor channel," in *IEEE International Conference on Communications*, May 2003, pp. 2879–2883.

[35] A. Batra, J. Balakrishnan, G. R. Aiello, J. R. Foerster, and A. Dabak, "Design of a multiband OFDM system for realistic UWB channel environments," *IEEE Transactions on Microwave Theory and Techniques*, vol. 52, pp. 2123–2138, Sep 2004.

[36] U. Onunkwo, Y. Li, and A. Swami, "Effect of timing jitter on OFDM-based UWB systems," *IEEE Journal on Selected Areas in Communications*, vol. 24, pp. 787–793, Apr 2006.

[37] Y. G. Li, A. F. Molisch, and J. Zhang, "Practical approaches to channel estimation and interference suppression for OFDM-based UWB communications," *IEEE Transactions on Wireless Communications*, vol. 5, no. 9, pp. 2317–2320, Sep 2006.

[38] G. F. Ross, "The transient analysis of certain TEM mode four-port networks," *IEEE Journal on Microwave Theory and Techniques*, vol. 14, no. 11, pp. 528–542, Nov 1966.

[39] C. L. Bennett and G. F. Ross, "Time-domain electromagnetics and its applications," *Proceedings of the IEEE*, vol. 66, no. 3, pp. 299–318, Mar 1978.

[40] J. D. Taylor, *Introduction to Ultra-Wideband Radar Systems*, CRC Press 1995.

[41] J. M. Cramer, R. A. Scholtz, and M. Z. Win, "Spatio-temporal diversity in ultra-wideband radio," in *IEEE Wireless Communications and Networking Conference*, Sep 1999, pp. 888–892.

[42] S. S. Ghassemzadeh, R. Jana, C. W. Rice, W. Turin, and V. Tarokh, "Measurement and modeling of an ultra-wide bandwidth indoor channel," *IEEE Transactions on Communications*, vol. 52, no. 10, pp. 1786–1796, Oct 2004.

[43] H. G. Schantz and L. Fullerton, "The diamond dipole: a Gaussian impulse antenna," in *IEEE Antennas and Propagation Society International Symposium*, vol. 4, Jul 2001, pp. 100–103.

[44] L. B. Michael, M. Ghavami, and R. Kohno, "Multiple pulse generator for ultra-wideband communication using Hermite polynomial based orthogonal pulses," in *IEEE Conference on Ultra Wideband Systems and Technologies*, May 2002, pp. 47–51.

[45] B. Parr, B. Cho, K. Wallace, and Z. Ding, "A novel ultra-wideband pulse design algorithm," *IEEE Communications Letters*, vol. 7, pp. 219–221, May 2003.

[46] B. Hu and N. C. Beaulieu, "Pulse Shaping in UWB Communication Systems," in *IEEE Vehicular Technology Conference*, Sep 2004, pp. 5175–5179.

[47] J. D. Choi and W. E. Stark, "Performance analysis of RAKE receivers for ultra-wideband communications with PPM and OOK in multipath channels," in *IEEE International Conference on Communications*, Apr 2002, pp. 1969–1973.

[48] V. S. Somayazulu, "Multiple access performance in UWB systems using time hopping vs. direct sequence spreading," in *IEEE Wireless Communications and Networking Conference*, Mar 2002, pp. 522–525.

[49] G. Yue, L. Ge, and S. Li, "Analysis of ultra wideband signal interference to DSSS receiver," in *IEEE Workshop on Signal Processing Advances in Wireless Communications*, Jun 2003, pp. 229–233.

[50] ——, "Ultra wideband impulse radio signal interference to code division multiple access system," in *IEEE International Symposium on Personal, Indoor and Mobile Radio Communications*, vol. 3, Sep 2003, pp. 2437–2441.

[51] R. C. Qiu, H. Liu, and X. Shen, "Ultra-Wideband for multiple access communications," *IEEE Communications Magazine*, pp. 80–87, Feb 2005.

[52] H. Liu, "Error performance of a pulse amplitude and position modulated ultra-wideband system over lognormal fading channels," *IEEE Communications Letters*, vol. 7, no. 11, pp. 531–533, Nov 2003.

[53] A. A. M. Saleh and R. A. Valenzuela, "A statistical model for indoor multipath propagation," *IEEE Journal on Selected Areas in Communications*, vol. 5, no. 2, pp. 128–137, 1987.

[54] J. R. Foerster, "Channel modeling sub-committee report final (doc: IEEE 802-15-02/490r1-sg3a)," Feb 2002.

[55] M. Z. Win and R. A. Scholtz, "On the robustness of ultra-wide bandwidth signals in dense multipath environments," *IEEE Communications Letters*, vol. 2, pp. 51–53, Feb 1998.

[56] ——, "On the energy capture of ultrawide bandwidth signals in dense multipath environments," *IEEE Communications Letters*, vol. 2, no. 9, pp. 245–247, Sep 1998.

[57] F. Ramirez-Mireles and R. A. Scholtz, "Multiple-access with time hopping and block waveform PPM modulation," in *IEEE International Conference on Communications*, Jun 1998, pp. 775–779.

[58] R. J. Cramer, M. Z. Win, and R. A. Scholtz, "Impulse radio multipath characteristics and diversity reception," in *IEEE International Conference on Communications*, Jun 1998, pp. 1650–1654.

[59] R. J. Cramer, R. A. Scholtz, and M. Z. Win, "On the analysis of uwb communication channels," in *IEEE Military Communications Conference*, Oct 1999, pp. 1191–1195.

[60] D. Cassioli, M. Z. Win, F. Vatalaro, and A. F. Molisch, "Performance of low-complexity RAKE reception in a realistic UWB channel," in *IEEE International Conference on Communications*, Apr 2002, pp. 763–767.

[61] A. Taha and K. M. Chugg, "Multipath diversity reception of wireless multiple access time-hopping digital impulse radio," in *IEEE Conference on Ultra Wideband Systems and Technologies*, May 2002, pp. 283–287.

[62] C. Rushforth, "Transmitted-reference techniques for random or unknown channels," *IEEE Transactions on Information Theory*, vol. 10, no. 1, pp. 39–42, Jan 1964.

[63] Y.-L. Chao and R. A. Scholtz, "Ultra-wideband transmitted reference systems," *IEEE Transactions on Vehicular Technology*, vol. 54, no. 5, pp. 1556–1569, Sep 2005.

[64] S. Franz and U. Mitra, "Generalized UWB transmitted reference systems," *IEEE Journal on Selected Areas in Communications*, vol. 24, no. 4, pp. 780–786, Apr 2006.

[65] K. Witrisal, C. Krall, G. Leus, and M. Pausini, "Equivalent system model and equalization of differential impulse radio UWB systems," *IEEE Journal on Selected Areas in Communications*, pp. 1851–1862, Sep 2005.

[66] M. Pausini, G. J. M. Janssen, and K. Witrisal, "Performance enhancement of differential UWB autocorrelation receivers under ISI," *IEEE Journal on Selected Areas in Communications*, vol. 24, no. 4, pp. 815–821, Apr 2006.

[67] G. F. Edelmann, H. C. Song, S. Kim, W. S. Hodgkiss, W. A. Kuperman, and T. Akal, "Underwater acoustic communications using time reversal," *IEEE Journal of Oceanic Engineering*, vol. 30, no. 4, pp. 852–864, Oct 2005.

[68] F. Ramirez-Mireles, "On the performance of Ultra-Wide-Band signals in Gaussian noise and dense multipath," *IEEE Transactions on Vehicular Technology*, vol. 50, no. 1, pp. 244–249, Jan 2001.

[69] ——, "Performance of ultrawideband SSMA using time hopping and M-ary PPM," *IEEE Journal on Selected Areas in Communications*, vol. 19, no. 6, pp. 1186–1196, Jun 2001.

[70] B. Hu and N. C. Beaulieu, "Exact bit error rate analysis of TH-PPM UWB systems in the presence of multiple-access interference," *IEEE Communications Letters*, vol. 7, no. 12, pp. 572–574, Dec 2003.

[71] ——, "Accurate evaluation of multiple-access performance in TH-PPM and TH-BPSK UWB systems," *IEEE Transactions on Communications*, vol. 52, no. 10, pp. 1758–1766, Oct 2004.

[72] M. Sabattini, E. Masry, and L. B. Milstein, "A non-Gaussian approach to the performance analysis of UWB TH-BPPM systems," in *IEEE Conference on Ultra Wideband Systems and Technologies*, Nov 2003, pp. 52–55.

[73] J. R. Foerster, "The effects of multipath interference on the performance of UWB systems in an indoor wireless channel," in *IEEE Vehicular Technology Conference*, May 2001, pp. 1176–1180.

[74] R. D. Wilson and R. A. Scholtz, "Comparison of CDMA and modulation schemes for UWB radio in a multipath environment," in *IEEE Global Telecommunications Conference*, Dec 2003, pp. 754–758.

[75] H. R. Ahmadi and M. Nasiri-Kenar, "Performance analysis of time-hopping ultra-wideband systems in multipath fading channels (uncoded and coded schemes)," in *IEEE International Symposium on Personal, Indoor and Mobile Radio Communications*, vol. 4, Sep 2002, pp. 1694–1698.

[76] N. Boubaker and K. B. Letaief, "MMSE multipath diversity combining for multi-access TH-UWB in the presence of NBI," *IEEE Transactions on Wireless Communications*, vol. 5, no. 4, pp. 712–719, Apr 2006.

[77] W. Cao, A. Nallanathan, B. Kannan, and C. C. Chai, "Exact BER analysis of DS-UWB multiple access system under imperfect power control," in *IEEE Vehicular Technology Conference*, Sep 2005, pp. 986–990.

[78] ——, "Exact BER analysis of DS PPM UWB multiple access system under imperfect power control," in *IEEE Military Communications Conference*, Oct 2005, pp. 977–982.

[79] S. Zhao and H. Liu, "On the optimal linear receiver for impulse radio systems in the presence of pulse overlapping," *IEEE Communications Letters*, vol. 9, no. 4, pp. 340–342, Apr 2005.

[80] L. Zhao and A. M. Haimovich, "Performance of ultra-wideband communications in the presence of interference," *IEEE Journal on Selected Areas in Communications*, vol. 20, no. 9, pp. 1684–1691, Dec 2002.

[81] X. Wu, G. V. Eleftheriades, and E. V. Deventer, "Design and characterization of single and multiple beam mm-wave circularly polarized substrate lens antennas for wireless communications," in *IEEE Antennas and Propagation Society International Symposium*, Jul 1999, pp. 2408–2411.

[82] G. Durisi and S. Benedetto, "Performance evaluation and comparison of different modulation schemes for UWB multiaccess systems," in *IEEE International Conference on Communications*, May 2003, pp. 2187–2191.

[83] T. C. Yang, "Temporal resolutions of time-reversal and passive-phase conjugation for underwater acoustic communications," *IEEE Journal on Oceanic Engineering*, vol. 28, no. 2, pp. 229–245, Apr 2003.

[84] S.-H. Jung, N.-M. Kim, and H.-J. Suh, "Pre-RAKE assisted RAKE receiver for TDD WCDMA system," in *IEEE Vehicular Technology Conference*, Apr 2003, pp. 1396–1400.

[85] N. Guo, R. C. Qiu, and B. M. Sadler, "An ultra-wideband autocorrelation demodulation scheme with low-complexity time reversal enhancement," in *IEEE Military Communications Conference*, Oct 2005, pp. 1–7.

[86] K. Popovski, B. J. Wysocki, and T.A.Wysocki, "Modelling and comparative performance analysis of a time-reversed UWB system," *EURASIP Journal on Wireless Communications and Networking*, vol. 2007, no. 71610, 2007.

[87] Y.-H. Chang, S.-H. Tsai, X. Yu, and C. C. J. Kuo, "Design and analysis of Channel-Phase-Precoded Ultra Wideband (CPPUWB) systems," in *IEEE Wireless Communications and Networking Conference*, Apr 2006, pp. 866–871.

[88] T. Q. S. Quek and M. Z. Win, "Analysis of UWB transmitted-reference communication systems in dense multipath channels," *IEEE Journal on Selected Areas in Communications*, vol. 23, no. 9, pp. 1863–1874, Sep 2005.

[89] Y. Wang and X. Dong, "Frequency domain channel estimation for SC-FDE in UWB communications," *IEEE Transactions on Communications*, vol. 54, no. 12, pp. 2155–2163, Dec 2006.

[90] S. E. El-Khamy, E. E. Sourour, and T. A. Kadous, "Wireless portable communications using pre-RAKE CDMA/TDD/QPSK systems with different combining techniques and imperfect channel estimation," in *IEEE International Symposium on Personal, Indoor and Mobile Radio Communications*, Sep 1997, pp. 529–533.

[91] S. S. Tan, B. Kannan, and A. Nallanathan, "Multiple access capacity of UWB M-ary impulse radio systems with antenna array," *IEEE Transactions on Wireless Communications*, vol. 5, no. 1, pp. 61–66, Jan 2006.

[92] W. Cao, A. Nallanathan, and C. C. Chai, "On the multiple access performance of Prerake DS UWB System," in *IEEE Military Communications Conference*, Oct 2006.

[93] H. T. Nguyen, I. Z. Kovacs, and P. C. F. Eggers, "A time reversal transmission approach for multiuser UWB communications," *IEEE Transactions on Antennas and Propagation*, vol. 54, no. 11, pp. 3216–3223, Nov 2006.

[94] M. Jun and T. Oh, "Performance of pre-rake combining time hopping UWB system," *IEEE Transactions on Consumer Electronics*, vol. 50, no. 4, pp. 1033–1037, Nov 2004.

[95] K.-S. Song, "A globally convergent and consistent method for estimating the shape parameter of a generalized Gaussian distribution," *IEEE Transaction on Information Theory*, vol. 52, no. 2, pp. 510–527, Feb 2006.

[96] K. Kokkinakis and A. K. Nandi, "Exponent parameter estimation for generalized gaussian probability density functions with application to speech modeling," *Signal Processing*, vol. 85, no. 9, pp. 1852–1858, Sep 2005.

Appendix A

Expectation Related to $\tilde{g}_{j,k}$

All expectation values related to $\tilde{g}_{j,k}$ are derived using the following convolution. To simplify the notation, we will drop the user index k in following derivation of expectation values.

$$\begin{aligned}\tilde{g}_{j,k} &= \sum_{n=\max[0,j-L+1]}^{\min[j,L_p-1]} \alpha_{j-n,k}\tilde{\alpha}_{L_p-1-n,k} \\ &= \sum_{n=\max[0,j-L+1]}^{\min[j,L_p-1]} \alpha_{j-n,k}\left(\alpha_{L_p-1-n,k} + n_{L_p-1-n,k}\right) \end{aligned} \tag{A.1}$$

In the derivations, the x^{th} (where x is an even number) moment of $\alpha_{l,k}$ is obtained by the x^{th} moment of $\beta_{l,k}$, i.e., $\mathrm{E}[(\beta_{l,k})^x] = \exp(x\eta_{y_{l,k}} + x^2\sigma^2_{y_{l,k}}/2)$, where $\beta_{l,k} = \exp(y_{l,k})$ and $y_{l,k} \sim \text{Gaussian}(\eta_{y_{l,k}}, \sigma^2_{y_{l,k}})$.

A.1 The 2nd Moment

A.1.1 $j \neq L_p - 1$

$$\begin{aligned}\mathrm{E}\left[\tilde{g}_j^2\right] &= \sum_{n=\max[0,j-L+1]}^{\min[j,\,L_p-1]} \mathrm{E}\left[\alpha^2_{j-n}\right]\mathrm{E}\left[\alpha^2_{L_p-1-n}\right] \\ &\quad + \frac{N_0}{2N_t}\sum_{n=\max[0,j-L+1]}^{\min[j,\,L_p-1]} \mathrm{E}\left[\alpha^2_{j-n}\right] \end{aligned} \tag{A.2}$$

A.1.2 $j = L_p - 1$

$$\begin{aligned} \mathrm{E}\left[\tilde{g}_j^2\right] &= \sum_{n=0}^{L_p-1} \mathrm{E}\left[\alpha_n^4\right] \\ &\quad + \sum_{n=0}^{L_p-1} \sum_{\substack{n'=0 \\ n' \neq n}}^{L_p-1} \mathrm{E}\left[\alpha_n^2\right] \mathrm{E}\left[\alpha_{n'}^2\right] \\ &\quad + \frac{N_0}{2N_t} \sum_{n=0}^{L_p-1} \mathrm{E}\left[\alpha_n^2\right] \end{aligned} \tag{A.3}$$

A.2 The 4th Moment

A.2.1 $j \neq L_p - 1$

The range of n and m in the following summation is $\{\max[0, j - L + 1], \cdots, \min[j, L_p - 1]\}$. To simplify the expression, we define $f_1 = j - n$, $f_2 = L_p - 1 - n$, $f_3 = j - m$ and $f_4 = L_p - 1 - m$.

$$\begin{aligned} \mathrm{E}\left[\tilde{g}_j^4\right] &= \sum_n \mathrm{E}\left[\alpha_{f_1}^4\right] \mathrm{E}\left[\alpha_{f_2}^4\right] \\ &\quad + 3 \sum_n \sum_{\substack{m, m \neq n \\ f_1 \neq f_4, f_2 \neq f_3}} \mathrm{E}\left[\alpha_{f_1}^2\right] \mathrm{E}\left[\alpha_{f_2}^2\right] \mathrm{E}\left[\alpha_{f_3}^2\right] \mathrm{E}\left[\alpha_{f_4}^2\right] \\ &\quad + 3 \sum_n \sum_{\substack{m, m \neq n \\ f_1 = f_4}} \mathrm{E}\left[\alpha_{f_1}^4\right] \mathrm{E}\left[\alpha_{f_2}^2\right] \mathrm{E}\left[\alpha_{f_3}^2\right] \\ &\quad + 3 \sum_n \sum_{\substack{m, m \neq n \\ f_2 = f_3}} \mathrm{E}\left[\alpha_{f_1}^2\right] \mathrm{E}\left[\alpha_{f_3}^4\right] \mathrm{E}\left[\alpha_{f_4}^2\right] \\ &\quad + \frac{3N_0^2}{4N_t^2} \sum_n \mathrm{E}\left[\alpha_{f_1}^4\right] \\ &\quad + \frac{3N_0^2}{4N_t^2} \sum_n \sum_{\substack{m \\ m \neq n}} \mathrm{E}\left[\alpha_{f_1}^2\right] \mathrm{E}\left[\alpha_{f_3}^2\right] \\ &\quad + \frac{3N_0}{Nt} \sum_n \mathrm{E}\left[\alpha_{f_1}^4\right] \mathrm{E}\left[\alpha_{f_2}^2\right] \\ &\quad + \frac{3N_0}{Nt} \sum_n \sum_{\substack{m, m \neq n \\ f_2 \neq f_3}} \mathrm{E}\left[\alpha_{f_1}^2\right] \mathrm{E}\left[\alpha_{f_2}^2\right] \mathrm{E}\left[\alpha_{f_3}^2\right] \end{aligned}$$

$$+\frac{3N_0}{Nt}\sum_{n}\sum_{\substack{m,m\neq n\\ f_2=f_3}} \mathrm{E}\left[\alpha_{f_1}^2\right]\mathrm{E}\left[\alpha_{f_3}^4\right] \tag{A.4}$$

A.2.2 $j = L_p - 1$

The range of n and m in the following summation is $\{0, \cdots, L_p - 1\}$.

$$\begin{aligned}
\mathrm{E}\left[\tilde{g}_j^4\right] &= \sum_n \mathrm{E}\left[\alpha_n^8\right] \\
&+3\sum_n\sum_{\substack{m\\ m\neq n}} \mathrm{E}\left[\alpha_n^4\right]\mathrm{E}\left[\alpha_m^4\right] \\
&+6\sum_n\sum_{\substack{m\\ m\neq n}}\sum_{\substack{l,l\neq n\\ l\neq m}} \mathrm{E}\left[\alpha_n^2\right]\mathrm{E}\left[\alpha_m^2\right]\mathrm{E}\left[\alpha_l^4\right] \\
&+\sum_n\sum_{\substack{m\\ m\neq n}}\sum_{\substack{l,l\neq n\\ l\neq m}}\sum_{\substack{p,p\neq n\\ p\neq m,p\neq l}} \mathrm{E}\left[\alpha_n^2\right]\mathrm{E}\left[\alpha_m^2\right]\mathrm{E}\left[\alpha_l^2\right]\mathrm{E}\left[\alpha_p^2\right] \\
&+4\sum_n\sum_{\substack{m\\ m\neq n}} \mathrm{E}\left[\alpha_n^2\right]\mathrm{E}\left[\alpha_m^6\right] \\
&+\frac{3N_0^2}{4N_t^2}\sum_n \mathrm{E}\left[\alpha_n^4\right] \\
&+\frac{3N_0^2}{4N_t^2}\sum_n\sum_{\substack{m\\ m\neq n}} \mathrm{E}\left[\alpha_n^2\right]\mathrm{E}\left[\alpha_m^2\right] \\
&+\frac{3N_0}{N_t}\sum_n \mathrm{E}\left[\alpha_n^6\right] \\
&+\frac{9N_0}{N_t}\sum_n\sum_{\substack{m\\ m\neq n}} \mathrm{E}\left[\alpha_n^4\right]\mathrm{E}\left[\alpha_m^2\right] \\
&+\frac{3N_0}{N_t}\sum_n\sum_{\substack{m\\ m\neq n}}\sum_{\substack{l,l\neq n\\ l\neq m}} \mathrm{E}\left[\alpha_n^2\right]\mathrm{E}\left[\alpha_m^2\right]\mathrm{E}\left[\alpha_l^2\right]
\end{aligned} \tag{A.5}$$

A.3 Expectation of Square Product

We assume $j_1 \neq j_2$. The range of n in the following summation is $\{\max[0, j_1 - L + 1], \cdots, \min[j_1, L_p - 1]\}$. The range of m is $\{\max[0, j_2 - L + 1], \cdots, \min[j_2, L_p - 1]\}$.

$$\begin{aligned}
\mathrm{E}\left[\tilde{g}_{j_1}^2\tilde{g}_{j_2}^2\right] &= \mathrm{E}\left[\left(\sum_n \alpha_{j_1-n}\alpha_{L_p-1-n}\right)^2\left(\sum_m \alpha_{j_2-m}\alpha_{L_p-1-m}\right)^2\right] \\
&+\frac{N_0}{2N_t}\mathrm{E}\left[\sum_n\sum_m \alpha_{j_1-n}^2\alpha_{L_p-1-n}^2\alpha_{j_2-m}^2\right]
\end{aligned}$$

$$+\frac{N_0}{2N_t}\mathrm{E}\left[\sum_n\sum_m \alpha_{j_1-n}^2\alpha_{j_2-m}^2\alpha_{L_p-1-m}^2\right]$$
$$+\mathrm{E}\left[\left(\sum_n \alpha_{j_1-n}n_{L_p-1-n}\right)^2\left(\sum_m \alpha_{j_2-m}n_{L_p-1-m}\right)^2\right] \quad \text{(A.6)}$$

List of Publications

1. Wei Cao, A. Nallanathan, C. C. Chai, "A novel high data rate Prerake DS UWB multiple access system: Interference modeling and tradeoff between energy capture and imperfect channel estimation effect", to appear in *IEEE Transactions on Wireless Communications*, 2008.

2. Wei Cao, A. Nallanathan, C. C. Chai, "Exact BER analysis and comparison of DS PAM UWB and DS PPM UWB multiple access system in lognormal multipath fading channels", to appear in *IEE Proceedings Communications*, 2007.

3. Wei Cao, A. Nallanathan, C. C. Chai, "Performance analysis of Prerake DS UWB multiple access system under imperfect channel estimation", *IEEE Transactions on Wireless Communications*, vol. 6, no. 11, pp. 3892-3896, Nov 2007.

4. Wei Cao, A. Nallanathan, C. C. Chai, "A novel high data rate Prerake DS UWB multiple access system and its accurate interference model", in *Proc. of IEEE Global Telecommunications Conference*, Nov 2007.

5. Wei Cao, A. Nallanathan, C. C. Chai, "A novel high data rate DS UWB communication system via superposition of chip waveforms", in *Proc. of IEEE International Conference on Ultra-Wideband*, Sep 2007.

6. Wei Cao, A. Nallanathan, C. C. Chai, "On the tradeoff between data rate and BER performance of Pre-RAKE DS UWB System", in *Proc. of IEEE Global Telecommunications Conference*, Nov 2006.

7. Wei Cao, A. Nallanathan, C. C. Chai, "Exact BER analysis of DS PPM UWB multiple access system in lognormal multipath fading channels", in *Proc. of IEEE Global Telecommunications Conference*, Nov 2006.

8. Wei Cao, A. Nallanathan, C. C. Chai, "On the multiple access performance of Prerake DS UWB System", in *Proc. of IEEE Military Communications Conference*, Oct 2006.

9. Wei Cao, A. Nallanathan, C. C. Chai, "Exact BER analysis of DS PAM UWB multiple access system in lognormal multipath fading channels", in *Proc. of IEEE Vehicular Technology Conference*, Sep 2006.

10. Wei Cao, A. Nallanathan, B. Kannan, C. C. Chai, "Exact BER analysis of DS PPM UWB multiple access system under imperfect power control", in *Proc. of IEEE Military Communications Conference*, pp.977-982, Oct 2005.

11. Wei Cao, A. Nallanathan, B. Kannan, C. C. Chai, "Exact BER analysis of DS-UWB multiple access system under imperfect power control", in *Proc. of IEEE Vehicular Technology Conference*, pp.986-990, Sep 2005.